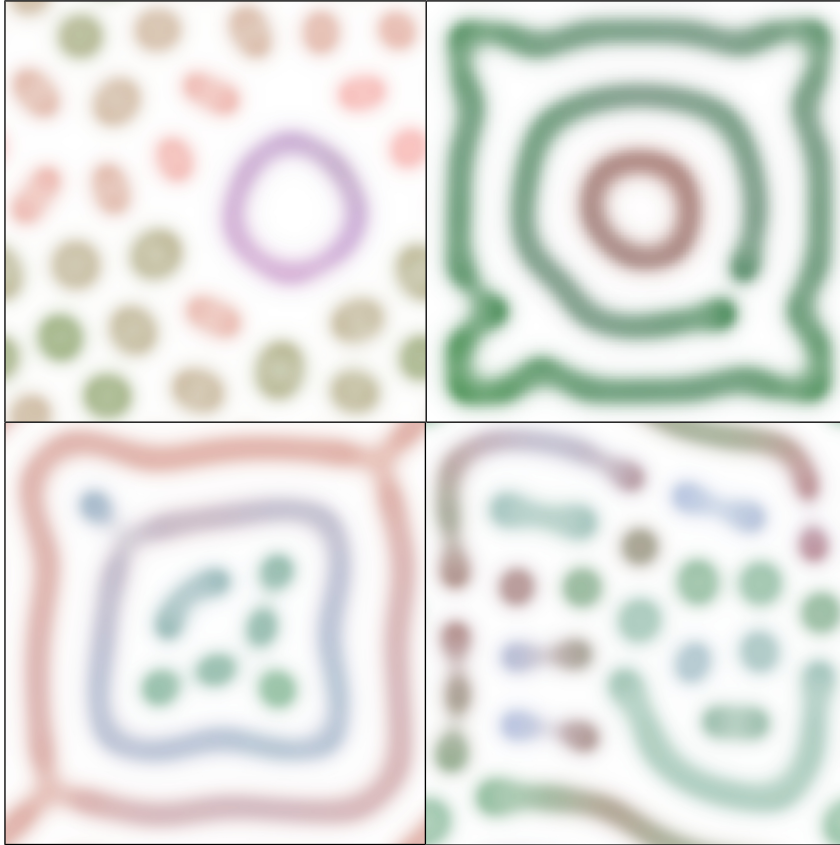




CHALMERS
UNIVERSITY OF TECHNOLOGY



Pattern formation and chemical evolution in extended Gray-Scott models

Master of Science thesis in Complex Adaptive Systems

FILIP BURIC

THESIS FOR THE DEGREE OF MASTER OF SCIENCE IN COMPLEX ADAPTIVE SYSTEMS

Pattern formation and chemical evolution
in extended Gray-Scott models

FILIP BURIC

Division of Physical Resource Theory
Department of Energy and Environment
CHALMERS UNIVERSITY OF TECHNOLOGY

Göteborg, Sweden, 2014

Pattern formation and chemical evolution in extended Gray-Scott models

FILIP BURIC

Supervisor: Kristian Lindgren

Thesis for the Degree of Master of Science in Complex Adaptive Systems

© FILIP BURIC, 2014

FRT 2014:04

Department of Energy and Environment
Division of Physical Resource Theory
CHALMERS UNIVERSITY OF TECHNOLOGY
SE-412 96 Göteborg
Sweden
Tel. +46-(0)31 772 1000

Cover: Examples of dynamic patterns produced by the most general reaction-diffusion model developed in this thesis.

Chalmers Reproservice
Göteborg, Sweden 2014

Abstract

Pattern formation in reaction-diffusion systems has been the subject of study in a variety of natural disciplines. In this thesis we investigate the behaviour of an abstract pattern-forming autocatalytic system based on the Gray-Scott model, featuring a small number of related chemical species.

The aim is to investigate the form of interaction that takes place between these species, whether competition or cooperation, and how this relates to the overall pattern generation. Through the perspective of chemical evolution we seek to observe what long-term behaviour emerges, both in terms of population composition and structure formation. The work is largely exploratory and we approached the observed system properties from various angles to characterise them.

We report that systems composed of 2 species were seen to be unstable and only achieve transient joint pattern formation, while the 3-species extension reached stability for a limited class of configurations. This class produced rich behaviour in the form of dynamic patterns with shifting structural features involving long transients, including a novel type of pattern, not seen in other studies of the Gray-Scott model or related models. Both systems are examples of catalytic hypercycles. In terms of pattern formation, the exhibited structural features reflect local species populations and in general are not themselves decisive for the outcome of species interactions. In an unconstrained evolution scenario, we report a strongly directed evolutionary path towards selfish species and loss of structure.

Keywords: *chemical evolution, complex systems, excitable media, Gray-Scott model, hypercycles, pattern formation, self-organization.*

Acknowledgements

I would like to thank my supervisor Kristian Lindgren for offering me the chance to work on this topic. It has been an enjoyable collaboration and a fruitful learning experience and I am grateful for his constant guidance and patience.

Thanks also go to all those in the CAS programme for the many stimulating conversations and words of encouragement.

Filip Buric, Göteborg 14th of June, 2014

Contents

1	Introduction	1
1.1	Pattern formation in reaction-diffusion systems	1
1.2	Terminology	1
1.3	Chemical evolution	1
1.4	Thesis considerations and results	3
2	The Gray-Scott model	4
2.1	Model	4
2.2	Pattern examples	5
2.3	Noise	8
3	Simple mutation	10
3.1	Model	10
3.2	Simulations	11
3.3	Parameter space sweep	17
4	Interacting catalysts	19
4.1	Model	19
4.2	Mutation outcomes	20
4.3	Evolution simulations	24
4.4	Special cases	27
4.5	The aggregate pattern case	31
4.6	Slight extension: full parametrisation	38
4.7	Mutation outcomes	39
4.8	Evolution simulations	41
4.9	Conclusions	48
5	Catalytic hypercycle	49
5.1	Model	49
5.2	Mutation outcomes	50
5.3	Stable hypercycle properties	61
5.4	Dynamic patterns	66
5.5	Novel pattern: expanding loop	73
5.6	Evolution simulations	86
5.7	Conclusions	90
6	Discussion	91
6.1	Overview	91
6.2	Parallels with existing models	91
6.3	On further extensions	93
A	On numerical issues	95
B	Simulation movie files	97
C	Software	98
	Bibliography	99

Chapter 1

Introduction

1.1 Pattern formation in reaction-diffusion systems

In the larger context of self-organising systems, the study of pattern formation in reaction-diffusion systems has a long history, starting with Alan Turing's paper in 1952 [Tur52], where such a mechanism was proposed as the basis of biological morphogenesis, the process by which organisms take shape from otherwise homogeneous and symmetrical incipient structures such as the morula of early embryonic life. Structure would emerge when certain chemical system in steady state were perturbed. A point of interest of these pattern-forming systems is the very long time spans in which they remain far from steady state, a property characteristic of living systems.

Reaction-diffusion systems capture the effect of spatial distribution of chemical reactions. While such transformations yield periodic oscillations in well-stirred environments that are effectively non-spatial, they become far more interesting when transport processes such as diffusion are allowed to extend these oscillation across a spatial domain. The interplay of these antagonistic feedback mechanisms (synthesis of new molecules and their dispersal) has been postulated to be essential for structure formation in the activator-inhibitor Gierer-Meinhardt model [GM72]. A closely related concept is that of *excitable media*, though most definitions refer strictly to media that allow the propagation of waves in a one-shot manner for a given time interval and as such, describe a sub-class of the behaviour exhibited by reaction-diffusion systems [Mer92]

Not surprisingly, these models have found applications in describing a wide range of natural phenomena across various scales, from microbiological processes such as chemotaxis (the directed cellular movement based on concentration gradients), neural activity, tumour growth, wound healing, and animal pigmentation patterns, to population dynamics, such as ecological dispersal and invasions, as well as spread of epidemics [Mur03].

1.2 Terminology

These systems are inspired by organic molecules that participate in biochemical reactions within living cells, most notably enzyme-facilitated transformations and replication.

Here we shall often speak of one chemical as *fuel* or *substrate*, by which we mean it acts as some building material that is transformed through reaction with a *catalyst* into another molecule or *species*, a transition that would otherwise have essentially null probability of happening. The catalysts or *enzymes* use these molecules to make copies of themselves, hence they are called *autocatalysts*. In this respect, the substrate becomes a *resource* present in the system in varying amounts. For the sake of alleviating repetition, we shall use the above terms interchangeably.

Following the definitions and treatment of [HS87], we call a chemical system featuring multiple chemical species a *permanent* system if all chemical species remain in the system (have non-null concentration) in the limit of time $t \rightarrow \infty$

1.3 Chemical evolution

One of the aims of this thesis is to explore the way structure formation is affected by the appearance of new types of molecules in the system. These are often slightly altered versions of existing molecules. This process of random alteration of chemicals is referred to as *mutation* since it is inspired by faulty biomolecule production inside the living cell. The entire process is termed *chemical* or *molecular evolution*.

In this type of abstract study however, the role of information-carrying molecules such as DNA and the transcriptional and translational machinery that produces the molecules based on these is ignored and the focus is placed upon the interactions of the end products themselves. Much of the terminology however comes from the classic macroscopic version of evolution, thus we speak of populations of various *species*, either *wild types* or mutants, that either survive or go extinct, with the sense of molecule species concentrations that either remain non-null or drop to zero.

Self-replicating molecules have been of great interest for their hypothesised role in abiogenesis and, in particular, in the emergence of key features of early life, cooperation between replication and later integration in the more complicated mechanism of translation [SS97], as well as the emergence of the first genomes, cellular compartments and cells [SS03].

This framework needs to account for variability in competing traits in order to allow for selection and thus evolution, but also for the establishment of cooperation at least for relatively small groups of replicators which would then need to resist destabilising influence from other groups [SS97]. Herein lies a problem with the well-known catalytic hypercycle model of cooperating replicators proposed by Eigen and Schuster in [ES77], that at least in a non-spatial, well-mixed environment it is known to be vulnerable to *parasites*, species that only receive replicative support from others but offer none in exchange [SS97]. That is, upon their interaction cycle species are outcompeted by a fitter parasite and become extinct, the system degenerating into a catalytic chain and ultimately leaving the parasite the sole species in the system [SS03].

Various solutions have been proposed to tackle this conundrum. The straightforward spatial extension of the hypercycle was seen to also be vulnerable [SCS⁺03] and so various constraints on global interactions that seek to emphasize locality have been investigated.

The metabolic model in [SCS⁺03] forces absolute cooperation of all species in the system. If any species goes extinct, the entire network does so as well. This architecture incorporates parasites and assures global survival, both in the mixed and spatial versions, at the cost of the stringent interaction requirement. Much emphasis has been placed on cyclic reaction networks since it was shown in [ES78] that more complex topologies devolve into hypercycles or strictly competing entities, at least when assuming uniform coupling. Another approach outlined in [SCS⁺03] and [HT03] is the so-called *stochastic correction principle*, a model “half-way” towards spatiality, which features vesicles of mixed competing species that undergo fission, each new vesicle containing a random fraction of the original contents, thus letting concentration drift “weed out” parasites by eventually producing vesicles free of these mutants. We shall not discuss this approach further. Models that introduce explicit spatial separation of chemical reactions in order to study the interplay between structure formation and the interaction between species in a catalytic network have been considered on different levels of dynamics.

One approach is to model the molecular dynamics microscopically using cellular automata [BH91], [HT03], [AS06], where there is strict particle exclusion in each cell of the grid and empty cells are thus a resource necessary for growth. The patterns in these are composed of largely segregated populations, with neighbouring populations tending to be formed by catalytically linked species [BH91]. The hypercycles in these environments were seen to resist invasion from parasites. In particular, the patterns considered in the referred papers are spirals that while rotating and expanding cause the parasite molecules to spread outwards and be pushed outside the system, going extinct. These studies also point out that such spatially extended populations undergo group evolution [BH91], i.e. selection that acts upon cooperating networks, which is an important step toward higher life-like systems.

However, there is a critical model dependence of the behaviour for the same classes of catalytic networks. In [CB94] it was shown that for the macroscopic partial differential equations modelling of the system in [BH91] the resistance disappears due to copies of the hypercycle possibly existing at every grid point, thus the inability to expel the molecules of strong parasites (fitter than their wild types) through spatial exclusion and the vulnerability to infection. A proposed solution explored in [CB97] is to employ a constraint on substrate availability along with a high concentration cut-off, i.e., whenever species levels drop below a certain threshold, they are considered null and excluded. This indeed allows for some structural features to remain isolated from others that have been infected, as the parasites cannot spread between low-concentration areas. Still, this cut-off needs to be unreasonably high to have effect. In this thesis, we do not use such a high cut-off. Neither do we rely on the possible lowest machine-representable positive number, as this was seen to induce what are considered spurious results. More on this in Appendix A. Another tactic to confer parasite resistance in the PDE description is to have heterogeneous space by varying parameters such as decay rates and fuel presence within the system [BH95b], which was seen to isolate infections within spiral fragments that were later pushed out of the system. In the present study, such spatial gradients were seen to have no impact on species interactions.

1.4 Thesis considerations and results

While spatial extension has thus been considered for its role in helping the prebiotic emergence of robust replicator cooperation, our perspective in the present study is somewhat different. Given an established chemical system that builds patterns we wish to explore how these molecular structures themselves are affected by mutation, especially at long time scales. Thus we do not restrict the properties of these new species to parasites, but let the system undergo general mutation. Beyond the trivial question of whether pattern-formation is able to sustain itself at all, we are particularly interested in how the structures change when their internal composition is spontaneously altered. We study various extensions of the Gray-Scott model featuring a small number of autocatalyst species that arise as mutations of an original. That is, they feature near-identical behaviour but have different intrinsic properties.

For the models explored here, we shall assume an aqueous isothermal solution containing the autocatalyst molecules, distributed on an effectively two-dimensional surface. A guiding principle in our model development was to impose as little external constraint as possible in order to observe self-organised behaviour. Replicators that are more probable to have existed in early life, capable of storing more information and having inherently higher variability are usually modelled as a nucleic-like polymer [SS03] and some models have explicitly built-in genetic information from which reaction behaviour is derived, such as the cellular automata model in [AS06]. However, small autocatalysts of more limited variability do exhibit essential mechanisms of replication. In this work a more abstract perspective is adopted, in which replicators possess continuous variability but behave as small molecules, emphasis being placed on their interactions. Similarly with the dynamics in [CB94] and [CB97], the Gray-Scott model and its extensions presented here specify a limited availability of substrate used in replication, and therefore introduce competition between species in fuel consumption, but unlike completely generalised models [TK01], we only consider one type of substrate and thus higher selective pressure.

Some forms of mutation assume an inherently faulty replication process in a network with a fixed number of species. In such models each catalytic replication yields alternative products with certain relative frequencies. Technically, the differential equations have a mutation term that acts as a perturbation of population growth [SS92]. The form of mutation we chose to use was sporadic appearance of a new species. Thus we have assumed a fixed number of species in the chemical systems studied here, with new species filling existing “slots”. A similar approach was taken in [HS98] for a non-spatial system but here we obtain different behaviour.

There has been much work regarding chemical systems undergoing mutation (invasion) only after the initial system has reached steady state, both in well-mixed conditions, e.g. [HS98], or in the spatial models mentioned earlier. This was argued in [HT03] to reflect ecological dynamics rather than evolutionary ones. However few studies focus on the effects of mutation on pattern formation while far from steady state. While experiments with spirals in different states of formation have been considered, we have only been able to find the previously mentioned paper relevant to our study, where this issue was considered explicitly and which reports contrasting results with the ecological-like studies. In our work, both scenarios are present but it is generally not assumed that the a priori (wild type) system is internally equilibrated (at steady state) or is even assumed to not be in some scenarios. Specifically, in the evolutionary experiments of the most general model presented here, it is essential that mutants are introduced before steady state. Mutants that appear in stable patterns were mainly considered in order to study immediate interaction between species, especially the perturbative effects of mutation, however we point out where results differ for mutation far from steady state.

We obtain here that 2-species systems, either non-interacting or catalytically linked are highly competitive, leading generally to at most one survivor but sometimes to the extinction of both. Except for the simplest unlinked model, patterns usually overlap in an infection-like manner. While subject to change due to species replacement, the patterns that are formed are still those of the original Gray-Scott model. Evolutionarily speaking, multiple mutation events quickly lead to structure loss due to the increase in autocatalyst self-preservation, which corresponds to homogeneous population distributions.

Interestingly, the addition of a properly linked third species is seen to stabilise the system and induce long-lived dynamic patterns, even if populations still overlap. We have also discovered a new type of pattern which does not occur in the original model. These systems, while assuring permanence, are rare however and until they are reached in an evolutionary setting, structure loss still occurs quite quickly. This seems to be the overwhelmingly probable fate of these systems. As we present our results we shall draw parallels and point out differences with the most relevant studies mentioned earlier, as well as give a review in the final discussion of this report.

Chapter 2

The Gray-Scott model

Originally published in [GS84] in a non-diffusive isothermal formulation, its pattern-forming behaviour was explored in the paper by Pearson [Pea93] across a range of parameter values. The physical plausibility of this rich set of patterns was demonstrated experimentally in [LMOS93]. Other aspects of this system, such as its information dynamics [LEE04] and the effects of noise perturbations [MS06] were subsequently studied.

Regarding its behaviour in an evolutionary setting and in particular steady state structure resistance to parasite invasion, the model was studied as a special case by Blomberg and Cronhjort [CB97], where it was shown that spatial separation of catalyst clusters by means of a high null concentration cut-off provides such resistance.

In the next chapters we shall extend upon this result by considering the case of mutants that lend catalytic support to wild type species, in contrast to the strictly parasitic type in the aforementioned paper.

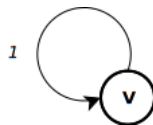
2.1 Model

The chemical system is composed of only two active chemical species U and V , along with a (virtual) inert product P . V is the species which catalyses its own replication through the conversion of the substrate U .



All reactions are irreversible and such will be the case for all model extensions presented here. P denotes inactivated V (incapable of further catalytic activity), which is eliminated from the system by a flow process. The degradation rate k controls how fast the inactivation occurs. All rates in this thesis are non-negative. Note that in actual systems, the reactions portrayed here may not be elementary, but they are typically treated as such in these models and the derived differential equation assume mass action kinetics.

A way to look at this system is that it describes a self-replicating molecule that consumes fuel to multiply and which only “lives” for a certain amount of time. We shall also use the following graphical notation to illustrate this point. The looped arrow corresponds to reaction (2.1) which occurs at dimensionless rate 1 (omitted above). The diagram omits that U is used in the self-catalysis and that V degrades, since all models shall use the same substrate and degrading catalysts.



Note that the arrows showing catalysed synthesis are ambiguous regarding the stoichiometry but since all models presented here use an autocatalysis ratio of 2:3, the diagram is kept unencumbered.

The dynamics take the shape of a system of non-linear parabolic partial differential equations composed of three terms, a *reaction* function, a *diffusion* term, and a *flow* process. This last term regulates the inflow of chemical U in the system which prevents its exhaustion, as well as the elimination of inactivated V . The system units and parameters have been non-dimensionalised

from the original model description in [GS84]. As a matter of notation, uppercase letters denote the name of the species, while lowercase their concentration.

$$\frac{\partial u}{\partial t} = -uv^2 + D_u \nabla^2 u + F(1 - u) \quad (2.3)$$

$$\frac{\partial v}{\partial t} = uv^2 + D_v \nabla^2 v - (F + k)v \quad (2.4)$$

The constants D_u and D_v are the diffusion coefficients of U and V , respectively, and F is the dimensionless feed rate. Following [Pea93], we set the initial conditions as $(u, v) = (1, 0)$ in the entire system space except a small area of concentration usually $(u, v) = (0.5, 0.25)$, which is randomised with Gaussian white noise to break the symmetry of the emerging pattern.

This initial-value problem was solved by means of the simple forward Euler explicit finite difference method on a two-dimensional lattice of $N \times N$ cells and physical size L (system length). Their ratio is the discrete space step size $\Delta x = L/N$. More on numerical issues in Appendix A. All simulations shown in this study have been performed on a torus, i.e a grid with periodic boundary conditions. We point out a need to have a sufficiently large initial population, otherwise the catalyst is unable to take hold due to diffusion and degradation, a phenomenon seen to be true also for CAs [AS06]. This will also become relevant in mutant invasion studies, as will be pointed out.

As a note on terminology, in the present work we will speak of pattern *steady state* to refer to a qualitative stable structure, ignoring small fluctuations and spatial translations or rotations. To be more rigorous one would refer to a periodic orbit reached by the dynamical system, but the informal sense is used for its qualitative insight.

2.2 Pattern examples

Here we show a few examples of patterns formed by this starting model. Since we will be interested in the behaviour of the self-replicator V (and its mutants later on), the animations showing the system time evolution will trace this concentration alone. Maxima of catalyst overlap perfectly with minima of substrate so plotting U would give the same patterns in the negative. From this perspective, one could also say there is a one-to-one correspondence between (catalyst-)empty space and high fuel concentration. This is often relevant in explaining the expansion and change in shape of structures, as this empty, resource-rich space tends to be optimally occupied by asymptotically time-independent patterns, i.e. those that reach steady state, or to be more accurate, a periodic orbit if one considers translation across the torus space.

Given the small integration time steps Δt , for convenience we record the system evolution using a specific time length called *generation*, computed as

$$1 \text{ generation} = \left\lceil \frac{LN}{\Delta t^2} \right\rceil \quad (2.5)$$

The term has been borrowed from population studies for its suggestiveness. The speed of system evolution is determined by the discretisation constants L , N , Δt , and the generation length was found to scale well with these values, spanning a largely consistent relative time interval, unless Δt was below 10^{-3} (which was deemed infeasible). Note that all simulation presented in this report use the same constants. The number of integration iteration steps comprising one generation is given throughout for reference. Its intuitive sense here is that of a time interval spanning visible change in the system and the above scaling was found largely satisfactory, even if it has been sometimes doubled when the interest was in long-term development. The convention used here is that the randomised initial conditions, before the dynamics are let to run, is counted as generation 0.

D_v	D_u	L	N	Δt
$1.4 \cdot 10^{-9}$	$2 \cdot D_v$	0.01	150	0.05

Table 2.1: System parameters used for the Gray-Scott patterns illustration in this section. The lengths were chosen in order to have the structural features at large enough size, with a grid of sufficient resolution but small enough size to allow fast computation. The diffusion coefficient D_v was computed with the heuristic described in Appendix A

When speaking about the size of pattern feature on the grid, we sometimes use the notion of Moore neighbourhood of a cell which defines the square of side $2r + 1$ centred on it and we refer r to as the Moore radius of this square, where the unit is one cell.

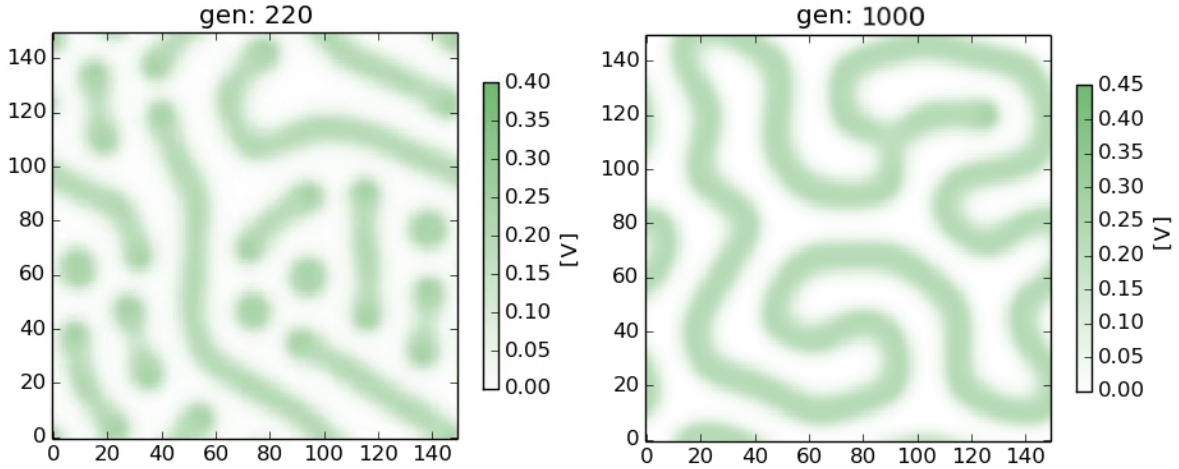


Figure 2.1: Examples of Gray-Scott patterns. These are frames from animations recording the time evolution of different systems. The catalyst concentration $[V]$ is plotted in shades of green across system space. The top label marks the generation number of the frame. The system parameters for all these are shown in Table 2.1. A generation has specific time length $\lceil \frac{LN}{\Delta t^2} \rceil = 600$ integration iterations.

The *first* pattern occurs for $(k, F) = (0.0634, 0.04)$ and is a mix of stripes and replicating spots. In the classification in [Pea93], these are κ (stripes) and λ (repl. spots), as this k is near the frontier between these two. In the top and bottom left of this frame we can see spots dividing.

The *second* pattern occurs for $(k, F) = (0.063, 0.062)$ and is composed of loops with stripes branching from bends. Although not clear due to the low resolution in [Pea93] this would be type κ or μ . The outward expansion of the structural features (waves) is slower than for the first pattern.

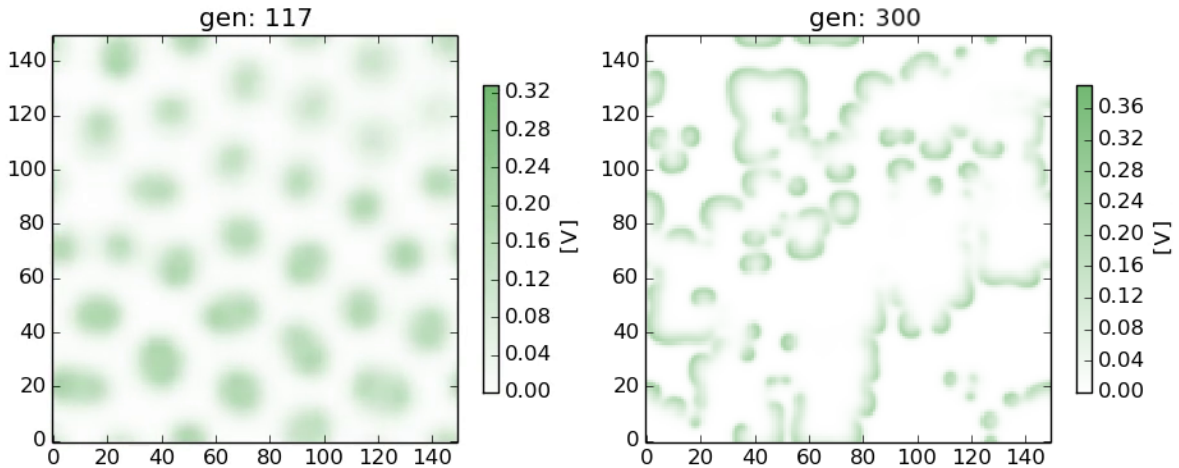


Figure 2.2: Examples of Gray-Scott patterns.

The *first* pattern is chaotic (Pearson ϵ), occurring for $(k, F) = (0.056, 0.02)$ and consists of dividing spots. These spots regularly disappear when in dense clusters, as can be see in the upper-right where a group is fading out, unlike the asymptotically time-independent type λ spots which fill the space and achieve steady state.

The *second* pattern occurs for $(k, F) = (0.045, 0.01)$ and is made up of thin spirals that annihilate when meeting. The spiral bodies exhibit irregularities (kinks) that nucleate new spirals. This corresponds to Pearson type β . The diffusion coefficient D_v was reduced to $1.4 \cdot 10^{-10}$ for this simulation, since it was slightly too high for the pattern waves to properly take shape.

The full extent of patterns that can be formed by this model is shown in the diagram below, of much higher resolution than the one provided in [Pea93]. This is taken from a study by Robert Munafò [Mun], which provides a very detailed inventory of structures in the Gray-Scott model, including an interesting regime named “u-skate world”, after a travelling structure reminiscent of the glider in Conway’s Game of Life.

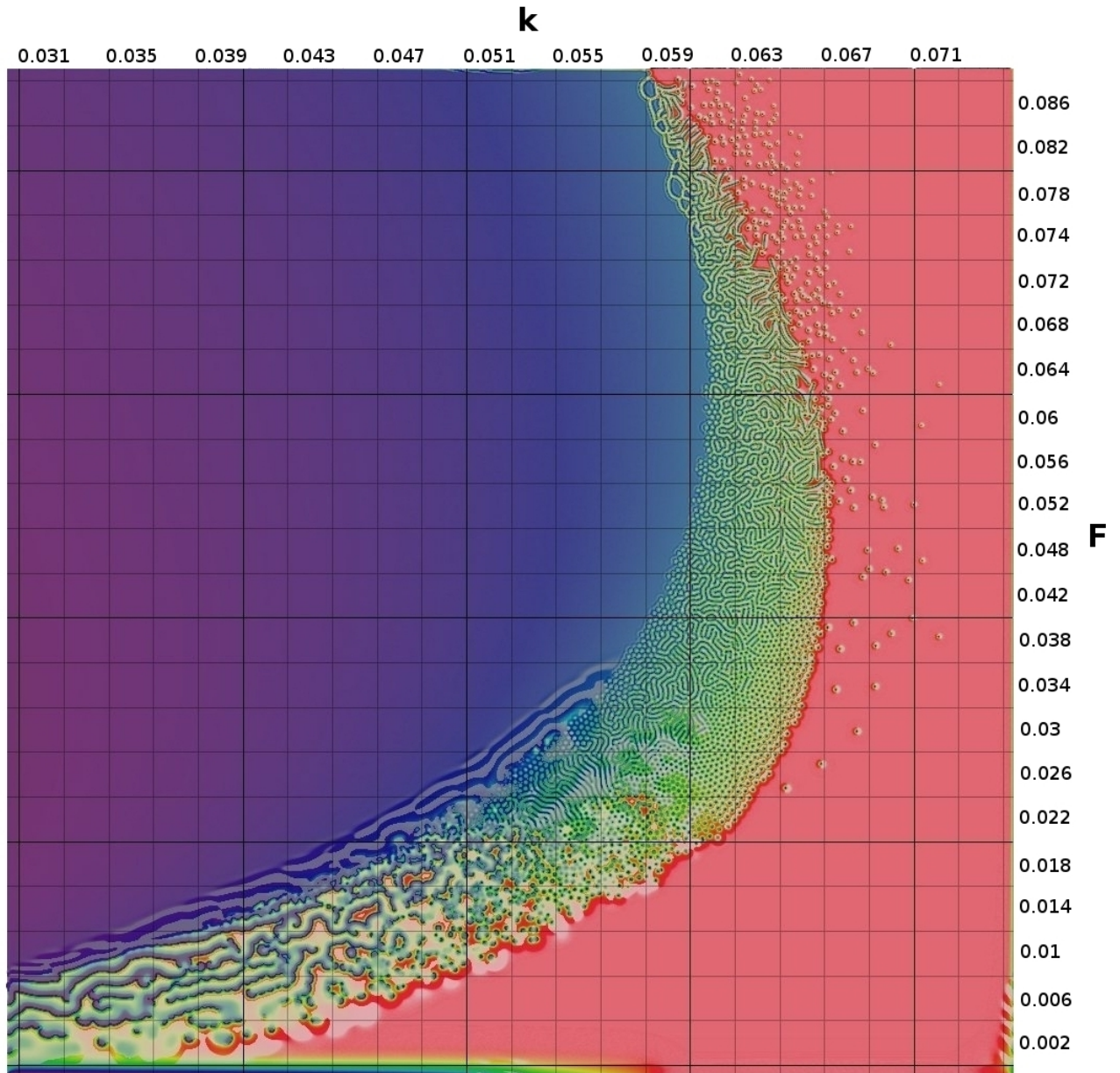


Figure 2.3: Phase diagram of pattern formation in the original Gray-Scott for varying k and F parameters, after [Mun] (axes added). The colour encodes the u concentration from dark blue (1.0) to dark red (0.0), following the scheme in [Pea93], that also gave the names of the two trivial states reachable by the system, the so-called “blue state” in the upper-left region, which contains a homogeneous mix of U and V at comparable concentrations, and the “red state” on the right, containing only $u = 1.0$ and so, void of catalyst.

2.3 Noise

In order to analyse the effect of stochastic perturbations on the emerging patterns, a noise term was added to the dynamics in some experiments. Both uniform and Gaussian noise distributions were used.

In keeping with standard practice [Kam07], random fluctuations intrinsic to chemical reactions scale as the square root of the number of particles, so for a certain chemical concentration c we would have the end quantity as

$$c = \hat{c} + \nu\sqrt{n} \quad (2.6)$$

where \hat{c} is the quantity computed by a deterministic differential equation, ν is a random number drawn from a normal distribution (the common case of Gaussian white noise) and n is the number of particles in \hat{c} . Then c is the perturbed quantity which is obtained at that time step. Strictly, any $c > 1$ after random perturbation is truncated to 1.

Since we concern ourselves with a continuous system, the above scaling presupposes an implicit discretisation. That is, to express the real concentration $c(\mathbf{x}) \in [0, 1]$ as a ratio of number of particles over the capacity of the grid cell corresponding to position \mathbf{x} . Note that technically speaking, this restriction from real to rational numbers is already effected by finite computer representation. We thus make the above equation more explicit as

$$c(\mathbf{x}) = \hat{c}(\mathbf{x}) + \lambda\nu \cdot \sqrt{\frac{\hat{c}(\mathbf{x})}{n^{\max}}}, \quad \forall \mathbf{x} \in \Omega \subset \mathbb{R}^2 \quad (2.7)$$

where Ω is the system space domain, and λ is an extrinsic noise amplification parameter since we wish to control the strength of these fluctuations.

Thus we need to decide values for two parameters, the standard deviation σ of the normal distribution from which ν is drawn and the grid cell capacity n^{\max} . In order to obtain the scales of these in a less arbitrary way, we turn to dimensional values in [LMOS93] for some orientation.

The stochastic process that yields ν values is the Langevin force $L(t)$ equating Gaussian white noise. As such, its variance is given as

$$\sigma^2 = \langle L(t)^2 \rangle = 2\gamma k_B T \quad (2.8)$$

for continuous time t , where γ is the damping coefficient in the corresponding Brownian motion equation and is inversely proportional to the diffusion coefficient D . Here we set it as $\gamma = D^{-1}$. We use the temperature of 303.15 K from [LMOS93] and obtain $\sigma^2 = 8.3766 \cdot 10^{-21} \cdot D^{-1}$, but approximate to

$$\sigma^2 = \frac{10^{-20}}{D} \quad (2.9)$$

Regarding maximum cell capacity, this needs to be taken as a function of the space discretisation step $\Delta x = L/N$, where L is the system size (length) and N is the number of cells comprising a side of the square 2D grid. For an estimation of the number of particles that would be contained in the entire reactor, we take sizes from [LMOS93], where the volume of the chamber was $7.6 \cdot 10^{-2}$ ml. Since we are dealing with an aqueous solution, we take the reference density as a tenth of the number of water molecules per ml, i.e. $3.34 \cdot 10^{21}$. So then the (three-dimensional) reactor capacity is $C_R = 10^{20}$ particles approximately, and we take a truncated linear density $\sqrt[3]{C_R} \approx 10^6$. Even if simulations may portray grids that would be physically implemented with larger chambers, we set this value as the maximum value. Note that this discretisation only comes into play when noise is present and does not otherwise influence computations so its level of rigour is not essential. Then we simply set

$$n^{\max} = \left(\Delta x \sqrt[3]{C_R} \right)^2 \quad (2.10)$$

To get an intuition for these values, in many simulations here we have set $\Delta x = 6.67 \cdot 10^{-5}$ which gives 4489 molecules per grid cell after the above formula. We stress again that this is an ad-hoc discretisation and unrelated to the rationale in choosing the concentration cut-off discussed in Appendix A.

In deciding how strong the noise should be in a realistic setting, the amplification parameter λ was set between $\lambda_{\min} = 10^5$ and $\lambda_{\max} = 10^6$. Anything below would have no noticeable effects and higher values gave unreasonably strong noise. To simplify notation when specifying noise strength, we shall use the notation $\bar{\lambda} = \frac{\lambda}{\lambda_{\max}}$ and speak of adjusting the *noise level* $\bar{\lambda}$ in the range $[0, 1]$.

Besides the normal distribution described above, experiments were also performed using a uniform distribution $\mathcal{U}(-\sigma, +\sigma)$. Although uniform noise of reasonably high strength manages to fragment the patterns more than the Gaussian, no essential destruction of these took place for the parameter values tried. The more natural Gaussian white noise which was used throughout this study was consistently seen to have little to no impact on the overall shape of these structures.

Effects of noise on the Gray-Scott system have been previously investigated in [LHMPM03] where it was seen to cause shifts between pattern types if the reaction parameters were set at the frontier between these, and in [MS06], where the number of structural features (spots and stripes) would vary as a function of noise strength. In this study we have found only a few cases of dynamics change due to noise, presented in special cases of the models. Beyond these results, noise influence was not pursued since it was seen to have essentially no impact on pattern formation in the context of evolution. Hence, while less chemically rigorous, deterministic dynamics have been used in general (besides the initial randomisation of initial conditions).

Chapter 3

Simple mutation

3.1 Model

This is a very simple extension of the Gray-Scott model, one that features a near-identical copy of the autocatalyst that appears at late time into the system's evolution via some process of mutation. There is no reaction between the wild type and mutant autocatalysts.



The corresponding differential equations are as follows

$$\begin{aligned} \frac{\partial u}{\partial t} &= -uv^2 - um^2 + F(1 - u) + D_u \nabla^2 u \\ \frac{\partial v}{\partial t} &= uv^2 - (F + k_1)v + D_v \nabla^2 v \\ \frac{\partial m}{\partial t} &= um^2 - (F + k_2)m + D_m \nabla^2 m \end{aligned} \tag{3.2}$$

where u , v , m , and D_u , D_v , D_m are the concentrations and diffusion coefficients of the three species, respectively. As before, F is the fuel feed rate and k_1 , k_2 are the degradation rates of the autocatalysts into the inert species P . Here we named the two degradation rates k_1 and k_2 for generality and simplicity of notation but in order to be more suggestive we will refer to them also as k_{wt} for the wild type autocatalyst V and k_{mut} for mutant M . To point out the relation between the two, we shall use $\Delta k = k_{\text{mut}} - k_{\text{wt}}$ in our discussion.

In all simulations presented here, we kept $D_v = D_m$ since the mutant is only slightly different. Different diffusion rates were tried but yielded no essential change in the dynamics. Hence the only differing parameter between the two species is the degradation rate k . Here we will focus on the mutant and talk about an *advantageous* degradation rate when $\Delta k < 0$ and *disadvantageous* when $\Delta k > 0$. We may use such a designation since obviously a lower degradation rates permits the autocatalyst to remain and replicate in the system longer.

3.2 Simulations

We considered the starting wild type species V in two pattern regimes, spirals and spots, and for these mutants with both advantageous and disadvantageous degradation rates. The mutation perturbation (or “drop”) was placed without subtracting it from the wild type catalyst quantity, i.e. $v^{t+1}(x, y) = v^t(x, y)$, when placing a concentration μ of mutant at coordinates (x, y) and time t . This was in order to focus more on species interaction and is also justified by the more plausible small mutant perturbations, which have low impact on wild type levels. This drop was placed in the system after the wild type formed patterns at either a minimum or maximum of wild type concentration.

In order to see how spread out a pattern is, i.e. how much space is occupied with the spatial structures of a certain species X , we use a very simplistic measure. Namely, we are interested in the number of cells that have “peaks” in concentration, that is, have a sufficiently higher than average concentration. This significant difference is discriminated by the mean absolute difference, since the population variance was found to be too restrictive:

$$\delta(\mathbf{x}) = \frac{1}{N^2} \sum_{i,j} |x_{i,j} - \bar{x}|$$

where \bar{x} is the average X concentration and N is the size of the grid. Then we simply construct the counting measure $\rho : \mathbb{R}^2 \rightarrow \mathbb{N}$ as:

$$\rho(\mathbf{x}) = |\{x_{i,j} : x_{i,j} > \bar{x} + \delta(\mathbf{x})\}| \quad (3.3)$$

For a trivial steady state with $\mathbf{x} = \text{const.}$ this measure is obviously null. We shall use this measure whenever it is more telling than a total concentration plot of the catalyst species. In the example to follow, tracing the relative spread of a species was considered relevant. When quantities are more relevant or when the spread plots are ambiguous, the concentration evolutions will be shown.

Now will follow the results of a few simulations. The system used had a grid of size $N = 150$, a physical size of $L = 0.01$, and periodic boundary conditions. For integration a time step $\Delta t = 0.05$ was used and the diffusion coefficients were taken $D_v = D_m = 1.4 \cdot 10^{-10}$, with $D_u = 2 \cdot D_v$ as usual. A generation has the specific length $\lceil \frac{LN}{\Delta t^2} \rceil = 600$ integration iterations.

The initial conditions are always a system with $u = 1$ and $v = 0$ except for a region of 20×20 cells where $u = 0.5$ and $v_0 = 0.25$. To reduce some of the symmetry in the initial pattern, we add Gaussian noise of level $\bar{\lambda} = 0.5$.

Due to this, the simulations have a certain degree of randomness, however the essential behaviour is reproducible for the same parameters.

Simulation 1 The spirals regime corresponds to $F = 0.01$ and $k_{wt} = 0.045$. The mutant placed had an advantageous degradation rate.

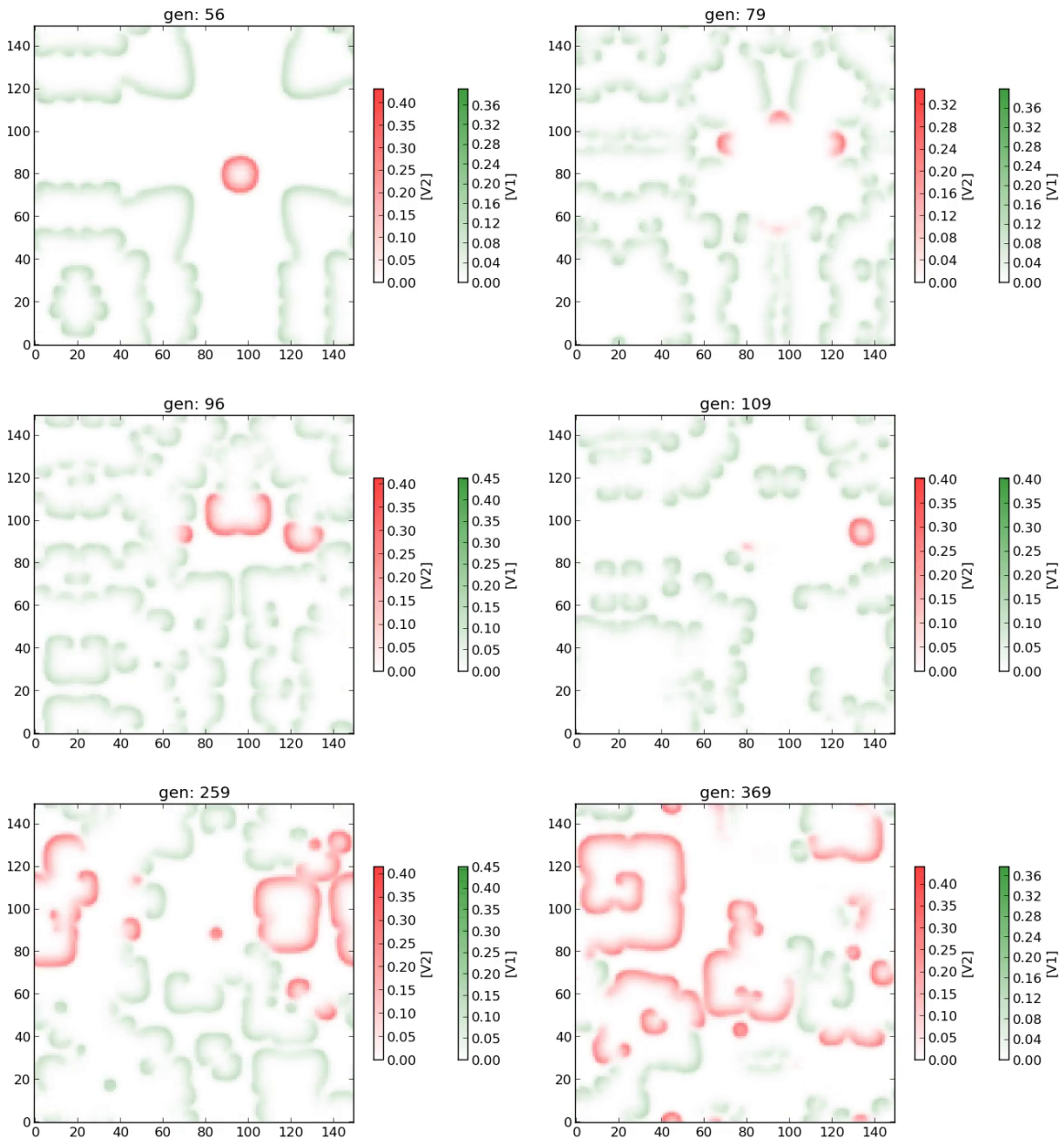


Figure 3.1: Movie frames from a simulation in the spiral patterns regime (in order left-right, top-bottom), featuring a mutant introduced at generation 50, which gradually spreads and occupies more space. Wild type (green) and mutant (red) concentrations are plotted. The mutant has an advantageous degradation rate with $\Delta k = -0.002$, the initial drop has concentration $\mu = 0.2$ and Moore radius $d_\mu = 1$ and placed at a non-null minimum of v .

The small mutant perturbation placed at low wild type concentration slowly spreads occupying more space. In this pattern regime, colliding wave fronts annihilate each other and this also holds between species. Initially, the spirals the mutant formed were destroyed by colliding with those of the wild type but nucleation sites managed to survive, generating subsequent spirals. Below is the ρ -spread of both species over the entire run of the simulation.

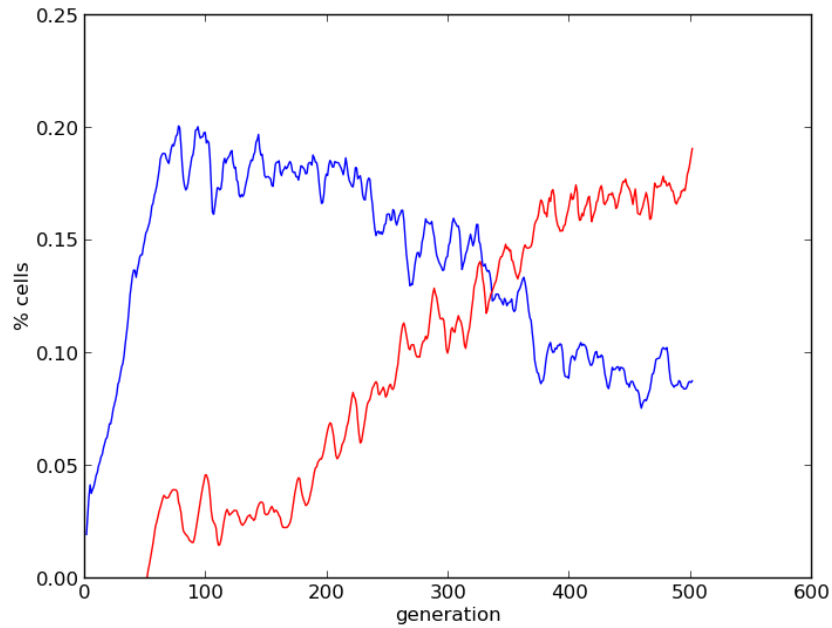


Figure 3.2: Spread of autocatalyst patterns of the wild type (blue) and mutant species (red) as cell percentages, measured with ρ . The trend of gradual mutant takeover is fairly obvious. The fluctuations are due to spiral annihilation, as seen in the frames above.

Simulation 2 Here we look at the evolution of a mutant at a degradative disadvantage. In all the simulations that were ran for mutants with $\Delta k > 0$ placed in small drops (low μ and d_μ) the outcome was the disappearance of the mutant.

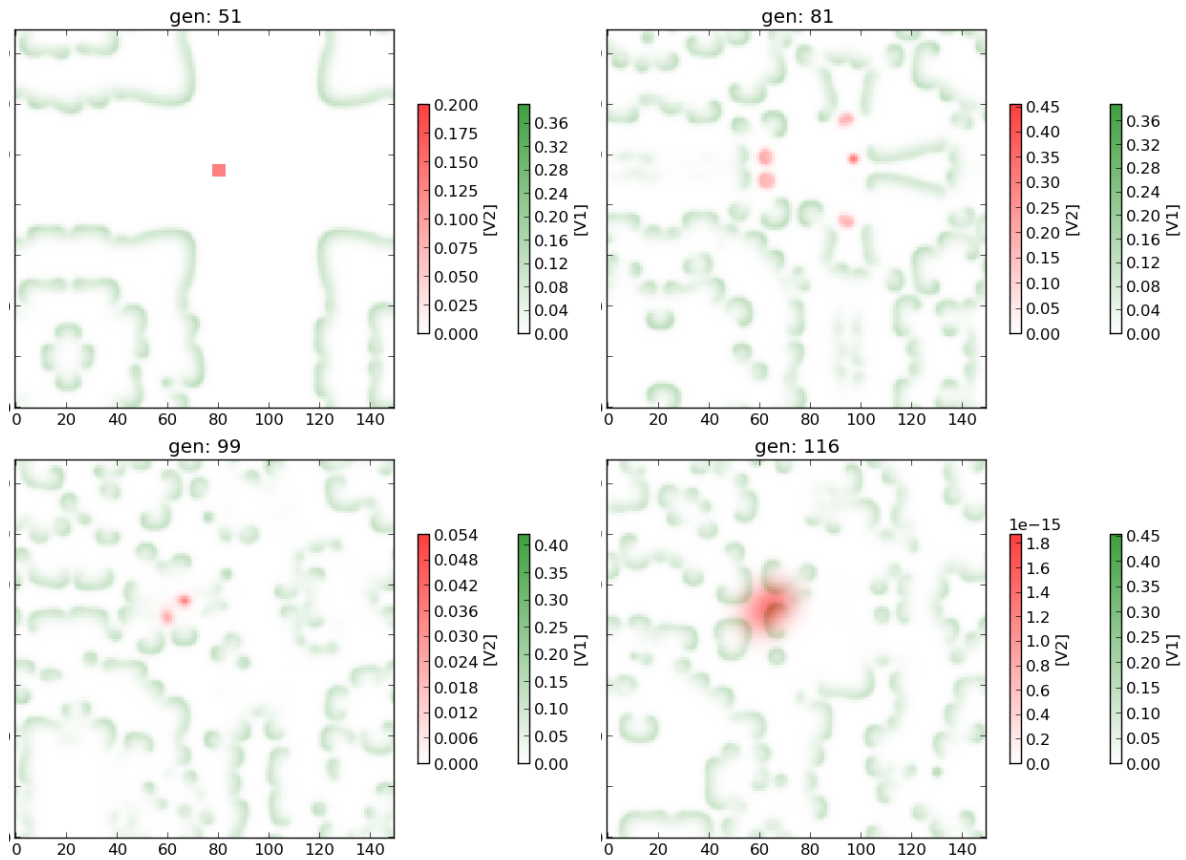


Figure 3.3: Simulation frames in the spiral patterns regime (left-right, top-bottom), featuring a mutant introduced at generation 50, which gradually disappears. Wild type (green) and mutant (red) concentrations are plotted. The mutant is not able to replicate and spread for very long, while being forced out of the system completely by generation 130. The mutant has a disadvantageous degradation rate with $\Delta k = +0.002$, the initial drop has concentration $\mu = 0.2$ and Moore radius $d_\mu = 2$ and placed at a non-null minimum of v .

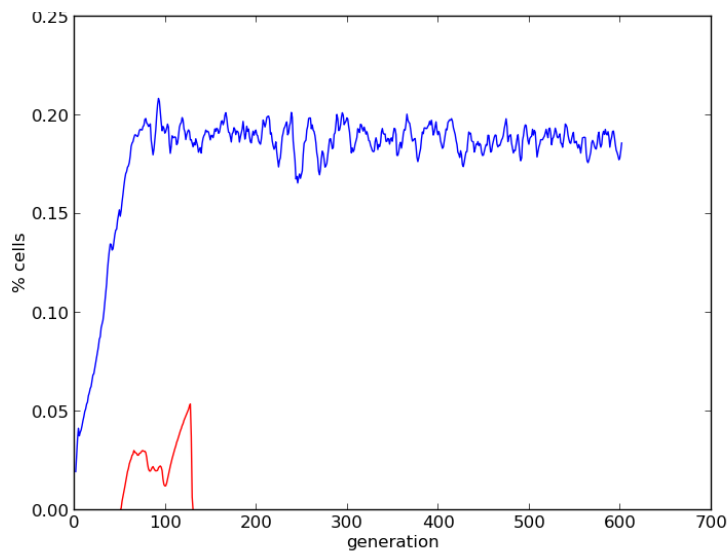


Figure 3.4: Spread of autocatalyst patterns of the wild type (blue) and mutant species (red) as cell percentages, measured with ρ . The mutant is not able to remain in the system for too long due to its higher degradation rate and initial disadvantage of occupying a limited space.

Simulation 3 We are interested in the dividing spots regime due to its stability. This corresponds to $F = 0.04$ and $k_{\text{wt}} = 0.065$. D_v is also increased to $1.4 \cdot 10^{-9}$. The mutant had an advantageous k . A generation has length $2 \cdot \lceil \frac{LN}{\Delta t^2} \rceil = 1200$ iterations since the dynamics in this regime are slower.

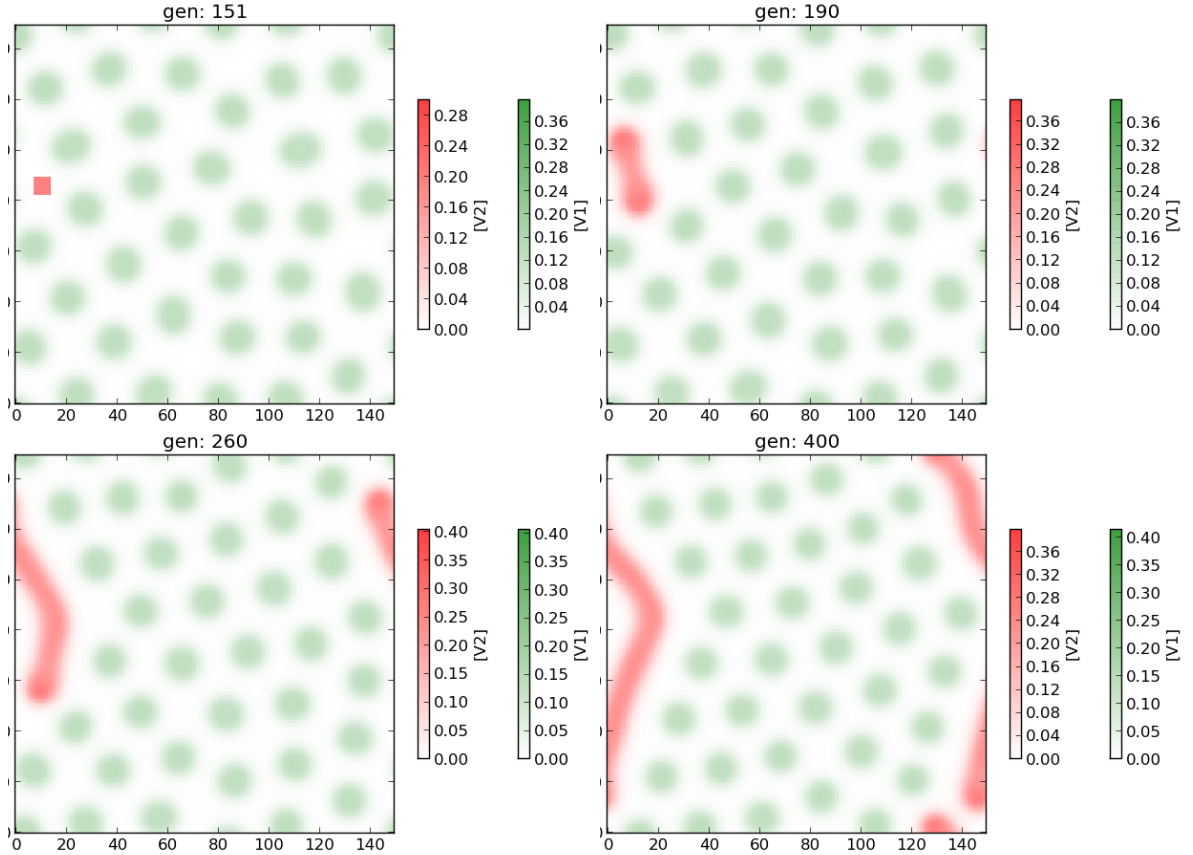


Figure 3.5: Frames from a simulation in the dividing spots regime (in order left-right, top-bottom), featuring a mutant introduced at generation 50, which gradually spreads and occupies more space. Wild type (green) and mutant (red) concentrations are plotted. Due to k deviation, the mutant forms stripes and gradually pushes away the V spots. The mutant has an advantageous degradation rate with $\Delta k = -0.002$, the initial drop has concentration $\mu = 0.3$ and Moore radius $d_\mu = 3$ and placed at a non-null minimum of v .

A plot of the catalyst spread ρ is omitted since the trend is quite obvious, with the mutant gradually taking over the space from the wild type. The size of the initial mutant drop needed to be larger than in the spirals regime and the concentration slightly higher for the mutant to be able to spread, otherwise the mutant very rapidly degraded out of the system. Interestingly, if the size of the drop was unreasonably large, e.g. $d_{\text{mut}} = 9$ the mutant was also unable to take hold. The reason was that due to its size it overlapped with existing wild type spots and, since both catalysts consume the fuel U , the two species disappeared in those areas of faster use. What was left of the mutant was insufficient for further spread.

Simulation 4 As before, we look at the evolution of a disadvantaged mutant. The system is otherwise the same

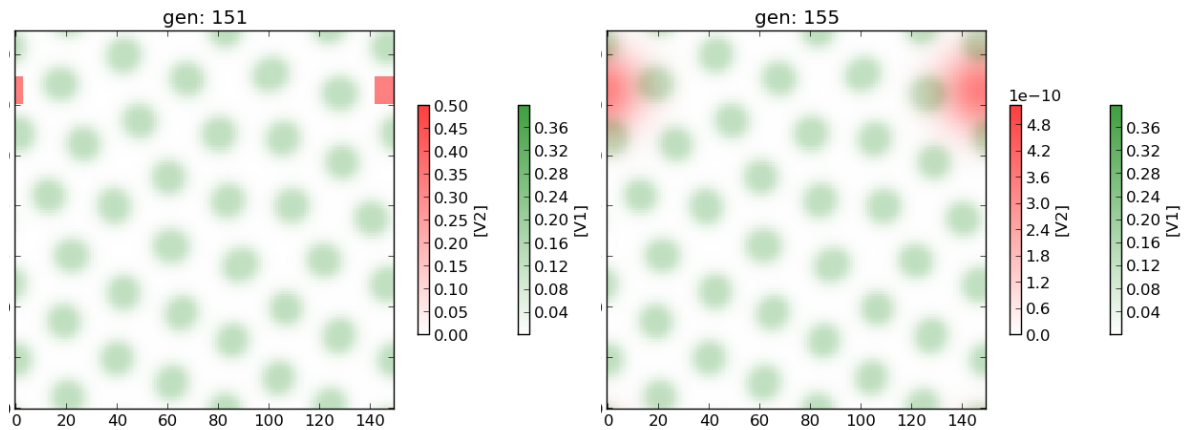


Figure 3.6: Frames from a simulation in the dividing spots regime (in order left-right, top-bottom), featuring a mutant introduced at generation 50, which gradually disappears. Wild type (green) and mutant (red) concentrations are plotted. The mutant introduced at generation 150 very quickly disappears from the system. The mutant has a disadvantageous degradation rate with $\Delta k = +0.002$, the initial drop has concentration $\mu = 0.5$ and Moore radius $d_\mu = 5$ and placed at a non-null minimum of v .

The concentration and size of the mutant perturbation were increased farther in this simulation but even at higher values the mutant was always unable to reproduce and degraded out of the system in a few generations.

These simulations show that between the two species there is mainly a competition for resource-rich space, the regions of structure formed by each being mutually exclusive and slightly repulsive. It was also apparent that only mutants with lower degradation rate were able to survive after being introduced.

Given this competition for space and by looking at various simulations, we deduce that the initial size of the mutant perturbation is important in deciding if the new species manages to establish a hold in the system and replicate, with extreme values being problematic. We therefore performed a sweep of (μ, r_μ) parameter space to map the values yielding surviving mutants.

3.3 Parameter space sweep

In this sweep we look for mutant “survival”, which is used here in a restricted sense, namely that the mutant managed to gain a hold on the system and self-replicated for a significant time. This includes cases where the mutant dies out eventually, alongside possible cases where it remains in balance with the wild type catalyst (up to long simulation times). As was seen in various simulations, if a mutant does not achieve this hold it very quickly disappears due to degradation and diffusion, hence the importance of this initial step. We considered mutants with $\Delta k < 0$ since one with a disadvantageous degradation rate was never seen to take hold.

To account for the initial randomization, each parameter combination is run through 10 simulations and the frequency of survival is recorded.

Algorithm 3.1 Simple Mutation Survival Sweep

```
for  $\mu \in \{0.1, \dots, 0.5\}$  and  $d_{\text{mut}} \in \{1, \dots, d_{\text{spot}} = 8\}$  do

  INITIALIZE()
  for  $run = 1, \dots, 10$  do

    repeat
      if (wt pattern steady state) then
        INTRODUCE MUTANT( $k_{\text{mut}}, position$ )
      end if
      SIMULATION STEP(())
    until ENDTIME

    if  $|\{(i, j) : m_{i,j} - \epsilon > 0\}| \neq 0$  then ▷  $\exists$  cells with mutant
      COUNT SURVIVOR CASE(())
    end if

  end for
  RECORD SURVIVOR FREQUENCY( $\mu, d_{\text{mut}}$ )
end for
```

The wild type pattern steady state is reached by generation 150 in this system and the mutant succeeds or fails to take hold by generation 200 (*ENDTIME*). ϵ is the effective null concentration. The position at which to insert the mutant was set to a non-null minimum concentration of v , a maximum of v , and random. Results for these three sweeps are below.

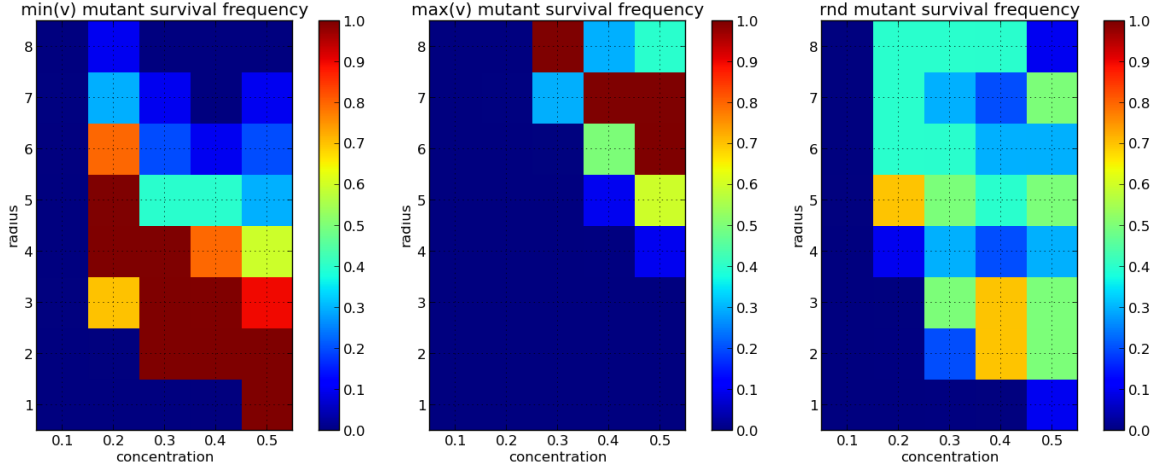


Figure 3.7: Frequency diagrams of mutant survival cases after placing the mutant at (left) $\min_{i,j}(v)$, (centre) $\max_{i,j}(v)$, and (right) $\text{rnd}(i,j)$. The values are averaged over 10 runs for each combination of concentration μ and Moore radius d_{mut} . Δk was taken to be -0.002 . For reference, the radius of a spot is $d_{\text{spot}} = 8$ and the distance between spots is about 5.

From the above frequency diagrams one can distinguish what was hinted at through simulations run for a mutant with $\Delta k < 0$ placed in this regime, namely that it is able to take hold in the system only for a narrow range of concentrations and sizes. The most favourable situation is when the mutant drop is placed in between wild type clusters, at a minimum of v . This way, this initial perturbation has more space available to spread. However, if the initial drop is larger than the inter-spot distance this becomes problematic as described before.

A sweep was performed for a mutant with $\Delta k = +0.002$ but this yielded only 1% survival for only a few parameter combinations, enforcing the previous observations that a disadvantaged mutant is unable to establish itself in the system.

One thing to note is that for this model, when a mutant is introduced at wild type steady state, it has a considerably lower chance of establishing itself initially, whatever the end outcome.

Chapter 4

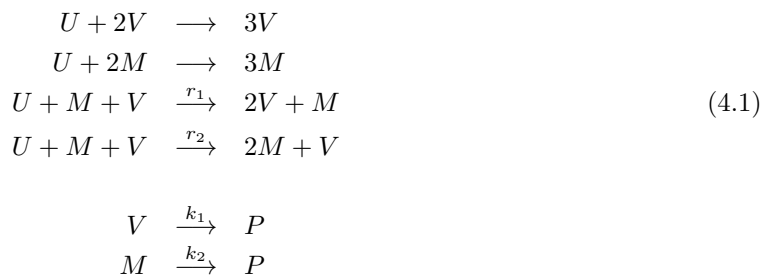
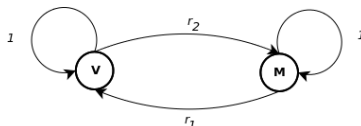
Interacting catalysts

4.1 Model

Building on the previous model, we add interactions between the wild type and mutated versions of the autocatalyst. Specifically, we allow for the two chemical species to provide catalytic support for the synthesis of the other.

The experimental realisation of a similar system was first reported by [LSYG97] as a cooperative 2-species cycle composed of self-replicating coiled coil peptides, however the molecules in question had quadratic autocatalysis and consumed three types of building material for replication and were also not described to degrade for the duration of the experiment. As we shall see, the model presented here exhibits essentially different behaviour, marked by general competition.

The question arises of how the two catalyst versions would interact with the substrate and each other. Here we considered that, since the mutation brings about only a minute change in the molecule, the two catalysts should interact in a largely similar manner with the substrate, hence we specifically allow for the concomitant binding of two differing catalyst molecules, which leads to two possible reactions products, namely the replication of one or the other catalyst species. We assign to these two possible evolutions reaction rates r_1 and r_2 . We could think of these as the rates of received catalytic support for V and M , respectively. Below are the reaction scheme and corresponding differential equations:



Here, for simplicity, the mutant M degrades into the same inert species as the wild type V as this only serves to remove them from the system. This reaction scheme could be classified as an elementary hypercycle composed of two replicators [ES77].

$$\begin{aligned}
\frac{\partial u}{\partial t} &= -u(v^2 + m^2 + (r_1 + r_2)vm) + F(1 - u) + D_u \nabla^2 u \\
\frac{\partial v}{\partial t} &= u(v^2 + r_1 vm) - (F + k_1)v + D_c \nabla^2 v \\
\frac{\partial m}{\partial t} &= u(m^2 + r_2 vm) - (F + k_2)m + D_c \nabla^2 m
\end{aligned} \tag{4.2}$$

Ignoring the differences in degradation rates, the scheme features an interaction between the substrate and a joint quantity of catalyst. Following this line of thought, the following constraint was imposed:

Constraint 1:

$$r_1 + r_2 = 2 \tag{4.3}$$

This yields a change in fuel as a function of the joint catalyst concentration. More precisely, the fuel rate can be written as:

$$\frac{\partial u}{\partial t} = -u(v + m)^2 + F(1 - u) + D_u \nabla^2 u$$

While this constraint is artificial, it was applied assuming that the species are very similar. So the relation captures the way they interact with the fuel as a single quantity, as opposed to emphasizing separate behaviour. It was seen in all models starting with this one that outcomes were determined by the comparative values of r_i (i.e if $r_1 < r_2$ or conversely), not their magnitude. So this constraint was not seen to obscure behaviour. The one exception to this found will be pointed out as a special case of this model. Technically, it also serves to relate the two possible reaction outcomes as the catalytic support rates become interdependent, thus resulting in parameter reduction.

We now have two parameters that govern the interaction of catalyst species, degradation rate and received catalytic support, namely rates r_1 and r_2 . We proceed to test how species of varying parameter values interact with each other.

4.2 Mutation outcomes

As a preliminary investigation of the impact of the two parameters on species interaction, we considered one mutation event, specifically the placing of a low concentration ($\mu = 0.2$) and low-spread (Moore radius $r_\mu = 2$) quantity of mutant catalyst at a peak of wild type catalyst, once its pattern had reached steady state. A system with periodic boundary conditions and with the following parameters was used:

D_u	F	L	N	Δt
$2 \cdot D_c$	0.04	0.01	150	0.05

Table 4.1: System parameters for single mutation outcome sweep.

The original (wild type) catalyst was always the same: $k_{\text{wt}} = 0.065$, which along with F places it in the dividing spots regime, and diffusion coefficient $D_c = 1.4 \cdot 10^{-9}$. The initial catalyst concentration was randomised using Gaussian noise, as in the previous model simulations. The mutant always has the same diffusion coefficient, the rationale being that small deviations in chemical properties should not lead to changes in diffusion. Slightly differing coefficients were tried, however, but had no effective impact on the dynamics. The sampling of values was rather sparse, as the apparent symmetry was hinted at through the various simulations.

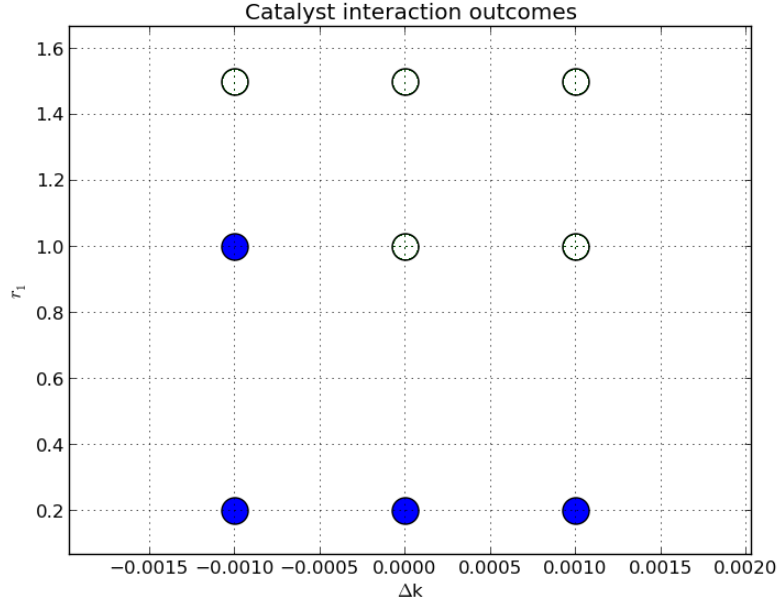


Figure 4.1: Scatter plot in parameter space of single mutation outcomes (dots), classified by the surviving species: *white* circles - wild type survived, *blue* circles - mutant survived. Δk is the change in mutant degradation rate with respect to the wild type, i.e. $k_{\text{mut}} = k_{\text{wt}} + \Delta k$. Rates r_1 and r_2 , which correspond to received catalytic support of the wild type and mutant, respectively, are set at the beginning of each simulation and obey Constraint 1, therefore only r_1 is needed for the plot.

In all simulations performed with Constraint 1, only one catalyst species remains as $t \rightarrow \infty$, as the mutant either replaces the wild type or disappears from the system. Indeed, the two parameters lie in symmetric balance, advantage of one species being conferred through lower degradation rate or higher received catalytic support. The case corresponding to identical species (central dot in the scatter plot above) yields a wild type survival outcome. This is due to the factor of “spatial hold”: the introduced minute mutant quantity with no intrinsic advantage in chemical parameters is not able to spread and take a hold inside the system, so it degrades out. Below are a few representative simulation examples to illustrate the behaviour. All are performed with the system described above and start with a wild type in the sots regime, i.e. $k_{\text{wt}} = 0.065$. A generation has length $2 \cdot \lceil \frac{LN}{\Delta t^2} \rceil = 1200$ integration iterations.

Simulation 1 We look at a mutant with advantageous k and r , introduced at a maximum of wild type pattern concentration, once this has achieved steady state.

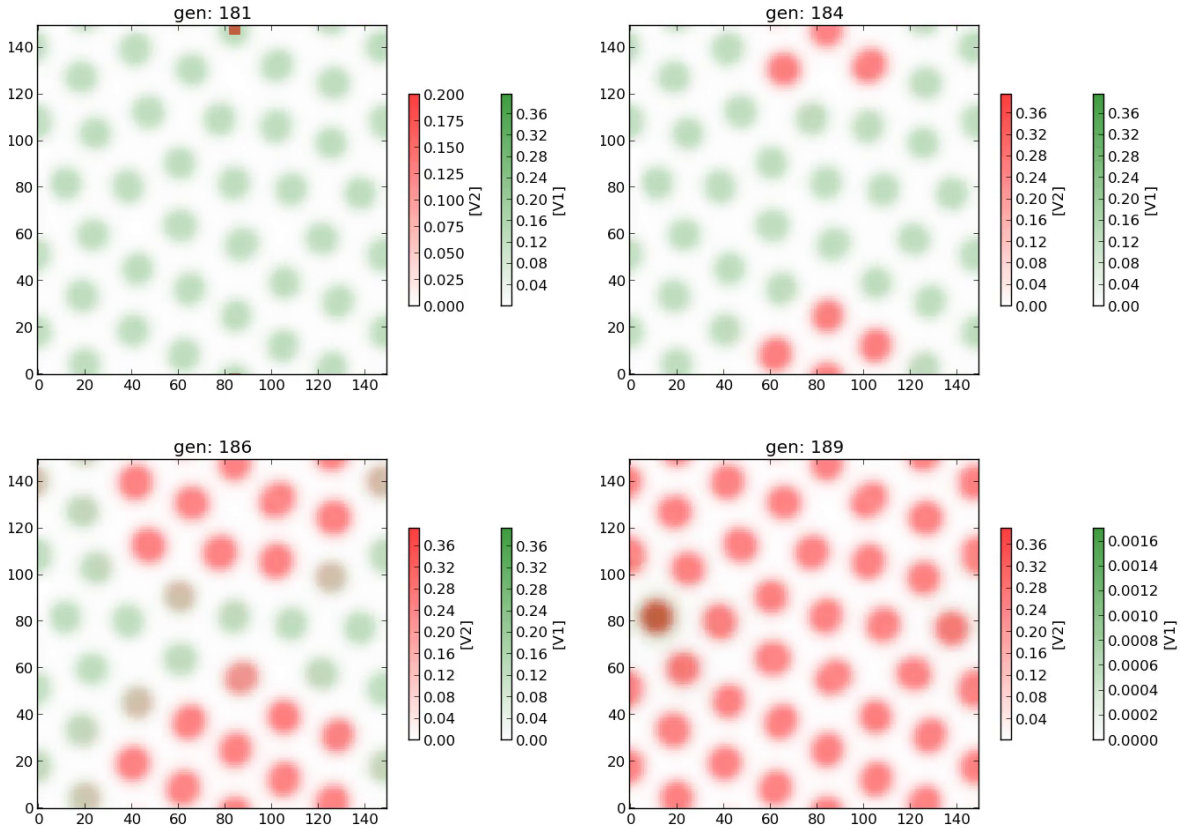


Figure 4.2: Frames from a simulation in the dividing spots regime (in order left-right, top-bottom), featuring a mutant replacing an existing species. Wild type (green) and mutant (red) concentrations are plotted. The mutant very quickly takes over after being introduced at generation 180. Its concentration peaks co-locate with the existing pattern but leads to their rapid degradation. The mutant has an advantageous degradation rate $\Delta k = -0.001$ and received catalytic support $r_2 = 1.8$, the initial drop has concentration $\mu = 0.2$ and Moore radius $d_\mu = 2$ and placed at $\max_{i,j}(v)$.

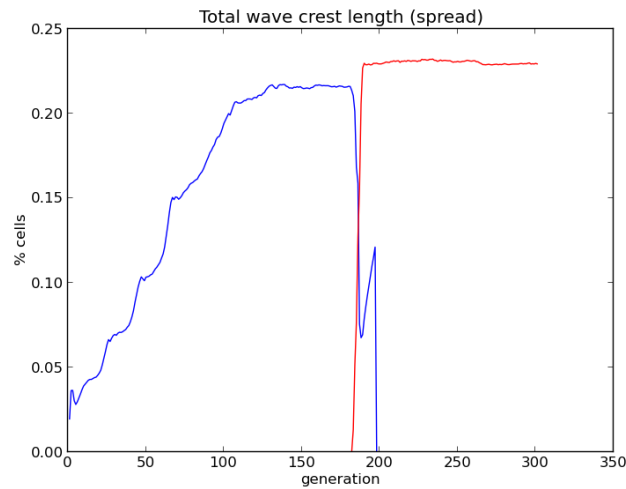


Figure 4.3: Spread of autocatalyst patterns of the wild type (blue) and mutant species (red) as cell percentages, measured with ρ . This shows the very fast species replacement after the mutation event at generation 180.

Given both the replicative and catalytic advantage, the mutant is able to quickly replace the wild type. This behaviour is the same for cases $\Delta k < 0$, $r_1 = r_2 = 1$, and the case $\Delta k = 0$, $r_1 < r_2$, the speed of replacement being dictated by the difference in parameters. Where the mutant perturbation is placed has little importance, as it very quickly co-locates with the existing patterns (“infects” them).

Simulation 2 In this simulation we tested a lower degradation rate but disadvantageous (lower) received catalytic support $r_2 = 0.5$, which implies a given support of $r_1 = 1.5$. Since the behaviour here is quite obvious, a spread plot is omitted.

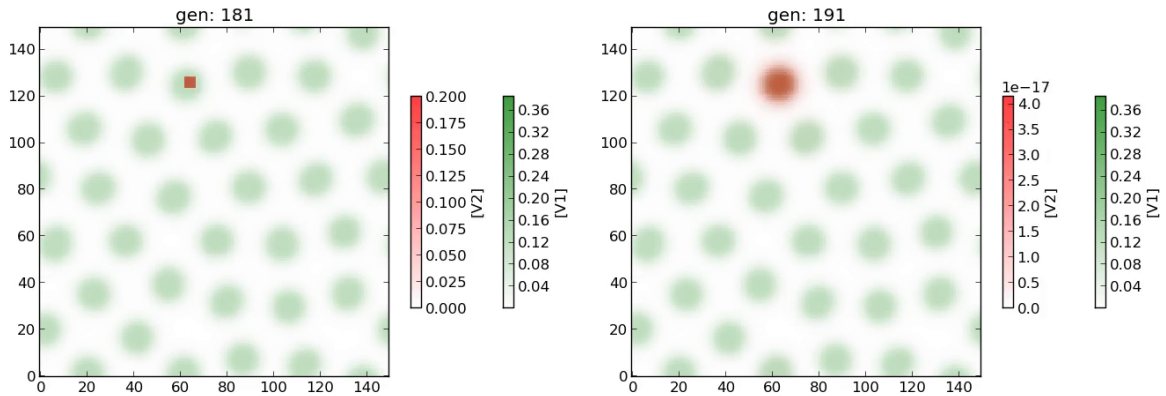


Figure 4.4: Two moments from a simulation in the dividing spots regime (in order left-right, top-bottom), featuring a mutant failing to spread. Wild type (green) and mutant (red) concentrations are plotted. While the mutant spot co-locates with the wild type’s, it is unable to spread farther and quickly degrades. The mutant has an advantageous degradation rate $\Delta k = -0.001$ but a disadvantageous received catalytic support $r_2 = 0.5$, the initial drop has concentration $\mu = 0.2$ and Moore radius $d_\mu = 2$ and placed at at generation 180, at a $max_{i,j}(v)$.

The same behaviour is obtained in the other cases of high mutant disadvantage, as can be seen in the mutation outcome diagram. The speed of mutant disappearance is influenced by the difference in parameter values.

Given that the model displays the behaviour of species replacement, we then proceeded to simulate multiple mutation events in succession, as investigation of an evolutionary process.

4.3 Evolution simulations

We considered systematic mutant placements, assuming only one other catalyst species present during placement. The simulations were stopped if both species disappeared from the system.

We wished to observe any tendency of the evolutionary process, so we performed long simulations in which we allow one species to form patterns in the entire available space, then introduce a mutant of small concentration $\mu = 0.2$ and Moore radius $r_\mu = 2$ and let sufficient time pass until only one species remains. Then the procedure is repeated until the limit time is reached.

We varied both degradation rate k and received catalytic support rate r , since it was fairly obvious that were only one to vary, the survivors would simply be those with the more advantageous value. We also allowed degradation rate values to fall outside the pattern-yielding range. Below is the algorithm of the simulations

Algorithm 4.1 Evolution Simulation 1

```

INITIALIZE()

repeat
    SIMULATION STEP( $k_{\text{wt}}, k_{\text{mut}}, r_{\text{wt}}, r_{\text{mut}}$ )

    if (another MTIME generations passed) then

        if ( $\sum v_{ij} \leq \epsilon$  and  $\sum m_{ij} \leq \epsilon$ ) then                                ▷ system “destroyed”
            STOP

        else if ( $\sum v_{ij} \leq \epsilon$  xor  $\sum m_{ij} \leq \epsilon$ ) then                            ▷ only one survivor
            RECORD(survivor)

             $k_{\text{mut}} \leftarrow k_{\text{wt}} + \Delta k \in \mathcal{N}(0, \sigma_{\Delta k}^2)$                     ▷ truncate if outside range

             $r_{\text{mut}} \leftarrow r_{\text{wt}} + \Delta r \in \mathcal{N}(0, \sigma_{\Delta r}^2)$ 

             $r_{\text{wt}} \leftarrow 2 - r_{\text{mut}}$                                             ▷ Constraint 1 imposed on wild type

            INTRODUCE MUTANT( $k_{\text{mut}}, r_{\text{mut}}$ , random position)

        end if
    end if
until ENDTIME

```

Algorithm notes:

1. The *survivor* is the species with non-null concentration, designated as “wild type”.
2. The simulation assumes at most one catalyst species survives, so the trivial equilibrium case was excluded.

The systems used in these simulations were

sim	D_u	F	L	N	Δt
1,2	$2 \cdot D_c$	0.04	0.01	150	0.05
3,4	$2 \cdot D_c$	0.04	0.01	300	0.01

Table 4.2: System parameters for evolution simulations of the interacting catalysts model. For the last two simulations, precision was increased as instabilities in the integration were suspected to occur.

And the catalyst parameter ranges were the ones in the following table.

sim	k	r	$\sigma_{\Delta k}$	$\sigma_{\Delta r}$	k_{wt}^0	F	ENDTIME
1	[0.06, 0.07]	[0.1, 1.9]	0.004	0.05	0.065	0.05	10^5 gen.
2	[0.06, 0.07]	[0.1, 1.9]	0.002	0.01	0.065	0.05	10^5 gen.
3	[0.055, 0.075]	[0.5, 1.5]	0.002	0.2	0.065	0.04	10^3 gen. (*)
4	[0.055, 0.07]	[0.8, 1.2]	0.002	0.025	0.0657	0.04	$3 \cdot 10^3$ gen. (*)

Table 4.3: Parameters of the system used in the above simulations. The rate r_{wt}^0 of the initial species was always 1. The standard deviations are the ones of the normal random process that generates mutant values. (*) The increased precision constrained the length of the simulation as the integration became much slower (generation size increased to $3 \cdot 10^5$ integration iterations from only 600 iterations).

The range and variance of r were set to both wide and narrow to see the impact of constraining one of the parameters. The fuel feed rate values were chosen to allow for a larger range of patterns. See the phase diagram in the original model for reference.

Below are the positions in parameter space of the survivors of these simulations

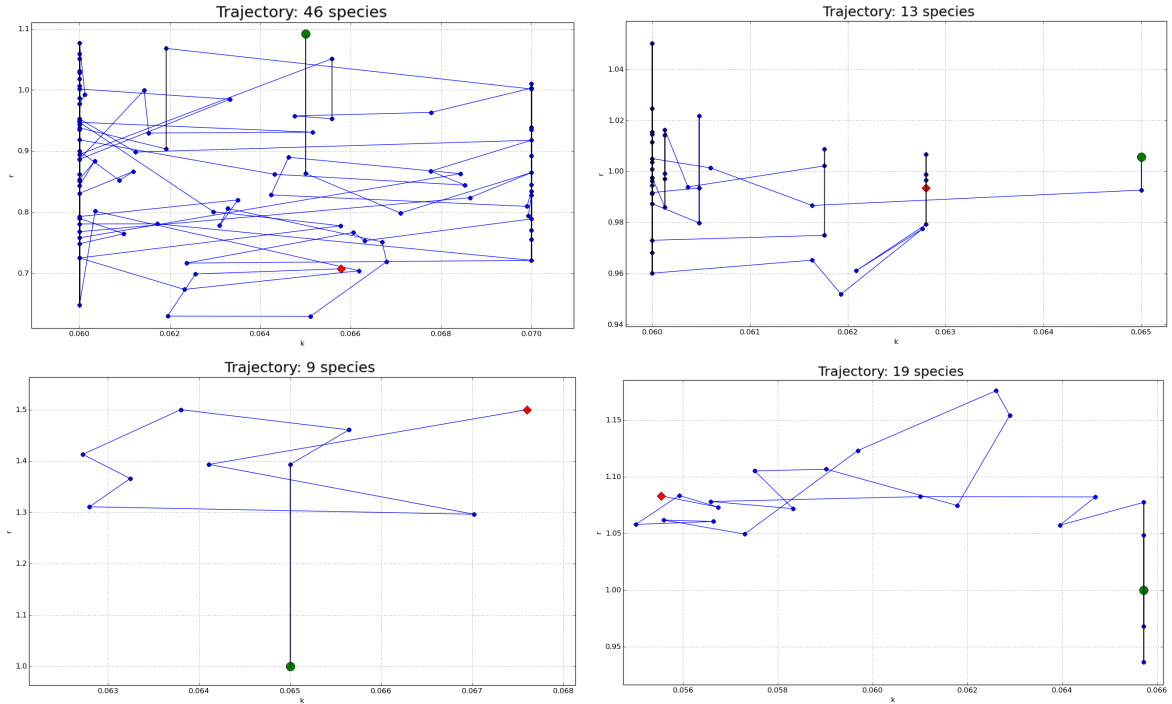


Figure 4.5: Trajectories in parameter space of surviving species in evolution simulations 1, 2 (top row) and 3, 4 (bottom row). The initial species is marked with a larger green dot while the last species is marked with a red diamond. Vertical lines (equal k) connect species that survived through successive mutation events but had their r parameter altered by imposing Constraint 1. The captions give the number of unique species. The large number of clustered points in the extreme left and right of the first two plots is due to parameter values k being truncated to the limits of the allowed range. One can see for simulation 4 how the survivors have a clear overall direction towards lowest k value (increasing label numbers to the left).

A common situation observed in these simulations is that a species would survive more than one mutation event but would have, due to Constraint 1, suffered change in its r parameter. As this rate is an extrinsic property defined in relation to the other catalyst, two species with the same degradation rate k and different received catalytic support rates r are considered identical.

From the above plots it is discernible that, given a narrow range and/or narrow variance of r (simulations 2, 4 - right column), the survivors are headed in the direction of minimal k , as evidenced by the clustering of the data series in that region. When r is given a large range and variance (simulations 1, 3), the survivor trajectories appear as random walks. Variance here has the higher impact, as the jumps in values become much larger for k .

Evolution example We reproduce here movie frames from evolution simulation 3.

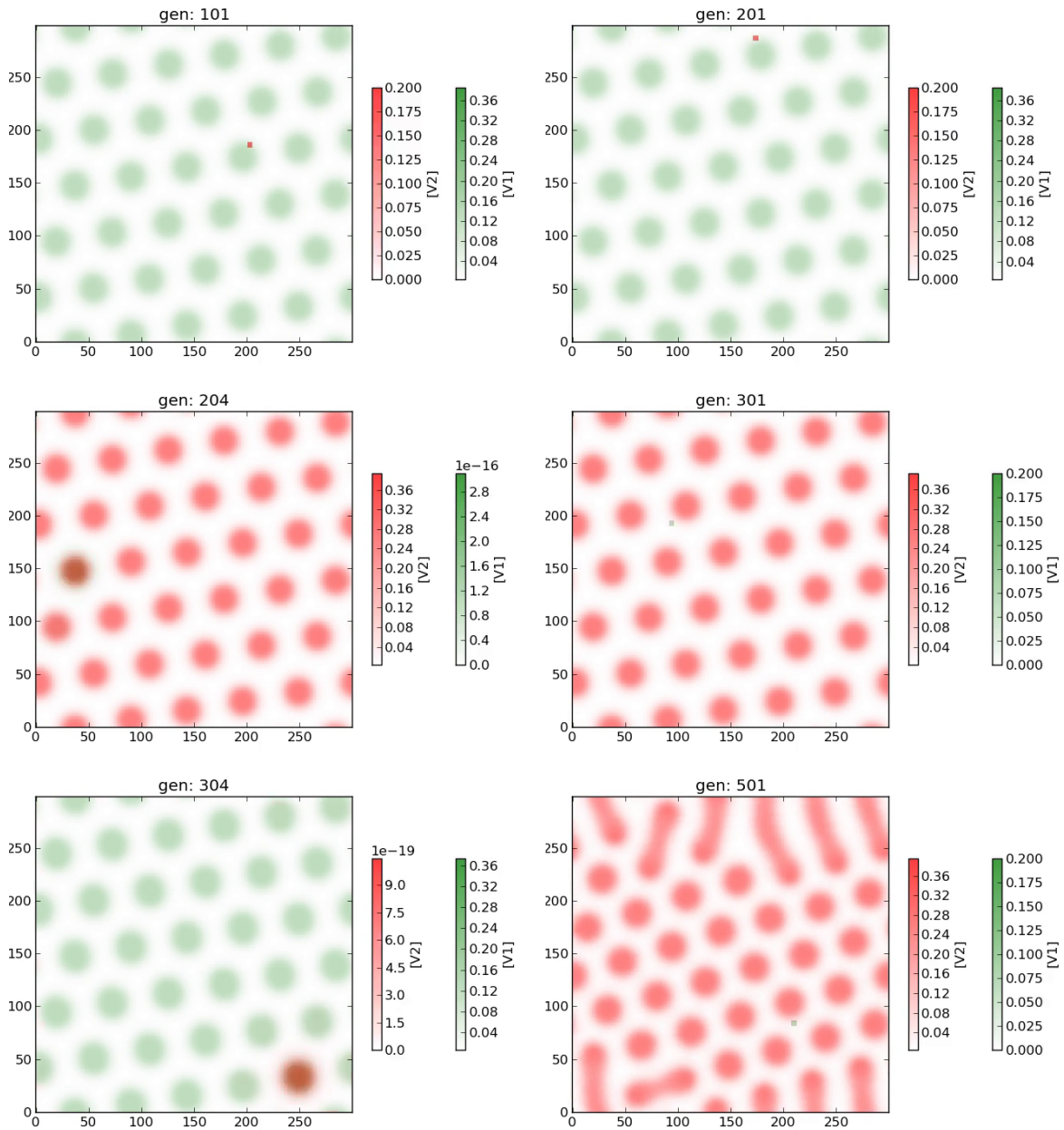


Figure 4.6: Movie frames from evolution simulation 3 (in order left-right, top-bottom). Colours alternate between designated wild type and mutant. A mutant was introduced every 100 generations, if only one species was present. The patterns mostly stayed in the spots regime. Key moments were reproduced here. At *gen. 101*: a mutation that fails; *gen. 201-204*: a mutant takes over; *gen. 301-304*: mutant takeover; *gen. 501*: a previous mutant took over and formed a different pattern, now another mutant is introduced. Subsequent mutations brought the system back into the spots regime.

4.4 Special cases

We consider here two cases where one of the received catalytic support rates r is effectively null. The simulations were done with the initial species in the dividing spots regime, as before. As reference for the placement of mutant concentrations, the radius of the Moore neighbourhood occupied by a spot was taken from the simulation frames as $d_{\text{spot}} = 8$.

Case 1: mutant at advantage

Setting $r_1 = 0$ yields an autocatalyst mutant that only receives catalytic support from the wild type but gives none itself. Perturbation values were taken from “reasonable” intervals of concentration $\mu \in \{0.1, \dots, 0.5\}$ and Moore radius $d_\mu \in \{1, \dots, d_{\text{spot}} = 8\}$. Generally, in this case a mutant will either disappear or destroy the system.

If the mutant has an *advantageous* (lower) degradation rate, it will spread and co-locate with the wild type (the spots overlap) and the two species subsequently disappear in tandem. This behaviour is actually that of the parasites studied in [CB97], which will be discussed further in the next, more general model. The placed concentration of mutant initially “infects” the closest clusters, leads to their complete joint degradation, then spreads to the next closest wild type clusters. The process is repeated until both species completely disappear from the system, an outcome which we call “system destruction” since it corresponds to a trivial steady state of $u = 1, v = m = 0$. What is remarkable in this behaviour is the timing of cluster destruction. Only after the closest, most infected (with highest mutant concentration) clusters completely disappear, do mutant levels increase in the surrounding clusters and start degrading themselves, and so on. Such an evolution is shown in the frames below.

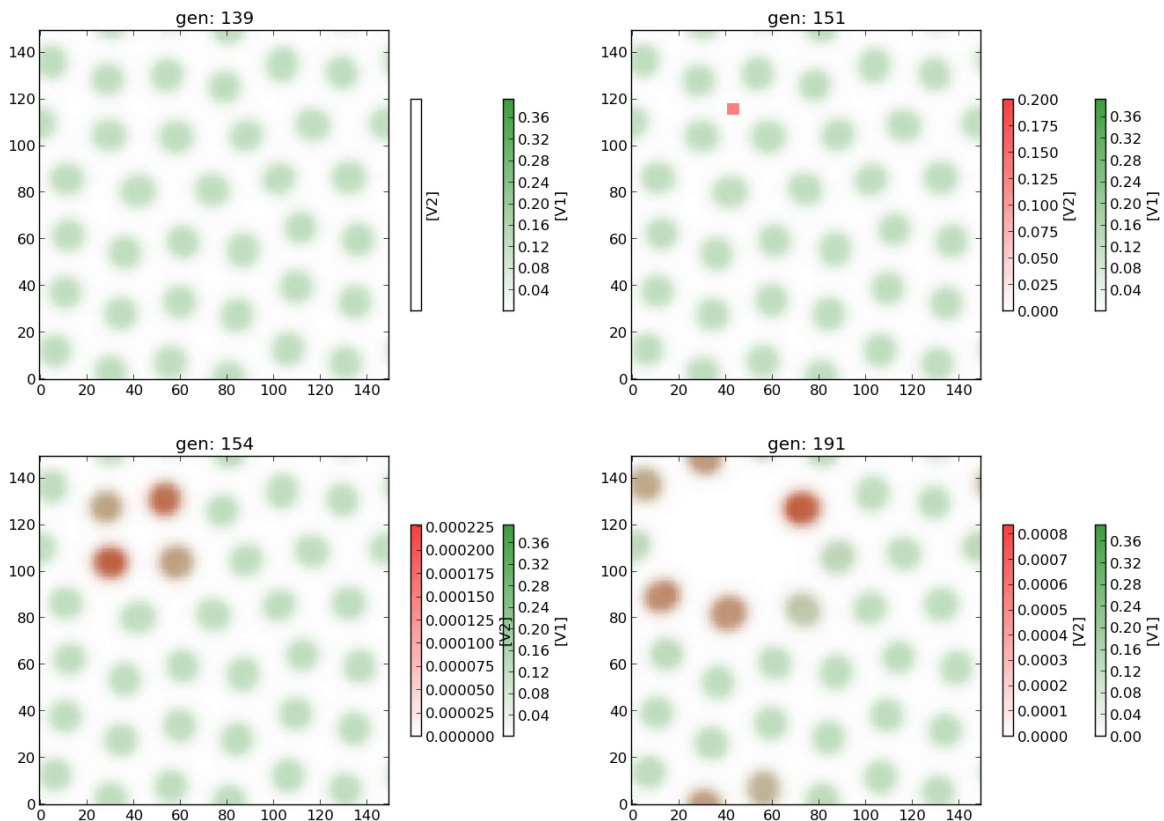


Figure 4.7: Frames of a simulation in which the mutant leads to system destruction. Wild type (green) and mutant (red) concentrations are plotted. At generation 139 the system is in steady state featuring wild type clusters. At generation 151 a mutant drop of concentration $\mu = 0.2$ and Moore radius of $d_\mu = 2$ is placed near coordinates (42, 118), a minimum of wild type concentration. At generation 154 the mutant has infected (co-locates with) the closest 4 clusters, starting their degradation. At generation 191 the initially infected clusters have disappeared and the closest 6 have had a sudden increase in co-located mutant. Very quickly the system is led to the complete degradation of both catalyst species.

However, rather extreme conditions were found in which a mutant with an advantageous degradation rate managed to replace the wild type and subsequently occupy the system by itself, though not really forming patterns. This was in a different regime, for a fuel feed rate $F = 0.008$ (≈ 0), $k_{wt} = 0.03$ and $k_{mut} = 0.029$ ($\approx k_{wt}$). Some frames of this simulation are below.

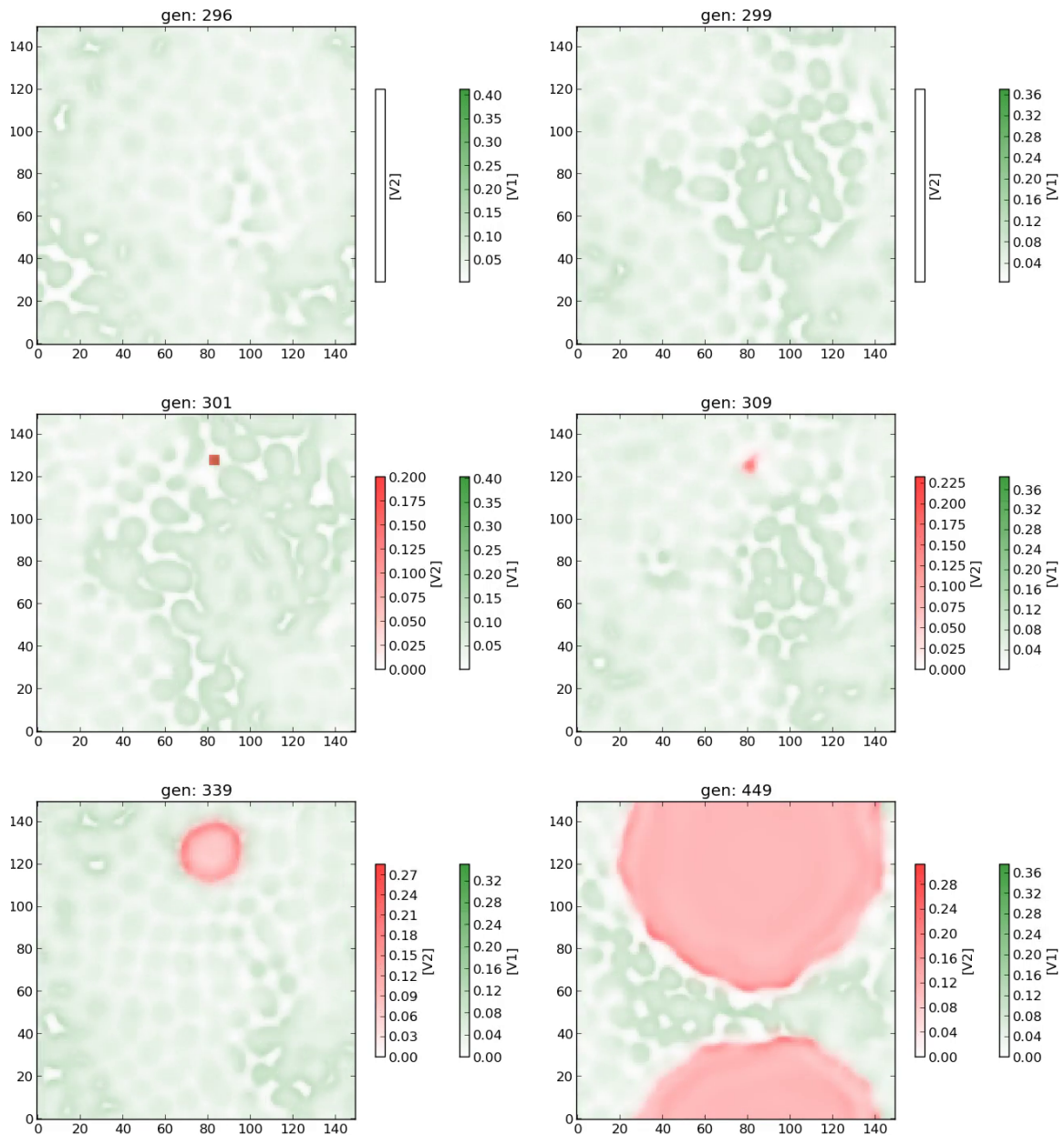


Figure 4.8: Frames of a simulation in which the mutant takes over. Wild type (green) and mutant (red) concentrations are plotted. By generation 299, the wild type spatial distribution arrived in a pattern orbit. At generation 301, A drop of $\mu = 0.2$ and $d_\mu = 2$ was placed at a maximum peak of wild type, near coordinates (85, 128). The region occupied solely by the mutant expands pushing away the wild type until it completely disappears from the system.

Case 2: mutant at disadvantage

The typical case for a parasitic mutant with a *disadvantageous* degradation rate is that it will spread and co-locate with (“infect”) the wild type spots but will eventually degrade and disappear. For such a mutant an interesting exception was found as well. Namely a mutant with $k_{\text{mut}} = k_{\text{wt}} + 0.0005 = 0.0655$ ($\approx k_{\text{wt}}$), high concentration and spread, placed in a steady state of wild type spots managed to form an independent spot (no co-location), which remained stable up until the simulation end. It is important to note that this behaviour was only found to be attainable by no longer applying Constraint 1 and setting $r_1 = 0$ and $r_2 = 1$.

The evolution of this simulation is presented in figure 4.9 below. In these frames, the independent mutant spot degrades the surrounding spots in much the same way as infection did in the other simulations. In the concentration cross-sections plotted at generations 169 and 196 it can be seen how the neighbouring peaks of mutant rise and interact with the wild type peaks, leading to their destruction and leaving space for newly divided clusters to fill, though the mutant is unable to divide. Thus a state of dynamic balance was achieved in which the two nearly identical catalysts both formed patterns independently and shared the available space. This event is however rare in more realistic evolutionary scenarios, due to larger parameter deviations, lower mutation concentrations and spread, and random mutant placement. And as we will show in the next section, this balance is unstable except for certain limit values, leading towards species replacement, given enough time.

Conversely, $r_2 = 0$ yields a mutant that only gives catalytic support to the wild type but receives none itself. This invariably leads to an inserted mutant not surviving, i.e. degrading out of the system, for placements of concentration $\mu \in \{0.1, \dots, 0.5\}$ and Moore radius $d_\mu \in \{1, \dots, d_{\text{spot}} = 8\}$. For this case, only mutants with $\Delta k = -0.002$ were inserted at a peak of wild type concentration.

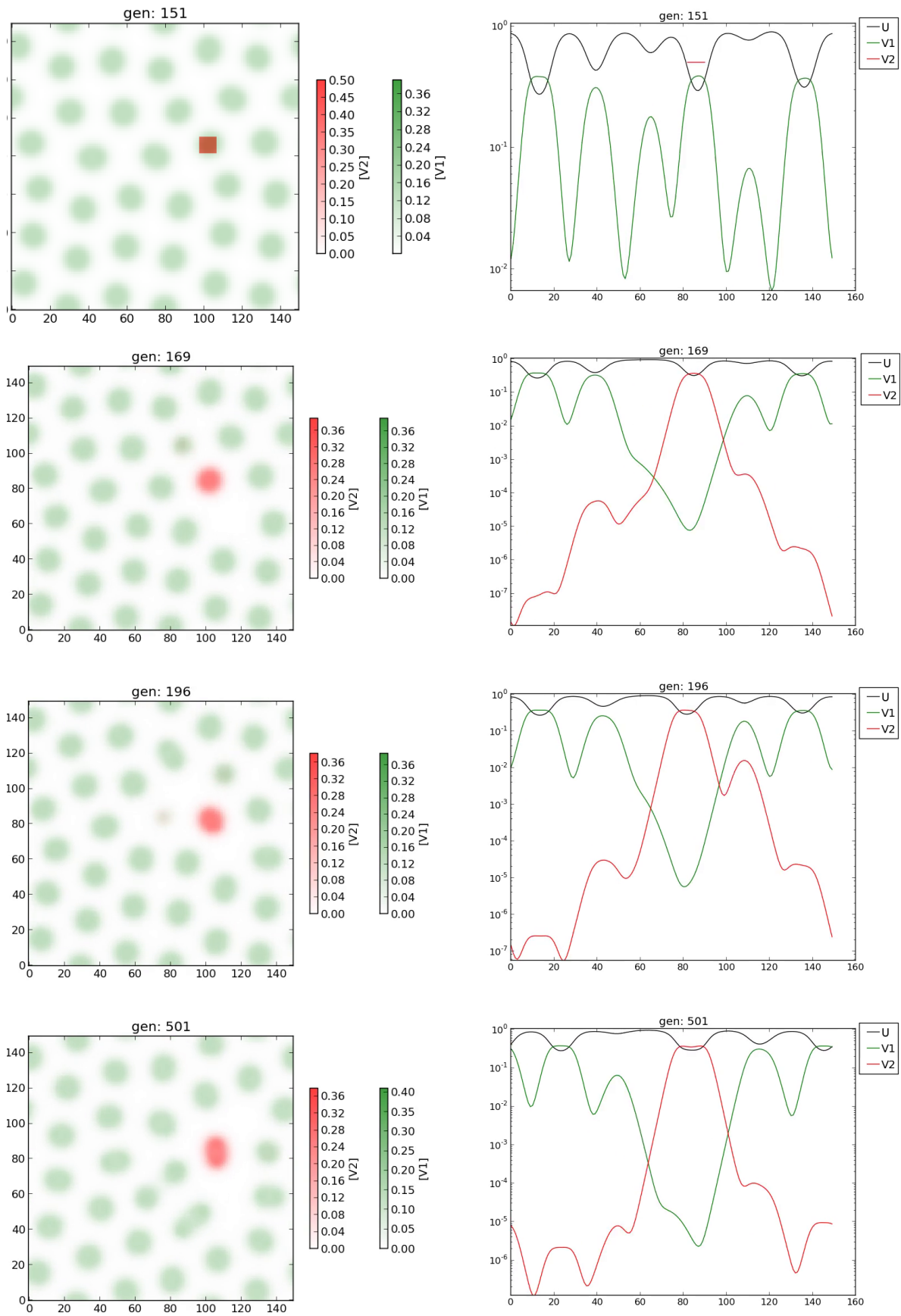


Figure 4.9: Simulation frames and 1-dimensional concentration plots. Wild type (green) and mutant (red) concentrations are plotted in the left column and the concentrations along the y axis for fixed $x = 105$ are plotted in the right, including fuel (black). At generation 151, after the wild type has reached steady state, a drop of mutant of high concentration $\mu = 0.5$ and radius $d_\mu = 4$ is placed at a maximum of wild type concentration, which it very quickly degrades and takes its place. It then slowly starts degrading neighbouring spots which are replaced as farther ones divide in the gaps. However, the mutant spot does not divide itself but only shifts position, though it tries to divide at e.g. generation 501. This behaviour repeats with no sign of change until simulation end.

4.5 The aggregate pattern case

We return to the special case in the previous section, where the mutant had formed an independent (non-colocating) spot and perform a series of experiments to investigate the behaviour of such aggregate structures. In particular, we wish to investigate the conditions in which such aggregate patterns might appear and how sensitive these are under perturbation and evolutionary scenarios (i.e. catalyst parameter change). We note again that this special case is in violation of Constraint 1. This may be justified by some silent braking of reaction rate r_1 , but we do not pursue such things here, given the abstraction of the model.

The asymmetry of the species interaction, specifically the degradation only seen in the wild type (of lower k), is due to the parasitic nature of the mutant. A value of $k_{\text{mut}} \leq 0$ leads to faster mutant takeover (without infection).

After a preliminary exploration, it became apparent that the parameter ranges that permit this behaviour are very narrow, with $r_1 \approx 1$ and $r_2 \in [0, 0.18)$. Outside of these, the interacting falls in the previously described cases (parasitic infection and at most single species survival). Furthermore, the aggregate is truly stable, with no w.t. degradation, only if the mutant is in the non-dividing spots regime, and occurs only for a small range of difference in species degradation rate (see below). The placing of the mutant also needs to be at a maximum of wild type concentration for it to have a good chance of taking hold.

Why the aggregate illustrated in the previous section is not truly stable becomes clear in very long simulations. In fact, the system remains in a metastable state characterized, as shown before, by successive destruction and division of wild type spots, which continuously prevent the mutant from dividing. However, given sufficient time, the introduced spot is able to divide once, after which the subsequent divisions will occur at decreasing time intervals, at an almost exponential pace, until finally the original species is forced out of the system. As such, in this case the initial single mutant spot is sufficient for takeover.

Below is a typical plot of the quantitative evolution of the two species in a much longer simulation with the same parameters as the one in Case 2 of the previous section, namely with $F = 0.04$, $k_{\text{mut}} = k_{\text{wt}} + 0.0005 = 0.0655$, $r_1 = 0$ and $r_2 = 1$, with a generation equal to 600 integration iterations. As usual, only the initial conditions feature randomisation, having no essential difference between runs.

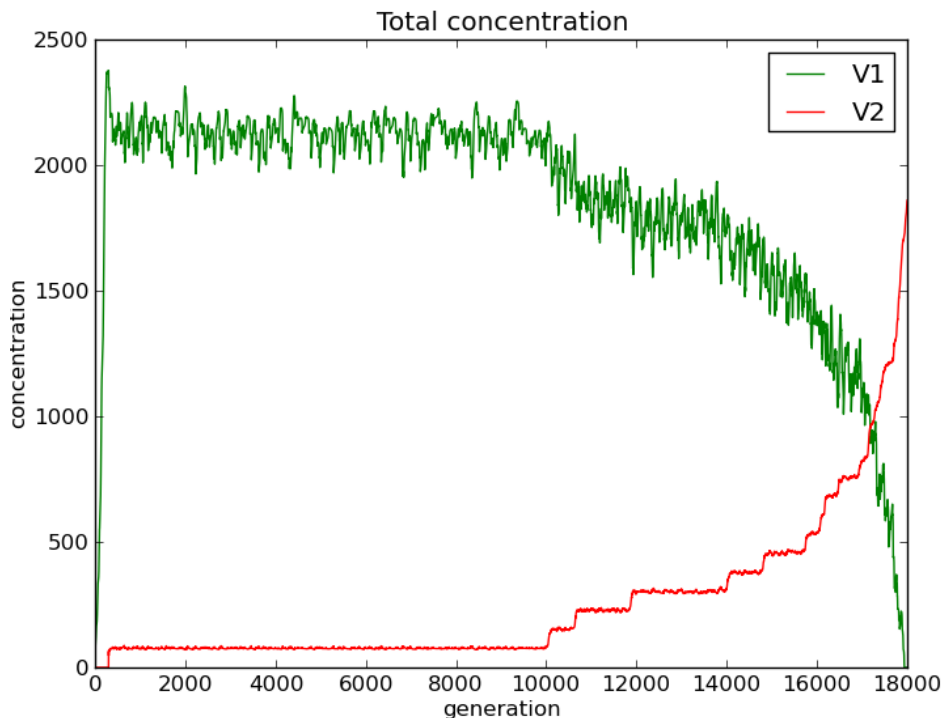


Figure 4.10: Total wild type (green) and mutant (red) concentrations. The mutant has been placed at generation 300 with a concentration $\mu = 0.5$ and radius $d_\mu = 4$ on a maximum peak of w.t. The large oscillations in w.t. level are due to the continuous spot destruction and division. The very long plateau in total mutant concentration is the metastable state, where no division occurs. Afterwards, each step in the mutant curve represents one spot division.

To better observe the interaction between species and to see how changes in conditions might affect the metastable state, we perturb the prevailing wild type population, by clearing an area around the mutant spot (w.t. concentration set to zero) when the state is reached to see how this spot behaves given enough space. Below is a plot of a typical such simulation, having all parameters as in the previous ones. As might be expected, the spot divides much sooner given the favourable open space (devoid of competing wild type).

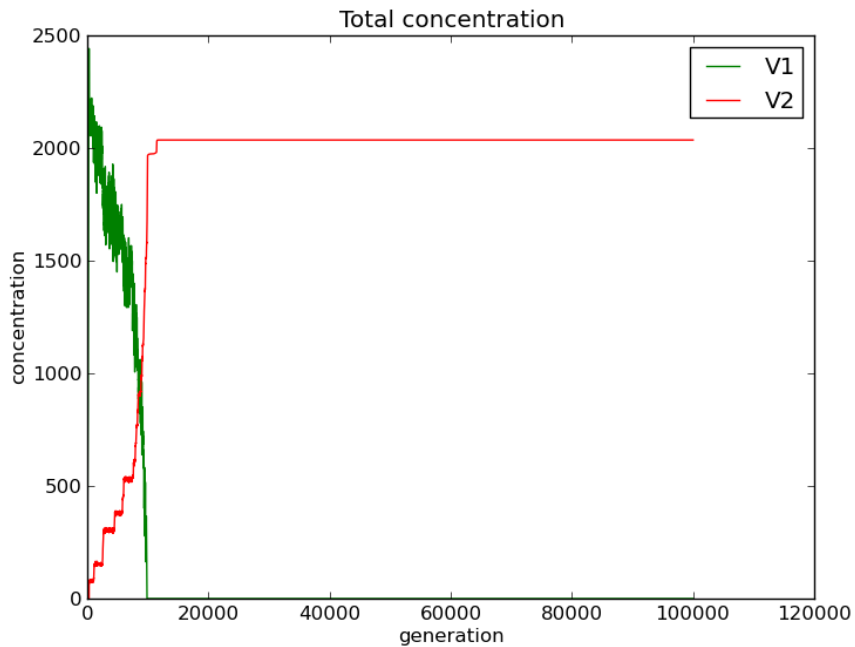


Figure 4.11: Total wild type (green) and mutant (red) concentrations. The mutant has been placed at generation 300 with a concentration $\mu = 0.5$ and radius $d_\mu = 4$ on a maximum peak of w.t. An area of Moore radius 20 centred on the mutant spot has been cleared of w.t. at generation 500. The free space permits this spot to divide much sooner, significantly shortening the metastable state and, consequently, the entire mutant growth period (to half of that in the previous simulation, ending just after gen. 10^5).

To see how the metastable aggregate pattern responds to stochastic perturbations we run simulations with high Gaussian noise ($\bar{\lambda} = 1$), even though such intrinsic noise levels would not be chemically realistic. This shortens the metastable state duration considerably. The fluctuations slow down wild type division, giving the mutant a higher chance of multiplying since empty, fuel-rich space is not occupied so quickly by the w.t. Below is the concentration plot of a typical such simulation. It must be noted that if the noise is too high patterns are broken down and the introduction of the mutant leads to the immediate disappearance of both species.

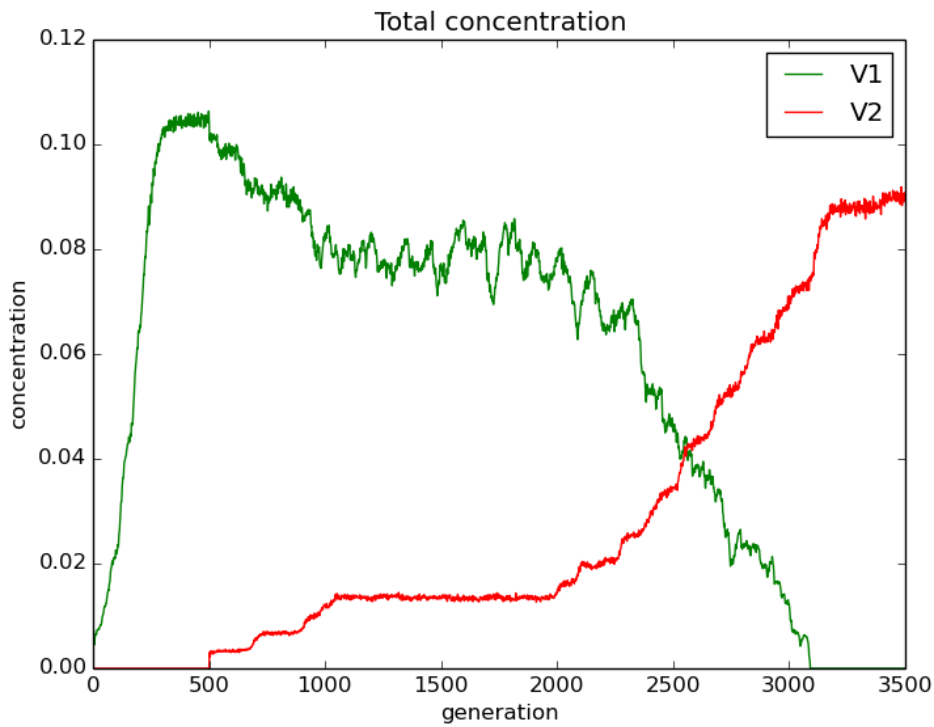


Figure 4.12: Total wild type (green) and mutant (red) concentrations in a noisy simulation. The mutant has been placed at generation 500 with a concentration $\mu = 0.5$ and radius $d_\mu = 4$ on a maximum peak of w.t. The noise is Gaussian, with a level $\bar{\lambda} = 1.0$. Complete mutant takeover takes place much quicker, under 5000 generations, due to the stochastic perturbation of w.t. division.

As mentioned before, a necessary condition for stable aggregate pattern formation is that the mutant be in the stable (non-dividing) spots regime, given by k roughly in $[0.067, 0.07]$ for $F = 0.04$. Since these clusters do not divide and spread (no increase of its concentration surrounding the initial cluster), there is no destructive interference with wild type clusters. The steady state of such a combination looks as below and is completely frozen, up to translation (given the torus topology of the system).

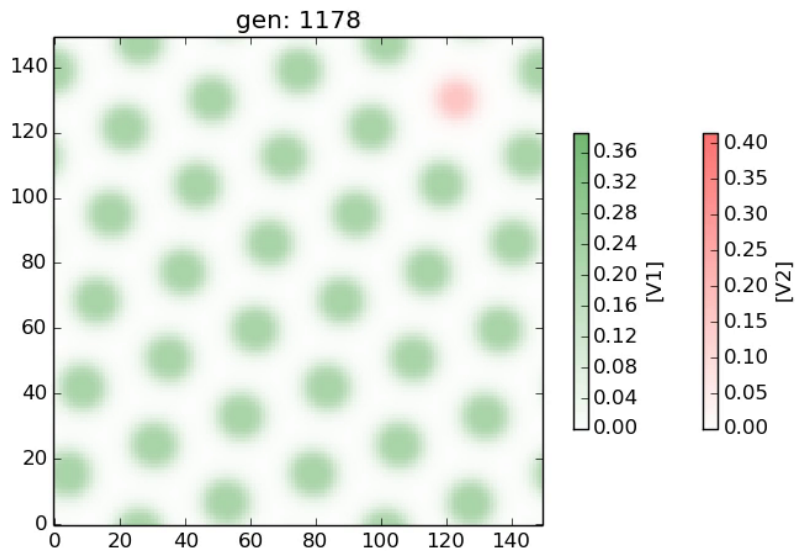


Figure 4.13: The steady state of the aggregate pattern composed of dividing spots (green), of $k_{wt} = 0.065$ and a non-dividing mutant spot (red), of $k_{mut} = 0.067$. The mutant had been introduced at generation 300 at the peak of a wild type spot, which it destroyed and replaced. No subsequent destruction of the original spots occurred and the system settled at about generation 700, when all wild type spots had achieved equilibrium relative positions.

Such a steady state is resistant to noise. This was tested on a steady state of a system with the same parameters as the above illustration. At generation 1000, the system was subjected to very high (effectively external) Gaussian noise $\bar{\lambda} = 10.0$ for a duration of 10 generations. This can be seen in the first frame below, where the spots are fuzzy due to concentration oscillations. When the noise is stopped, wild type spots shrink and disappear, to be replaced by dividing neighbours in a span of about 100 generations.

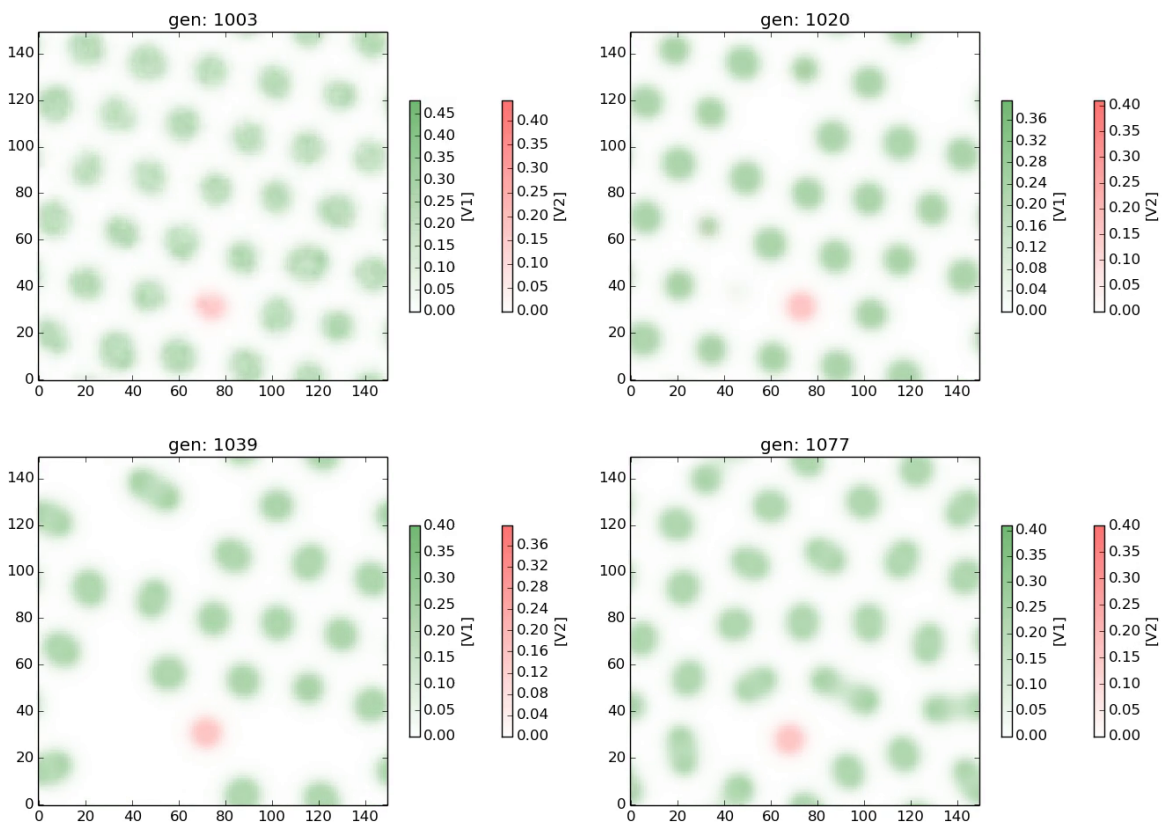


Figure 4.14: Simulation frames showing the noise perturbation of the aggregate pattern steady state. The top-left frame shows the system under high noise, with distorted (fuzzy) patterns, which takes place between generations 1000-1010. The following two frames (top-right, bottom-left) show the disappearance of wild type spots, followed by their replacement due to the division of remaining spots, almost complete before generation 1080 (bottom-right frame).

Another limiting condition in the formation of aggregates is the difference in the degradation rates of the two species involved, which cannot be too large, otherwise the mutant exhibits infection of w.t. spots and subsequently degrades out of the system, as seen in the general case. This maximum difference varies with the catalytic support r_1 given by the mutant, as shown in the plot below. For a fixed r_1 , the maximum differences (found by approximation) did not essentially vary with the starting k_{wt} . Note that this difference does not depend upon one of the species being in the non-dividing regime (and consequently, that the aggregate being stable). Still, for this sweep a starting wild type close to it was chosen.

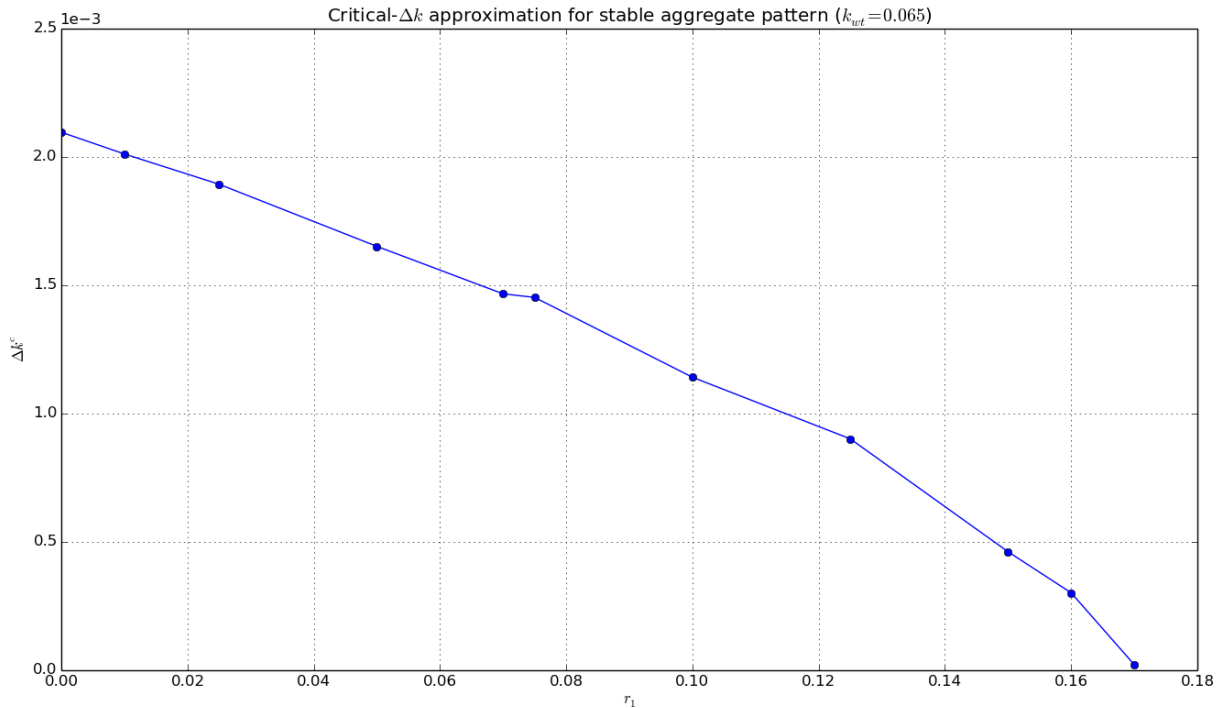


Figure 4.15: Curve showing approximate values of the maximum difference in degradation rates Δk^c which permits aggregate behaviour, as a function of r_1 , for a starting $k_{wt} = 0.065$. This quickly shrinks to null for $r_1 > 0.12$. The values were found by running multiple simulations for each r_1 to probe the critical Δk value by interval halving until 2-digit approximations were obtained.

To conclude this special case investigation, we can say that stable aggregates may be formed with catalytically parasitic mutants within the non-dividing spots regime, which are introduced into a wild type population of lower, but necessarily close, degradation rate. These non-dividing species must appear second otherwise only replacement takes place, because dividing (expanding) patterns are subjected to less competition from the non-dividing ones.

As may be observed, this special case allows for an increase in k in a multiple mutation events scenario. So evolutionarily speaking, this is in opposition to the tendency described elsewhere for the surviving species to have diminishing degradation rates. However, as shown in the proof sketch below, the direction of change with highest probability is always towards decreasing k values.

Claim. *Evolutionarily, the degradation rate k tends to lower values within the aggregate case.*

Proof sketch. Assume the evolution scenario \mathcal{E}_{aggr} defined as:

1. without Constraint 1
2. fixed $r_2 = 1$
3. jumps in degradation rate Δk drawn from $\mathcal{N}(0, \sigma_{\Delta k})$
4. new parasites use old ones: previous parasite offers $r_2 = 1$ support to new mutant
5. evolution is a stationary stochastic process

So then what are the probabilities of left $P(\leftarrow)$ and right jumps $P(\rightarrow)$, respectively?

Let i denote the current species, j the introduced, and s the survivor (successor) species.

Assume without loss of generality the simplifying assumption

$$\sigma_{\Delta k} = \frac{\Delta k^c}{3} \quad (\text{A1})$$

This ratio gives the interval $[k_i - \Delta k^c, k_i + \Delta k^c]$ (centred at k_i), which holds 99.7% of values drawn from the jumps distribution, i.e. the newly generated species. We divide this interval in three portions corresponding to outcome cases in the evolutionary process. As evidenced by the vast majority of simulations, the survivor s of a mutation process is:

$$s = \begin{cases} i & \text{if } k_i < k_j \text{ and } k_j - k_i > \Delta k^c \quad (1) \\ j & \text{if } k_i < k_j \text{ and } k_j - k_i < \Delta k^c \quad (2) \\ j & \text{if } k_j < k_i \quad (3) \end{cases}$$

To be clearer, the current species i survives mutation for $k_i + \Delta k^c < k_j$ (case 1), and is replaced by the mutant for $k_j \in (k_i, k_i + \Delta k^c)$ (case 2) or $k_j \in [k_{min}, k_i)$ (case 3), where $k_{min} < k_i - \Delta k^c$. Observe that we do not consider stable aggregates with $k_j - k_i \approx \Delta k^c$, since this stops the evolution process. Note that the probability of generated values to fall in the subinterval (3) is equal to that of the reunion of (1) and (2) and equal to 0.5 (probabilities of negative or positive jumps, respectively).

So we have the probabilities of each case as:

$$\begin{aligned} P((1)) &= \frac{1}{2} \cdot \frac{0.3}{100} = 0.0015 && \equiv P(\bullet) \quad (\text{no change}) \\ P((2)) &= \frac{1}{2} \cdot \frac{99.7}{100} = 0.4985 && \equiv P(\rightarrow) \\ P((3)) &= 0.5 && \equiv P(\leftarrow) \end{aligned}$$

One can easily see that even with variation of divisions (1) and (2) (lower k species always replace, so (3) is fixed), jumps to lower values are always of probability 0.5 and the probability that the current species surviving (no change in k) is never null (this would only happen for $k_j = k_i = k_{max}^a$, the highest admissible value for non-dividing spots and patterns in general, but this implies $\Delta k^c = 0 \Rightarrow k_j - k_i = 0 = \Delta k^c$, which was excluded above). This also justifies the simplifying assumption (A1) used here. So then we have:

$$P(\leftarrow) > P(\rightarrow), \quad \forall k_i \in [k_{min}^a, k_{max}^a] \quad (4.4)$$

where $[k_{min}^a, k_{max}^a]$ is the allowed range for aggregate patterns. Let n designate the number of the current species and have the evolution process stop at both ends of this range. Then the above implies

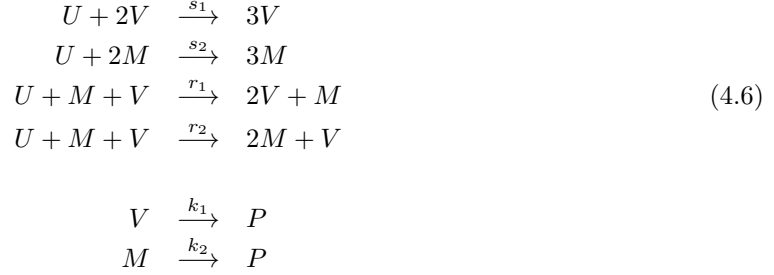
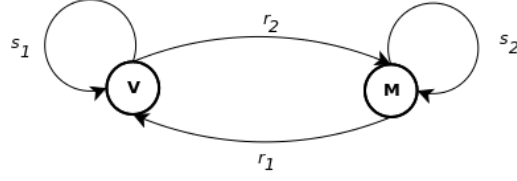
$$\lim_{n \rightarrow \infty} k_n = k_{min}^a \quad (4.5)$$

□

Thus we have a consistent direction of the evolution of species described by this model.

4.6 Slight extension: full parametrisation

We now allow for the catalyst self-replication rates to take arbitrary values and also adapt Constraint 1 accordingly. This more general reaction scheme looks like



with the corresponding differential equations:

$$\begin{aligned}
 \frac{\partial u}{\partial t} &= -u(s_1 v^2 + s_2 m^2 + (r_1 + r_2)vm) + F(1 - u) + D_u \nabla^2 u \\
 \frac{\partial v}{\partial t} &= u(s_1 v^2 + r_1 vm) - (F + k_1)v + D_c \nabla^2 v \\
 \frac{\partial m}{\partial t} &= u(s_2 m^2 + r_2 vm) - (F + k_2)m + D_c \nabla^2 m
 \end{aligned} \tag{4.7}$$

While the self-replication rates s_1, s_2 are unconstrained, the mutual reaction rates r_1, r_2 depend on the interaction between species, as in the previous scheme. Such as with Constraint 1, we seek to capture the reaction of fuel and joint catalyst quantities. Hence, we equate the first reaction rate with a quadratic form (obeying non-negativity of rates):

$$s_1 v^2 + s_2 m^2 + (r_1 + r_2)vm = (\sqrt{s_1}v + \sqrt{s_2}m)^2 \tag{4.8}$$

and derive

Constraint 2:

$$r_1 + r_2 = 2\sqrt{s_1 s_2} \tag{4.9}$$

We can easily see how this reduces to Constraint 1 for $s_1 = s_2 = 1$.

As a matter of range, given reaction rates $r_1, r_2 \geq 0$, then $r_1 = 2\sqrt{s_1 s_2} - r_2 \geq 0$, which means $r_2 \leq 2\sqrt{s_1 s_2}$ and symmetrically $r_1 \leq 2\sqrt{s_1 s_2}$.

We would also like to see the impact of change in catalyst self-replication rates on the overall rate of reactions. Of interest is the fuel feed term, since this reflects the variation in fuel use which occurs upon mutation. We therefore set $\tau \equiv ts_1$ and rescale the system with respect to time and get:

$$\begin{aligned}
 \frac{\partial u}{\partial \tau} &= -uv^2 - \frac{s_2}{s_1}um^2 - \frac{r_1 + r_2}{s_1}uvm + \frac{F}{s_1}(1 - u) + \frac{D_u}{s_1}\nabla^2 u \\
 \frac{\partial v}{\partial \tau} &= uv^2 + \frac{r_1}{s_1}uvm - \frac{F + k_1}{s_1}v + \frac{D_c}{s_1}\nabla^2 v \\
 \frac{\partial m}{\partial \tau} &= \frac{s_2}{s_1}um^2 + \frac{r_2}{s_1}uvm - \frac{F + k_2}{s_1}m + \frac{D_c}{s_1}\nabla^2 m
 \end{aligned} \tag{4.10}$$

We do not rename parameters as the reduction in their number is not the aim and this formulation is more suggestive. Here we chose to rescale time with respect to species S but the system is perfectly symmetrical. We use this form of the PDEs in the evolution simulations, along with Constraint 2.

4.7 Mutation outcomes

We wish to see for different parameter values which of the two species remains in the system after the introduction of a mutant. We perform a sweep over combinations of these values. For these simulations, a system with periodic boundary conditions and the following parameters was used:

D_u	F	L	N	Δt	ENDTIME
$2 \cdot D_c$	0.04	0.01	150	0.05	1000 gen.

Table 4.4: System parameters for single mutation outcome sweep. 1000 generations was deemed sufficient to allow for the disappearance of at least one species. One generation here equals 1200 integration iterations.

The original (wild type) catalyst was always the same, in the dividing spots regime: $k_{wt} = 0.065$, $s_1 = 1$, with diffusion coefficient $D_c = 1.4 \cdot 10^{-9}$ for both species. The initial catalyst concentration was slightly randomised using Gaussian noise, as in the previous model simulations. The mutant perturbation introduced was always of concentration $\mu = 0.2$ and Moore radius $r_\mu = 2$. For each combination of parameters, the mutant was introduced at a point of maximum concentration, after the original catalyst formed patterns across the entire available space. Then the simulation was left to run for sufficiently long and the final outcome was recorded. A single simulation run (i.e. using a single random seed) was performed for each parameter combination since it was seen that the outcome was not sensitive to randomisation of initial conditions, as was the case in the non-interacting catalysts model, where an outcome likelihood (frequency) plot was produced. Below is the diagram of the outcomes in parameter space.

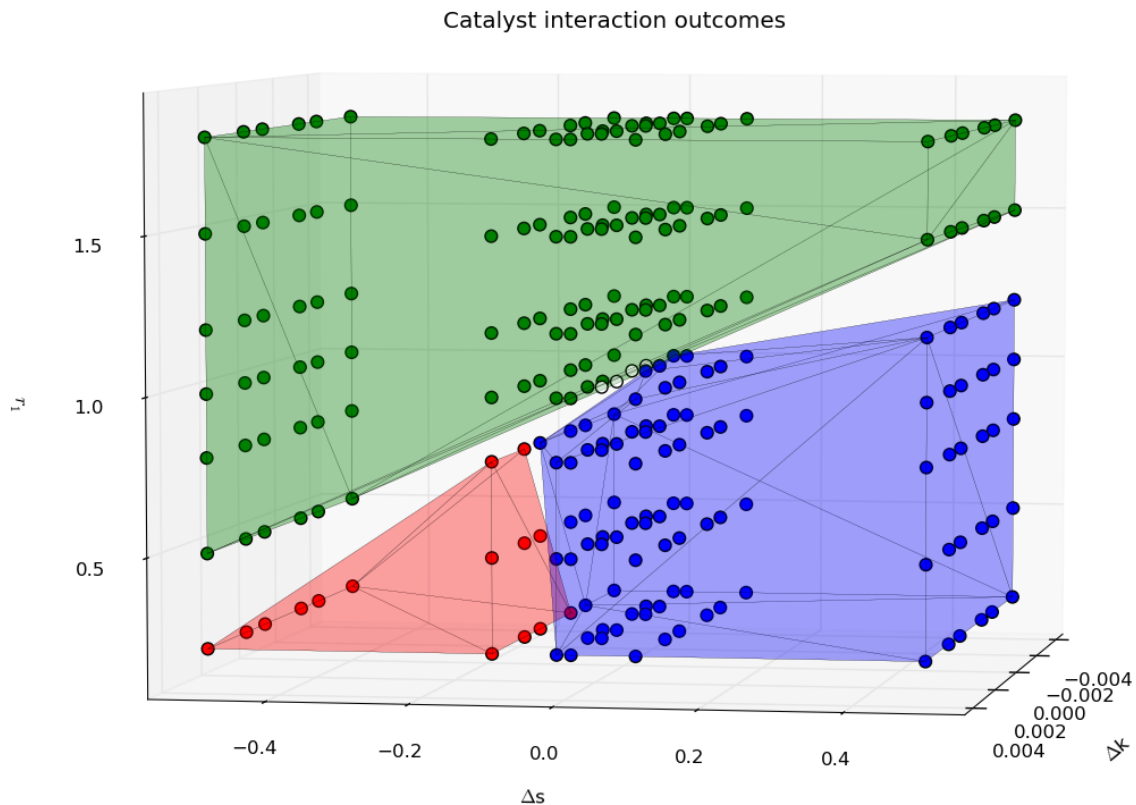


Figure 4.16: Scatter plot in parameter space of single mutation outcomes (dots), classified by the surviving species. The colours represent as follows, *green*: wild type survived; *blue*: mutant survived; *white*: quasi-equilibrium cases, where both species remained in the system up to the allotted time; *red*: both species disappeared. Except for the quasi-equilibrium cases at the centre, the subvolumes of this space containing the cases have been outlined with the semi-transparent envelopes featuring the appropriate colours. Δk is the change in mutant degradation rate with respect to the wild type, i.e. $k_{mut} = k_{wt} + \Delta k$. Similarly, Δs is the change in self-replication rate. Rates r_1 and r_2 , which correspond to wild type and mutant, respectively, are set at the beginning of each simulation and obey Constraint 2, therefore only r_1 is needed for the plot.

The above volume of parameter space is divided into regions for which one species survives the mutation event. Namely, a mutant has an advantage on the wild type in terms of reaction dynamics if it falls either in $\Delta k < 0$ (lower degradation rate), $\Delta s > 0$ (higher replication rate), or $r_1 < 1$ (offers less catalytic help to the wild type and, due to Constraint 2, receives more itself). As can be seen from the above scatter plot, quite predictably, there is a balance of outcomes between these parameters, with the subvolumes corresponding to an all-advantageous mutant being populated with replacement events and conversely, for advantageous wild types, with survival events.

However, there is also a subvolume comprised of cases where both catalysts disappeared, in the region of low r_1 - high r_2 , $\Delta s < 0$, and $\Delta k > 0$, in other words, for parasitic mutants that get more catalytic help but offer little and which also degrade quicker, thanks to low replication rate and higher k . When such a mutant is introduced into the system, the concentration peaks co-locate with the wild type and both disappear, leading to the destruction of the system.

This is the behaviour of the parasites in the paper by Cronhjort and Blomberg [CB97], and is the same as the special case illustrated in Figure 4.7 for the previous model. In fact, the single component plus parasite model that the authors used in their simulations is a special case of the one here, obtained by setting $r_1 = 0$ and $s_2 = 0$ (and to be rigorous, $k_1 = k_2$), as the model in the paper does not feature parasite autocatalysis. However, $r_1 = 0$ is sufficient to achieve the same behaviour.

The behaviour exhibited by this model is richer since it comprises the ones observed in previous models, but does not add any novel phenomena, so animation frames for various mutation outcomes were omitted. The replacement scenario allows for an equilibrium outcome, as evidenced by the species with only minute differences near the centre of the above volume. However, these states were seen to be transient in other simulations. Given enough time, they will resolve to a single survivor replacement case. As mentioned before, an interesting phenomenon in the competition between species is that space is an important resource. Even if the introduced mutant is identical with the existing wild type, if its pattern does not initially spread over enough (free) space it will disappear.

4.8 Evolution simulations

Our aim here, as before, is to observe the trajectory of surviving species in parameter space in order to identify any tendencies of the evolutionary process. We have performed a number of simulations using the algorithm described below, using different parameter ranges. Here we include the results of these simulations.

Algorithm 4.2 Evolution Simulation 2

```

INITIALIZE()

repeat

    SIMULATION STEP( $k_{wt}, k_{mut}, s_{wt}, s_{mut}, r_{wt}, r_{mut}$ )

    if (another MTIME generations passed) then

        if ( $\sum v_{ij} \leq \epsilon$  and  $\sum m_{ij} \leq \epsilon$ ) then ▷ system “destroyed”
            STOP

        else if ( $\sum v_{ij} \leq \epsilon$  xor  $\sum m_{ij} \leq \epsilon$ ) then ▷ only one survivor

            RECORD(survivor)

             $k_{mut} \leftarrow k_{wt} + \Delta k \in \mathcal{N}(0, \sigma_{\Delta k}^2)$ 

             $s_{mut} \leftarrow s_{wt} + \Delta r \in \mathcal{N}(0, \sigma_{\Delta s}^2)$ 

             $r_{mut} \leftarrow r_{wt} + \Delta r \in \mathcal{N}(0, \sigma_{\Delta r}^2)$ 

             $r_{wt} \leftarrow 2\sqrt{s_1 s_2} - r_{mut}$  ▷ Constraint 2 imposed on wild type

            INTRODUCE MUTANT( $k_{mut}, s_{mut}, r_{mut}$ , random position)

        end if
    end if

until ENDTIME

```

As before, the most plausible scenario of mutation was considered that of normally distributed deviation of small variance from the existing species' attributes.

For these simulations, a system with the following parameters were used

D_c	D_u	F	$\sigma_{\Delta k}$	$\sigma_{\Delta s}$	$\sigma_{\Delta r}$	μ	r_μ	L	N	Δt
$1.4 \cdot 10^{-9}$	$2 \cdot D_c$	0.04	0.01	0.005	0.005	0.2	2	0.01	150	0.05

Table 4.5: Parameters of the system used in the above simulations. The starting parameter values were $s = r = 1$ and $k = 0.065$. The standard deviations are the ones of the normal random process that generates mutant values and μ, r_μ are the mutant concentration and Moore radius of the introduced quantity, respectively.

The first three simulations were set with wide value ranges in order to see any strong tendencies. As it turned out, s and r values remained in the vicinity of 1. Small standard deviations were chosen for the mutant generating process because mutation here was considered a slight variation of the original but also to avoid hitting extreme values which lead to system destruction (complete decay of both catalysts).

The parameters for the four simulations considered for analysis are

sim	k	s	r	ENDTIME	survivors
1	[0.05, 0.07]	[0, 10]	[0, 2]	$5 \cdot 10^5$ gen.	197
2	[0.05, 0.07]	[0, 10]	[0, 2]	$5 \cdot 10^5$ gen.	134
3	[0.05, 0.07]	[0, 10]	[0, 2]	$2 \cdot 10^6$ gen.	251
4	[0.06, 0.07]	[0.9, 1.1]	[0.8, 1.2]	$2 \cdot 10^6$ gen.	129

Table 4.6: Parameter ranges for 4 Gaussian random walk simulations. The intervals are the limit values of the parameters, to which any higher deviations are truncated. The length is measured in generations, with 1 generation being equal here to 1200 integration iterations.

All of the above simulations exhibited the same overall behaviour. The small number of catalyst species recorded as survivors of mutation events is due to either the disappearance of both species or to very minute differences in parameter values, which lead to extremely slow replacement processes that exhaust the amount of time allocated. As a typical evolution example, below is the parameter-space trajectory of the survivors in simulation 4.

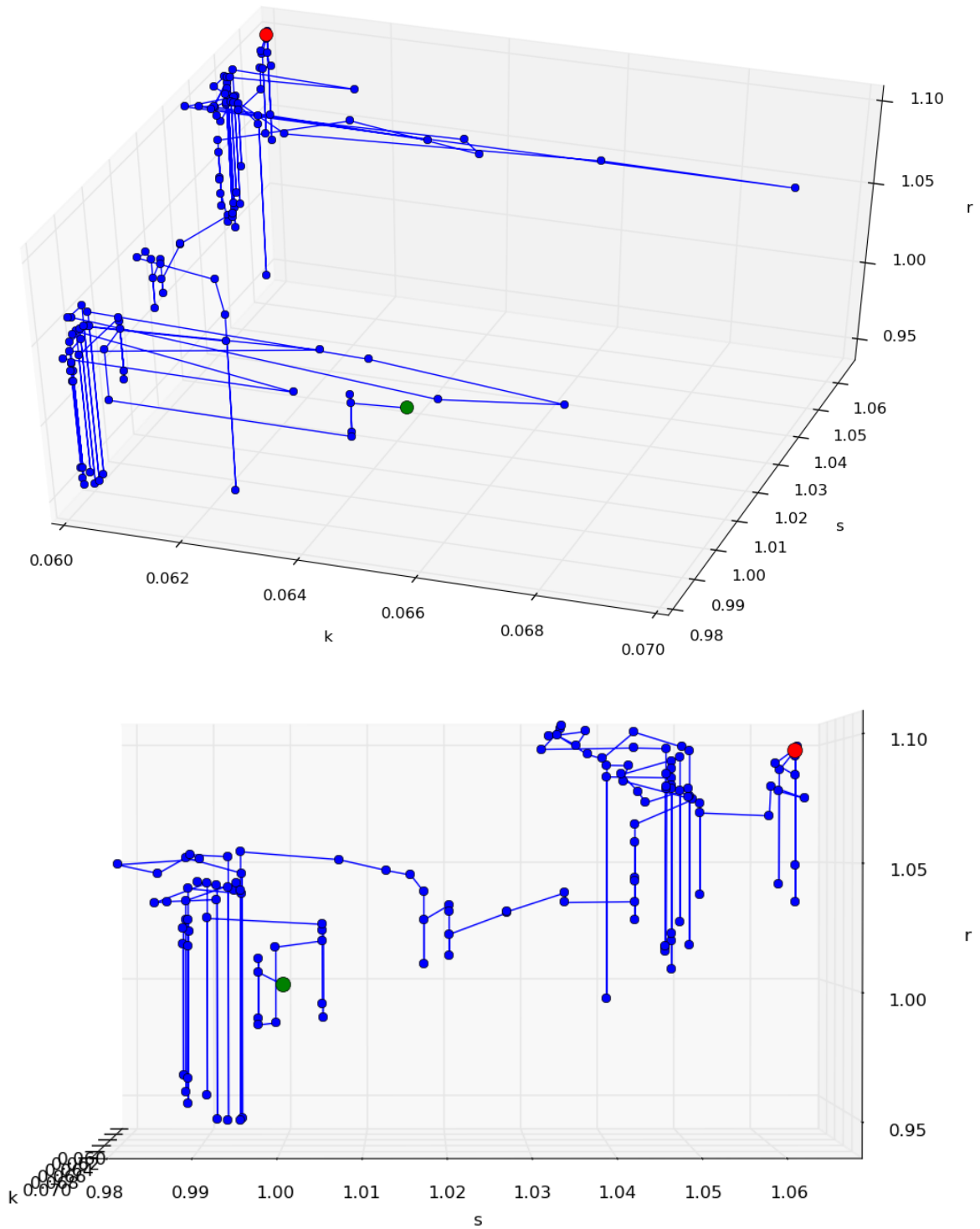


Figure 4.17: The trajectory in parameter space of surviving species obtained in simulation 4, in two perspectives. The starting species is marked with the larger, green dot, while the species in the system at the end of the simulation is marked with the larger, red dot. It is obvious that the majority of surviving species had their degradation rate k at the minimum of the allowed range, with a few very short incursions into greater values.

In order to test for tendencies in the data series, we look for deviations from a Gaussian random walk assumption. The very obvious is the tendency of the degradation rate toward the lowest value. There also seems to be a preference for $r > 1$, as evidenced by the distribution of the data series and the one-point jumps into lower r values for the same s values. The points that vary only in r , an extrinsic parameter, and are stationary in k and s are considered identical species since, as with the last model, they are due to failed mutations only altering the received catalytic support rate through Constraint 2. This situation occurred frequently when k arrived at the lower end of the allowed range, as visible in the figure above, since subsequent decreases were neglected.

We also plot the histograms of the jumps in catalytic rates Δs and Δr between data points, as well as the normal probability plots (quantile-quantile plots with a normal distribution as reference) of these sets.

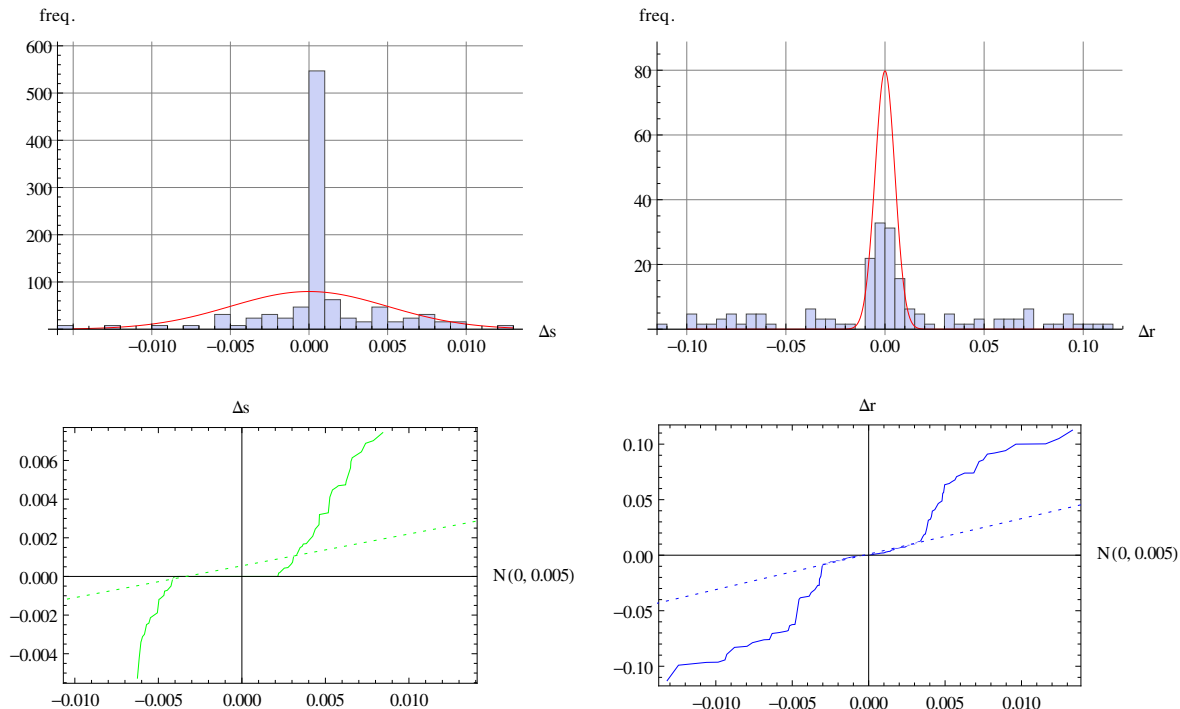


Figure 4.18: Histograms (top row) and quantile-quantile plots (bottom row) of the distribution of jumps in parameter values between consecutive points in the time series representing species parameters. The number of bins is 32 (a quarter of the data series) and the histograms feature a superimposed normal distribution with $\mu = 0$ and $\sigma = 0.005$ (red curve), which is also used as reference in the Q-Q plots. It is easily seen that the jumps do not match the normal distribution from which the evolution simulation drew the mutations. Indeed, they are not normally distributed, as evidenced by both the histograms and the Q-Q plots, although one could say that for a narrow range of values, i.e. $(-0.003, 0.003)$, the jumps in r do follow a normal distribution with fat tails. One can also note the central peak in s jumps, which holds a large number of null jumps.

An average over the 4 simulations shows that jumps in synthesis rate Δs are roughly 50% zero, while increases and decreases are in equal percentage (25%). These stationary values are paired with stationary k values, meaning that these are the failed mutations that only alter r . As for the previous model results, we wish to look at distinct species which are here distinguished by unique (k, s) pairs. Therefore we remove consecutive data points that have only different r values. We choose to keep only the first instance of these points since we are considering only change from the original surviving wild type.

After filtering out duplicate instances of species, we are left with roughly half of the data series. This indicates a high number of stationary species, that survived a few to several mutations. This is a significantly higher percentage than in the previous model and due to the extra dimension available for exploration.

We now redo the previous plots with the filtered data series. Only these unique species will be used in the following analysis.

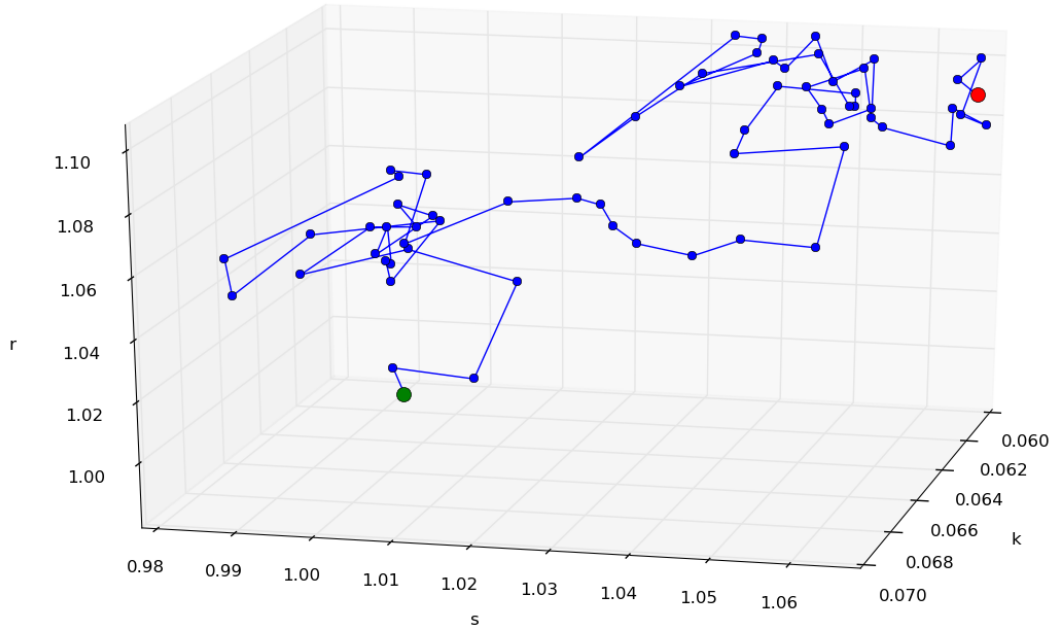


Figure 4.19: The trajectory in parameter space of unique surviving species obtained in simulation 4 (65 data points). The starting species is marked with the larger, green dot, while the species in the system at the end of the simulation is marked with the larger, red dot.

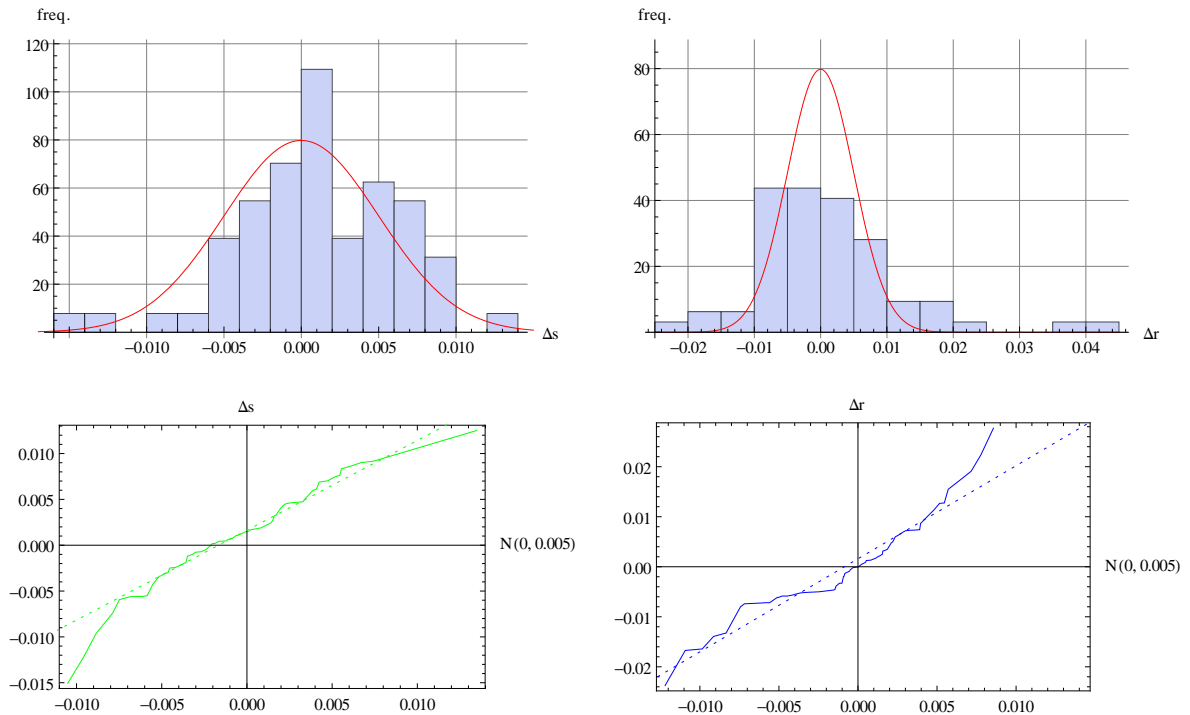


Figure 4.20: Histograms (top row) and quantile-quantile plots (bottom row) of the distribution of jumps in parameter values between unique consecutive species, as obtained in simulation 4. The number of bins is a quarter of the data series and the histograms feature a superimposed normal distribution with $\mu = 0$ and $\sigma = 0.005$ (red curve), which is also used as reference in the Q-Q plots. The Δs and Δr distributions more closely match the normal distribution of the mutant generating process used by the evolution algorithm. The distributions are skewed however and feature heavier tails on one side.

We now see that the jumps between unique species is almost normally distributed, but skewed to one side and featuring a heavier tail on the other. Which side varies between simulations.

Across the simulations considered here, there seems to be a preference for received catalytic support $r > 1$, having an average of 89% of (unique) species in this interval. For s this is not as clear, with an average of 55% (unique) species with $s > 1$ but featuring a wide variation, with as little as 6% in simulation 1.

We are interested in the interplay of species parameter variation with respect to the evolutionary trajectory. Since the distributions are not exactly normal, we compute the Spearman rank correlation coefficient between each pair of variables, after centering the data sets. The only significant correlation is between s and r values, with significant positive correlation in all simulations considered here (see table below). This indicates a tendency for tandem increase in the two values, something hinted at in the evolution trajectory above, though not readily visible in other simulations performed. The correlation is not surprising, given Constraint 2, which adjusts the existing species' r as a function of s . However, this decreases with data series size.

sim	n	$\rho_{s,r}$	p-value
2	62	0.56	$2.1 \cdot 10^{-6}$
4	65	0.61	$6.08 \cdot 10^{-8}$
3	100	0.21	$2.8 \cdot 10^{-2}$
1	101	0.34	$4.7 \cdot 10^{-4}$

Table 4.7: Spearman rank correlation coefficients and associated (two-sided) p-values between data series $\{s\}$ and $\{r\}$. The entries are sorted by the number of unique species n yielded by the simulations, since there is the issue of small population sizes. One can notice a trend of decreasing correlation and significance with population increase.

Between simulations there appears no discernible difference in system behaviour when considering large variations in mutant values or large parameter limits, except for the more likely possibility of catalyst degradation due to extreme values. One difficulty with these simulations is the frequent system destruction or extremely slow replacement events, as mentioned previously. This leaves us with small data series to be analysed. Thus the slight preference for higher values r might be particular to these simulations. Due to the extra parameter dimension, some species survive several mutation events by only having r change, in contrast with the previous model, where this was more rare.

Besides the obvious tendency toward the lowest admissible k values, a tentative conclusion is that there is a weak tendency of the s and r rates to increase in tandem through the evolutionary process, though it is not clear if this holds for much longer time series. Overall, this indicates that “selfish” species, ones that degrade less, self-synthesize more, and receive more catalytic support (and consequently, offer less) are the ones favoured by the evolutionary process. There is a limit to this however, as parasitic species that effectively offer no catalytic support lead to system destruction. Nevertheless, evolution quite clearly leads the system outside of the patter-forming range of values, so we could say that systematic mutation leads towards the destruction of structure-forming chemical systems.

As an illustration of these evolutionary simulations, we reproduce below some animation frames from a run performed before the time-rescaling of the differential equations was undertaken, though the behaviour is essentially the same. This was chosen because of its greater diversity of exhibited patterns. The only difference in system parameters are the higher standard deviation of r jumps $\sigma_{\Delta r} = 0.05$. The parameter ranges were $k \in [0.05, 0.07]$, $s \in [0.95, 1.05]$, and $r \in [0.8, 1.2]$.

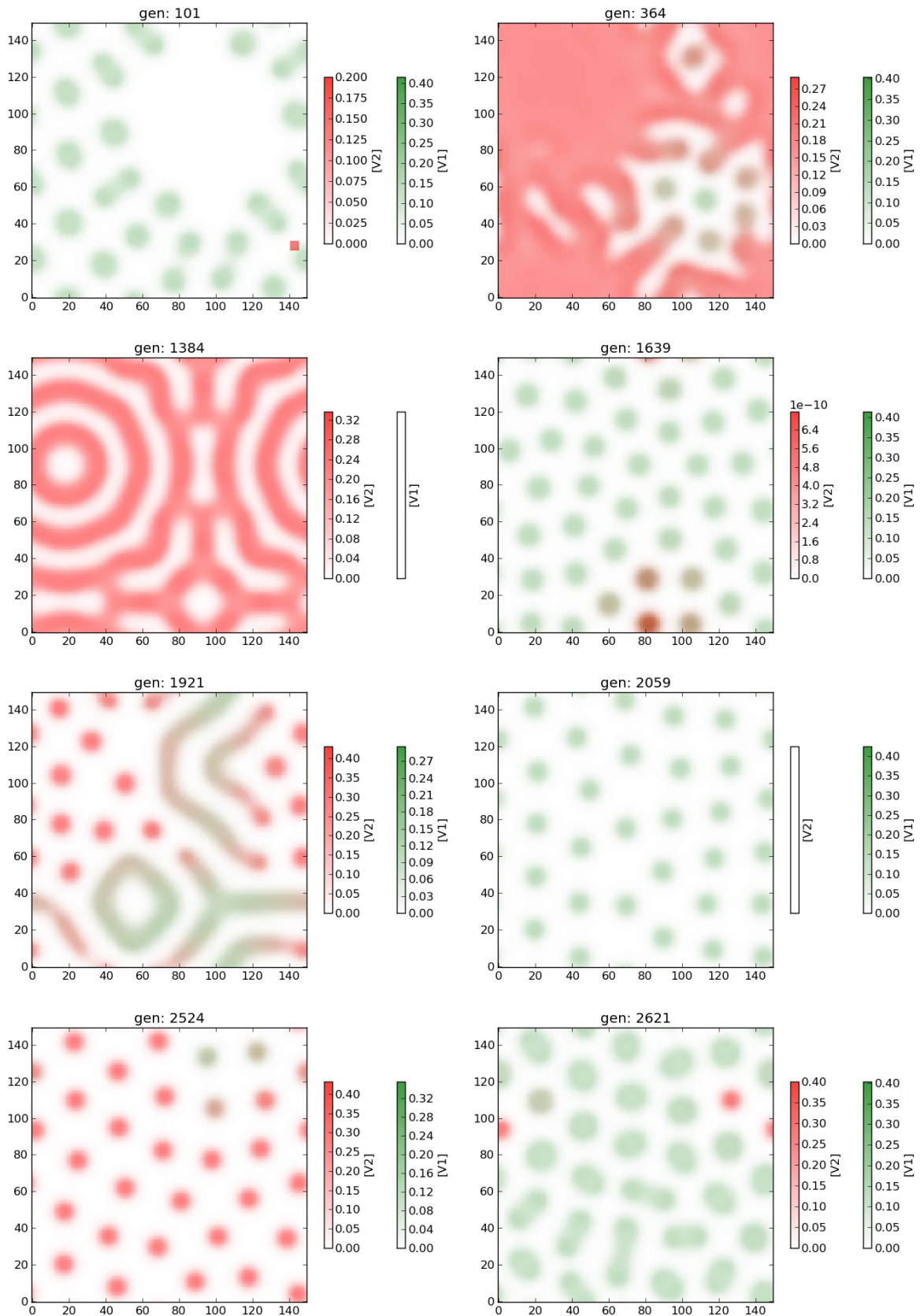


Figure 4.21: Movie frames from an evolution simulation (in order left-right, top-bottom). Colours alternate between designated wild type and mutant. A mutant was introduced every 100 generations, if only one species was present. At *101*: a mutant that fails; *364*: a mutant producing the homogeneous steady state takes over; *1384*: after a few more homogeneous species, a stripes mutant takes over; *1639*: after two stripes species, a spots mutant takes over; *1921*: the system passed through another homogeneous state, followed by stripes, now spots. Subsequent species stayed close to the spots regime, but final species in the simulation were homogeneous states.

4.9 Conclusions

The above results show that for the model of catalyst competition in the shape of a 2-component hypercycle, coexistence of the two species is generally not possible, and that their simultaneous presence in the system leads either to the elimination of one or both of them, in the form of a dramatic system destruction.

This is in contrast with the non-spatial elementary 2-cycles in [ES78] composed of species with no resource competition. These were shown to be cooperative leading to a non-trivial stable steady state. Here the added dynamics and spatial extension resulted in opposite results. It is also in contrast with the spatial model in [SS06], which looked at a 2-cycle without autocatalysis and relaxed resource competition through temporary fuel sequestration (i.e. catalysts consume and degrade back into fuel). To underline the importance of local interaction in hypercycle dynamics, the authors used both discrete (asynchronous cellular automata) and stochastic (mean-field theory) spatial models. The outcomes of these were either the survival or extinction of both species, with no discernible patterns formed but simply randomly spread concentration gradients.

In an evolutionary context, the system is shifted by systematic mutation in the direction of selfish chemical species, which are fitter assuming constant substrate concentrations. Subsequent survivors mutation events are those that tend toward lower degradation and higher synthesis rate and are ultimately of a type that does not produce spatial structures.

Therefore, these systems are purely competitive, with transient balance reached only in case of near-identity of the competing catalyst species. Furthermore, unless an unrealistically high concentration cut-off is imposed that would isolate spatial structures, the patterns formed play no deciding role in this competition but simply reflect local population sizes.

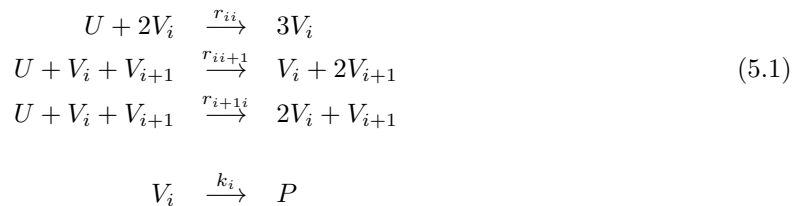
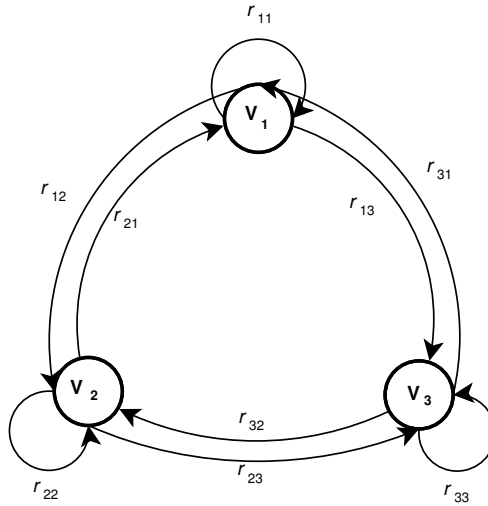
Chapter 5

Catalytic hypercycle

We consider here the hypercyclic linkage of replicators and adapt it to the spatial Gray-Scott model. The name comes from the closed chain of catalysed replication that connects autocatalysts, which in turn comprise catalytic cycles. In contrast with studies considering cycles of second-order replicators (see for instance review [SS03]), each species features cubic autocatalysis, following the original model. The catalytic linkage between them is less critical to their survival since they are fully functional self-replicative units in their own right and the mutual catalysis of cycle neighbour replication appears as an additional feature. Furthermore, since these species are considered to have arisen through mutation and are near-identical, the cycle considered here features both forward and backward catalytic reactions, as described below.

5.1 Model

The extension of the Gray-Scott model to three near-identical species takes the form of a compound hypercycle, following the classification in [ES78]. Note that the replicators in the respective study do not consume their substrates when copying themselves so here we have the added constraint of limited fuel supply.



Here we renamed the self-replication rates as r_{ii} for uniformity of notation, $i \in \{1, 2, 3\}$ and $i = 4 \equiv 1$ given the circular reaction graph. For each species V_i we speak of *forward* catalytic link r_{ii+1} and *backward* link r_{i+1i} where this becomes relevant.

The corresponding PDEs are:

$$\begin{aligned}
\frac{\partial u}{\partial t} &= -u[r_{11}v_1^2 + r_{22}v_2^2 + r_{33}v_3^2 + (r_{12} + r_{21})v_1v_2 + (r_{23} + r_{32})v_2v_3 + (r_{13} + r_{31})v_1v_3] \\
&\quad + F(1 - u) + D_u \nabla^2 u \\
\frac{\partial v_1}{\partial t} &= u(r_{11}v_1^2 + r_{21}v_1v_2 + r_{31}v_1v_3) - (F + k_1)v_1 + D_c \nabla^2 v_1 \\
\frac{\partial v_2}{\partial t} &= u(r_{22}v_2^2 + r_{12}v_1v_2 + r_{32}v_2v_3) - (F + k_2)v_2 + D_c \nabla^2 v_2 \\
\frac{\partial v_3}{\partial t} &= u(r_{33}v_3^2 + r_{23}v_2v_3 + r_{13}v_1v_3) - (F + k_3)v_3 + D_c \nabla^2 v_3
\end{aligned} \tag{5.2}$$

The constraints used in the previous models extend naturally as

Constraint 3:

$$r_{ij} + r_{ji} = 2\sqrt{r_{ii}r_{jj}}, \quad \forall i \neq j \in \{1, 2, 3\} \tag{5.3}$$

As a reminder, this comes from equating the rate of fuel consumption to a quadratic form, as $\frac{\partial u}{\partial t} = -u(r_{11}v_1 + r_{22}v_2 + r_{33}v_3)^2 + (\dots)$, justified by the near identity of the three species, which react with u as a joint quantity.

5.2 Mutation outcomes

We consider the evolutionary scenario in which two mutations occur, such that the above defined cycle appears. As we have seen in the previous sections, once a mutant appears, unless all reaction parameters are nearly identical, the species holding a chemical advantage will quite quickly cause the disappearance of the other. Thus, for three species to simultaneously exist, there is only a narrow window in which the second mutation ought to occur. This greatly limits the probability of the emergence of the hypercycle from one original species, assuming nothing like cascade mutation. Indeed, the realistic global odds of cycle formation are ignored here, as we are mainly interested in the properties of this system.

We shall therefore begin by initialising the system with one species, then introducing a small quantity of a mutant species, followed shortly after by the introduction of a second. Here we do not generate mutant parameters randomly based on their wild types but only observe behaviour for different values. We place the mutant perturbations at a maximum of wild type concentration, as this was seen in the previous system to increase the chances of initial mutant survival. Again, we are placing ourselves within a rather narrow island of probability in order to study this system. Note that the order of mutant placement does not affect the resulting dynamics.

D_c	D_u	L	N	Δt
$1.4 \cdot 10^{-9}$	$2 \cdot D_c$	0.01	150	0.05

Table 5.1: System parameters for hypercycle formation simulations.

Simulation 1: spots and stripes

We start with species in and near the dividing spots region. Reaction scheme parameters are below. As before, we place mutant quantities of concentration $\mu = 0.2$ and Moore radius $r_\mu = 2$. The simulation ran for 800 generations, with one generation spanning $2\lceil \frac{LN}{\Delta t^2} \rceil = 1200$ forward Euler integration iterations, so twice the specific length.

F	0.04
k_1	0.065 (dividing spots - Pearson λ)
k_2	0.064 (stripes and spots - Pearson κ, λ)
k_3	0.063 (stripes - Pearson κ)
\mathbf{r}	$\begin{bmatrix} 1 & 1.7 & 0.2 \\ 0.3 & 1 & 1.9 \\ 1.8 & 0.1 & 1 \end{bmatrix}$

Table 5.2: Reaction scheme parameters for hypercycle simulation 1. Observe that reaction rates \mathbf{r} obey Constraint 3.

As an easier to grasp visual alternative to parameter notation we shall use an extension of the model diagram, as illustrated below. Note that as with previous graphic notation, as a simplification we omit the fact that U takes part in all catalysis reactions. The reason why for each pair of species we mark the higher of the forward and backward catalytic rates (considering increasing V indices as forwards) will become apparent later, as we shall see these play a role in the cycle's stability. Note that V_2 is effectively parasitic to V_1 , due to its high received replication rate and low given rate. Similarly, V_3 is parasitic to V_2 .

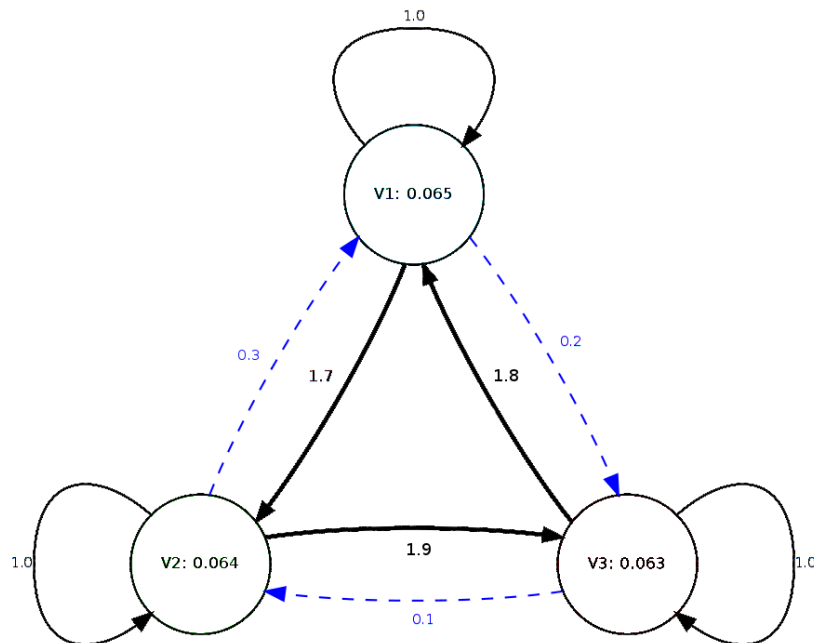


Figure 5.1: Hypercycle diagram depicting degradation and catalytic rates of the system in simulation 1. The values appearing next to the species label denote their degradation rates. The thick arrows depict the rate with higher value of the forwards and backwards rates for each pair of species, while the dashed arrow the smaller of the two. The colours depict their order of appearance, namely *blue* (top): first, *green* (lower-left): second, and *red* (lower-right): third.

Below are movie frames from the time evolution of this system.

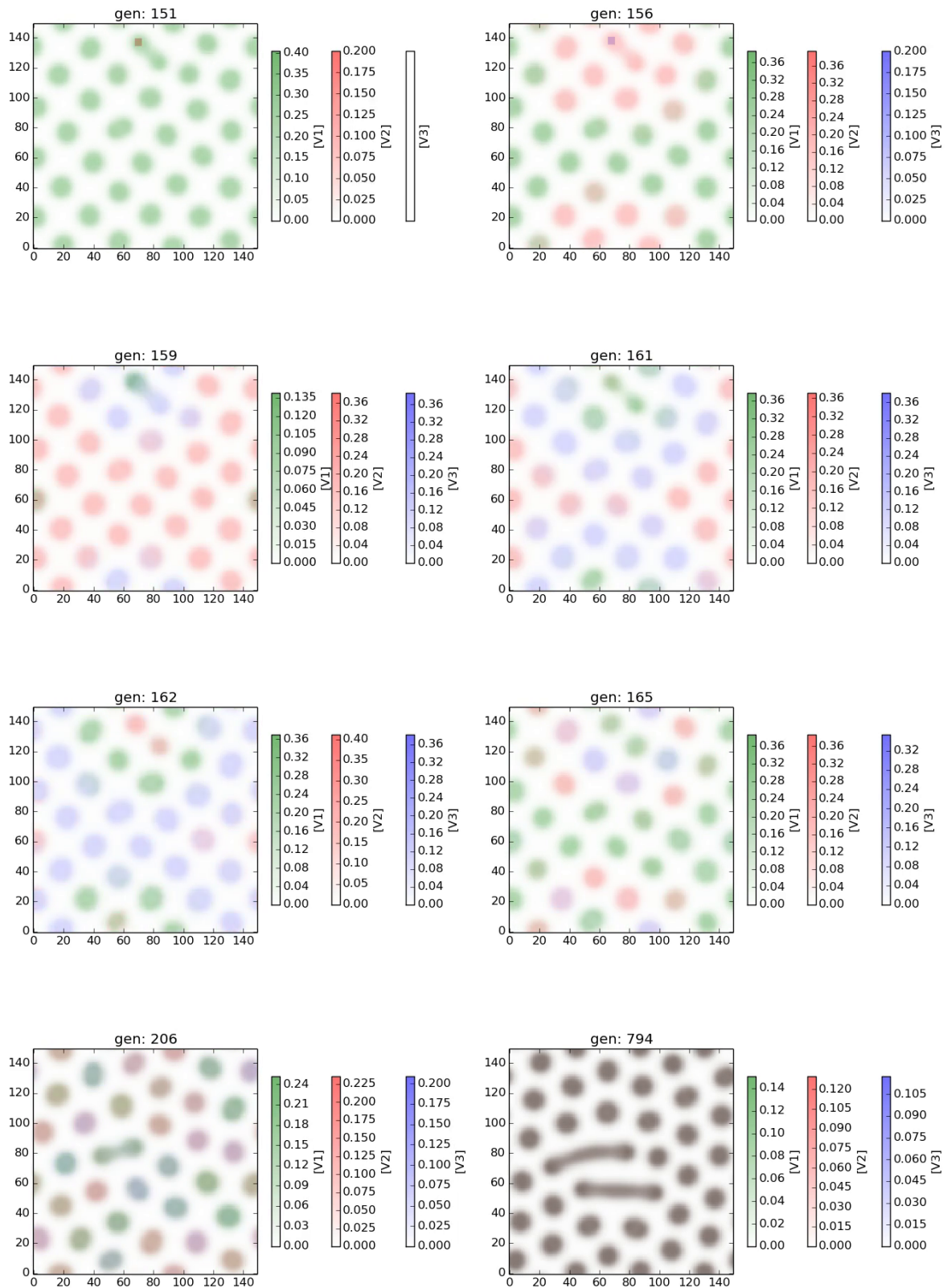


Figure 5.2: Simulation 1 frames, showing the formation of a compound hypercycle. The three species concentrations are marked with green, red, and blue, respectively. At gen. 151, after V_1 has formed its pattern across the entire space, a perturbation of mutant V_2 is introduced at a maximum of wild type V_1 , close to coord. (70, 138). This quickly spreads, infecting the surrounding spots and removing the wild type. At gen. 156, a perturbation of V_3 is placed at a maximum peak of V_2 , close to (70, 138). Similarly, V_3 starts infecting and replacing V_2 , but in the wake of its infection, V_1 levels are restored (gen. 159 - 161), followed by concentration fluctuations, with each spot holding one dominant species, as distinguishable by its coloration (gen. 162 - 206). Ultimately, the fluctuations settle, with each species arriving at about the same global concentration level. Almost at steady state (gen. 794), the pattern observed corresponds to neither species alone.

Remarkably, the introduction of the third species has led to the restoration of the original, which had started to be driven out by the first mutant, and so to the stabilisation of the chemical system. V_3 infects V_2 but since it acts as a promoter of V_1 , it leads to its concentration increase given sufficient time. Note that this would not be possible if we had set a high concentration cut-off, as flow of V_1 between spots would have been stopped and would not have been available to V_3 for replication.

Hence we observe overall cooperative behaviour of mutual replication, which was generally impossible with only two competitive species. While strictly speaking, the three species are competing for fuel and may have advantageous received catalytic and degradation rates with respect to one another, the cyclic nature of the model allows for the emergence of collaboration. The three species exchange local dominance in each spot through fluctuating concentration levels, but finally achieve steady state. Furthermore, the compound pattern they form appears as a combination of the ones formed by each species individually, lying somewhere between k_2 and k_1 in pattern space.

To see these global concentration oscillations we plot total concentrations during the simulation.

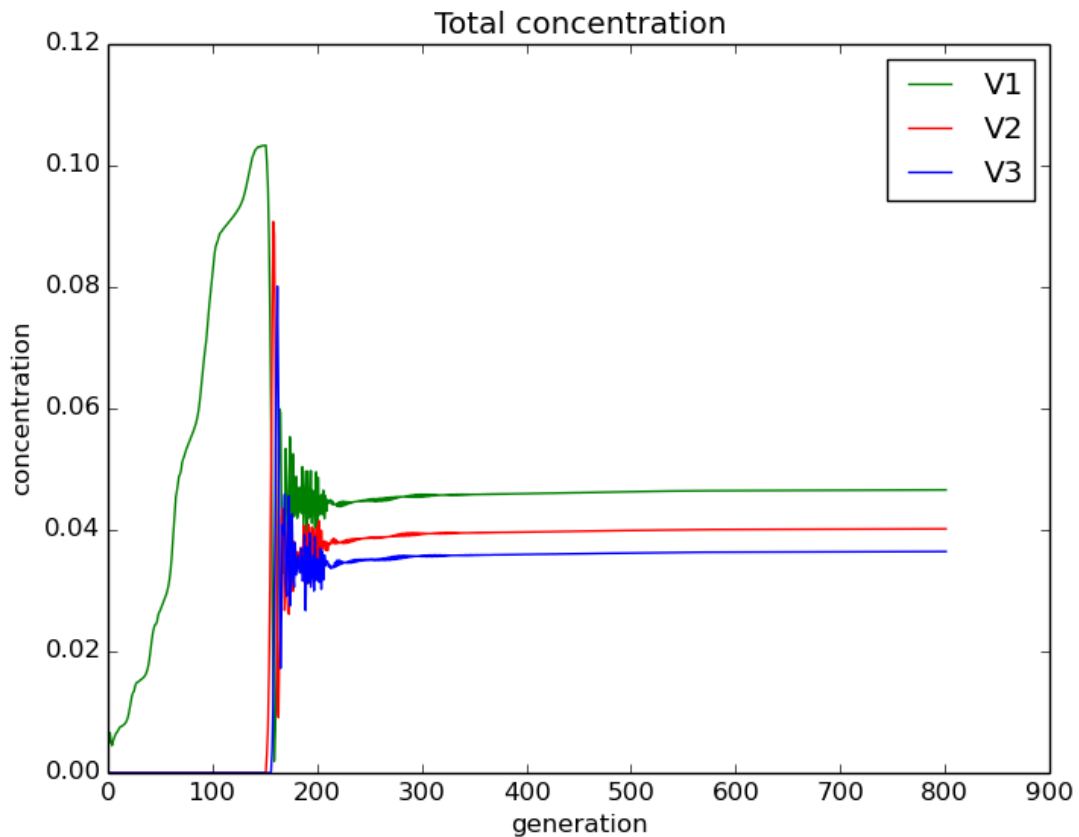


Figure 5.3: Total concentration of the three hypercycle species in simulation 1 (normalised over grid size). V_1 levels lie on top after generation 200, V_3 lowest, and V_2 middle level. A periodic orbit or steady state is reached shortly before generation 800.

One can see in the above figure how V_1 levels very quickly drop when the effectively parasitic mutant is introduced but before it disappears completely, it is recovered by the introduction of V_3 . The three species then start oscillating with decreasing amplitudes, until they reach a steady concentration, at about generation 450.

Simulation 2: fledgling spirals

We have looked at other species placement within parameter space. In the following simulation we chose more closely related species that form short-lived spirals. Placed mutant quantities are of concentration $\mu = 0.2$ and Moore radius $r_\mu = 2$. The simulation ran for 800 generations of same length as the previous simulation. Below are the parameters and movie frames.

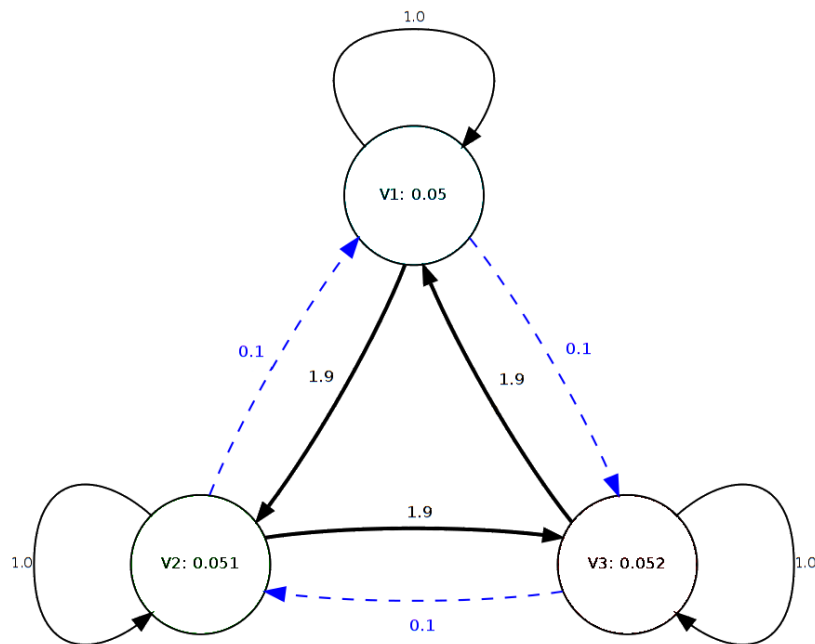


Figure 5.4: Compound hypercycle diagram depicting parameters for simulation 2. Replication rates \mathbf{r} obey Constraint 3. The fuel feed rate is $F = 0.01$, which in conjunction with k_i , places the species within fledgling spirals (Pearson α) pattern regime

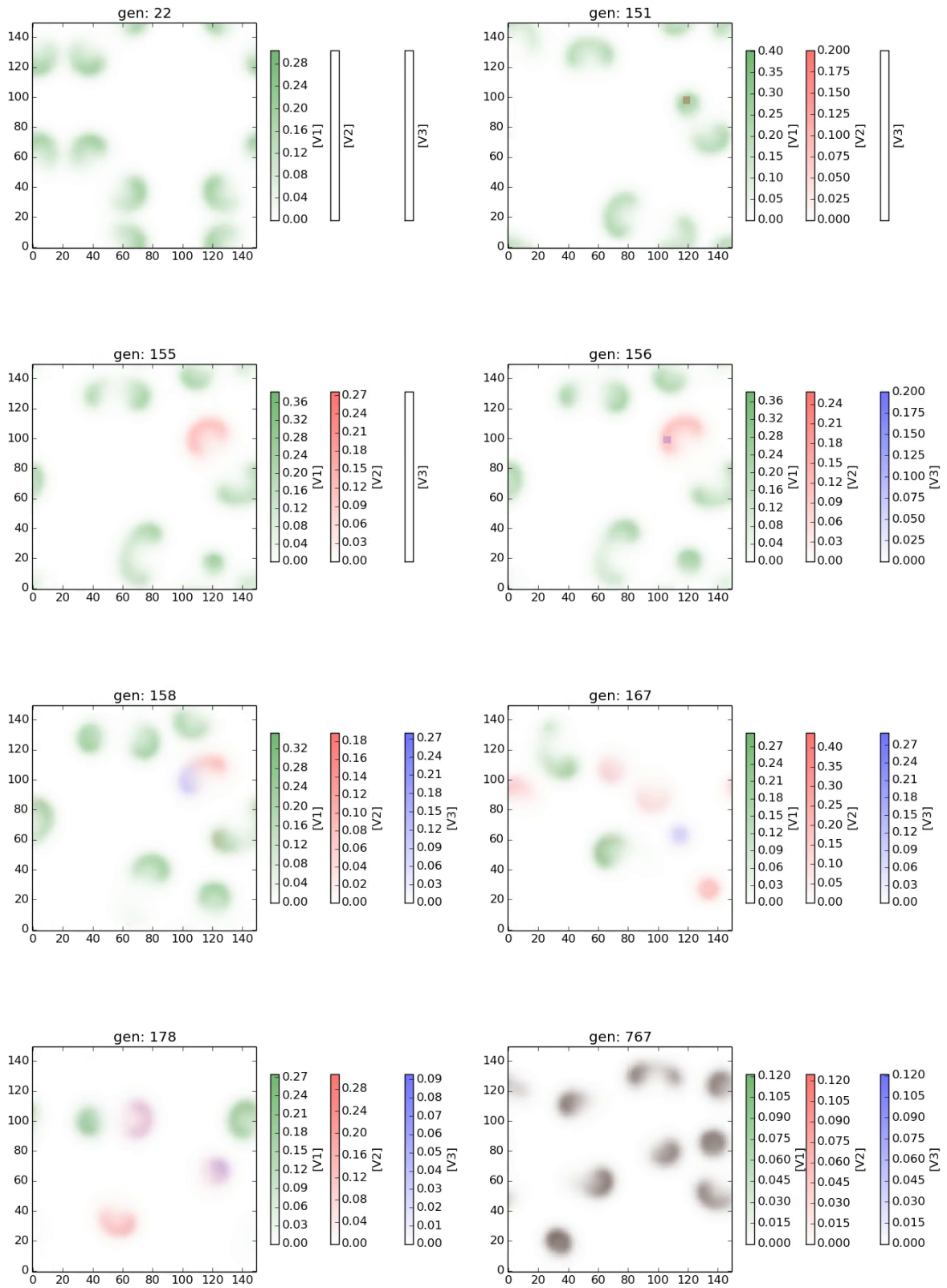


Figure 5.5: Simulation 2 frames, showing the formation of a compound hypercycle. The three species concentrations are marked with green, red, and blue, respectively. At gen. 151 an amount of mutant V_2 is placed near coord. (118,100). By generation 155, the infected spiral is virtually only composed of mutant, and in the next generation is subjected to the introduction of V_3 at peak V_2 concentration near coord. (108,100), and subsequently starts spreading. Afterwards, the autocatalysts' levels start oscillating, with one species dominant in each spiral. This goes one for some time, until about gen. 300, after which concentration curves overlap, fluctuating in tandem.

Once again we have seen that while initially species levels oscillate out of phase with each other, each one achieving peak concentration while the other two are at low levels, after enough time the peaks synchronise and fluctuate in tandem. This is visible in the animation frames above as a somewhat violet colour that comes from comparable (if not identical) levels of species in each structural feature. There is only the matter of offsets in amplitude between the three concentration curves. In contrast with Simulation 1, here V_1 and V_3 overlap perfectly at a very small offset from the V_2 curve. This is seen in the global concentration evolution plot below.

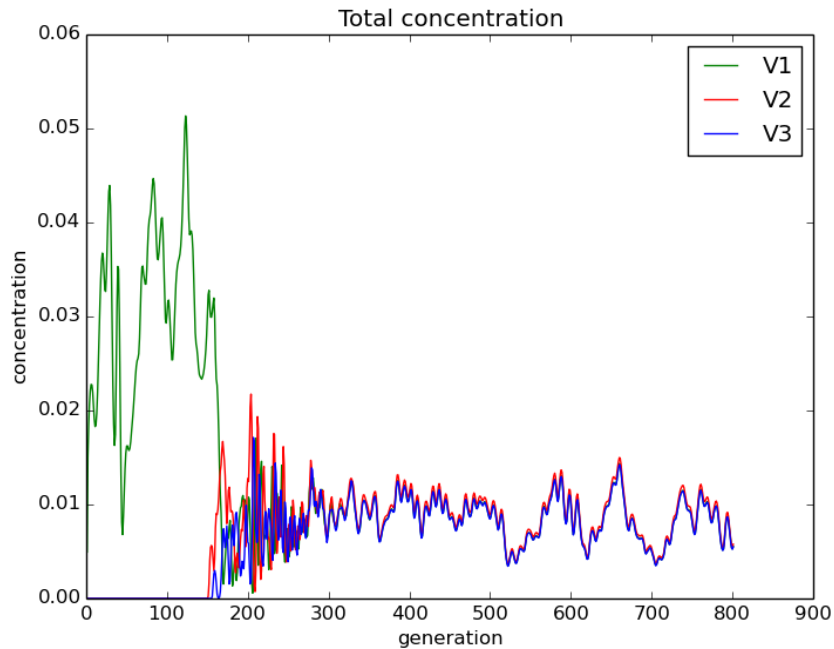


Figure 5.6: Total concentration of the three hypercycle species in simulation 2 (normalised over grid size). After generation 300, the V_1 and V_3 curves are indistinguishable, with V_2 synchronised at a narrow amplitude offset (top curve).

To better describe this behaviour we look in simulation 3 at a short time interval following initial infection, at a slowed animation rate (shorter generations).

Simulation 3: species interaction

To have a clearer picture of the narrow time interval in which the two mutations occur, we shorten the length of a generation to $\left\lfloor \frac{1}{32} \cdot \left\lceil \frac{LN}{\Delta t^2} \right\rceil \right\rfloor = 18$ integration iterations. Below are the simulation parameters. The simulation ran for 20000 generations.

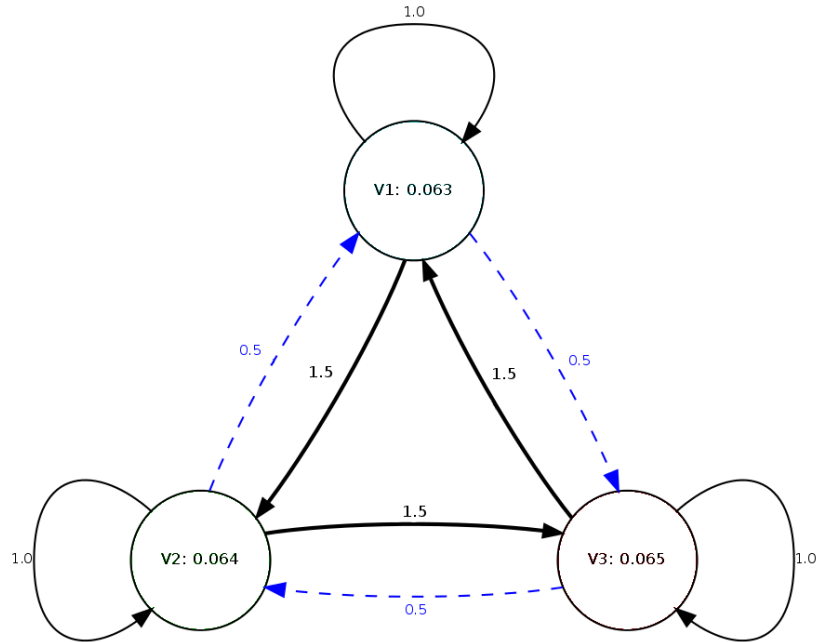


Figure 5.7: Compound hypercycle diagram depicting parameters for simulation 3. V_1 corresponds to stripe patterns, V_2 to a mix of stripes and spots, and V_3 to dividing spots (Pearson λ) Replication rates \mathbf{r} obey Constraint 3. The fuel feed rate is $F = 0.04$.

Note that these are the same species as in simulation 1, except with lower forward catalytic rates and placed in a different order. As noted above, the different order of placement has no impact on the end steady state. The mutants were placed at gen. 4800 and 5200. Below are two frames showing the system state a short time after each of these events.

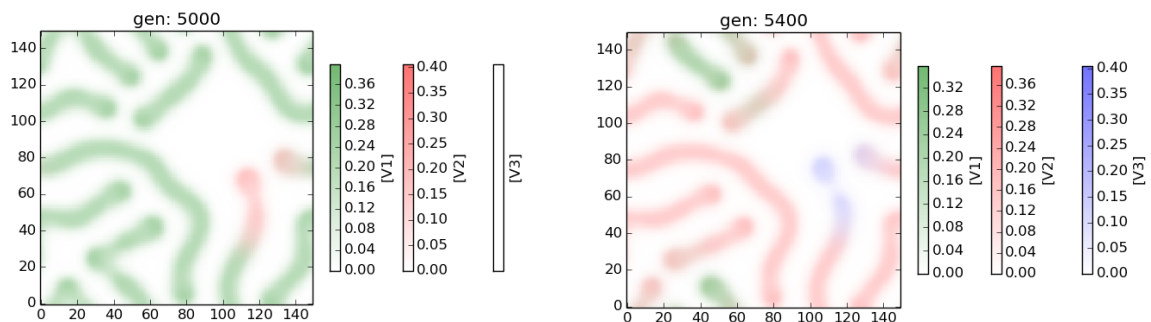


Figure 5.8: Simulation 3 frames, showing system state shortly after placement of mutant V_2 (left) and V_3 (right). The three species concentrations are marked with green, red, and blue, respectively. V_2 infects the original species and starts spreading from close to coordinates (110, 70), also affecting the pattern (spots start breaking off). Since V_3 is placed at a peak of V_2 , this second mutant starts spreading from the same region, with a more pronounced change in pattern, since it forms dividing spots exclusively.

In order to study the interaction between species in this narrow window of the mutation events, we look at the concentration evolution of a single grid point, namely (110, 70), where we saw in the above figures that the new species enter the system and can be found in greater concentrations shortly thereafter.

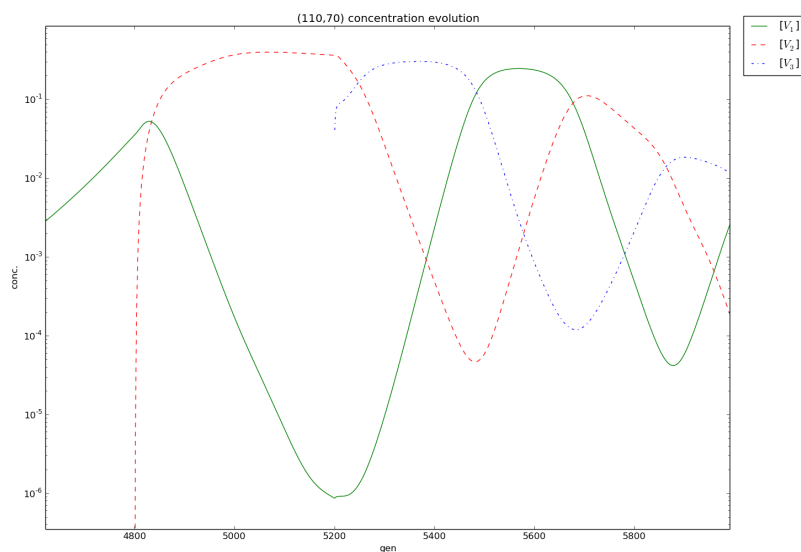
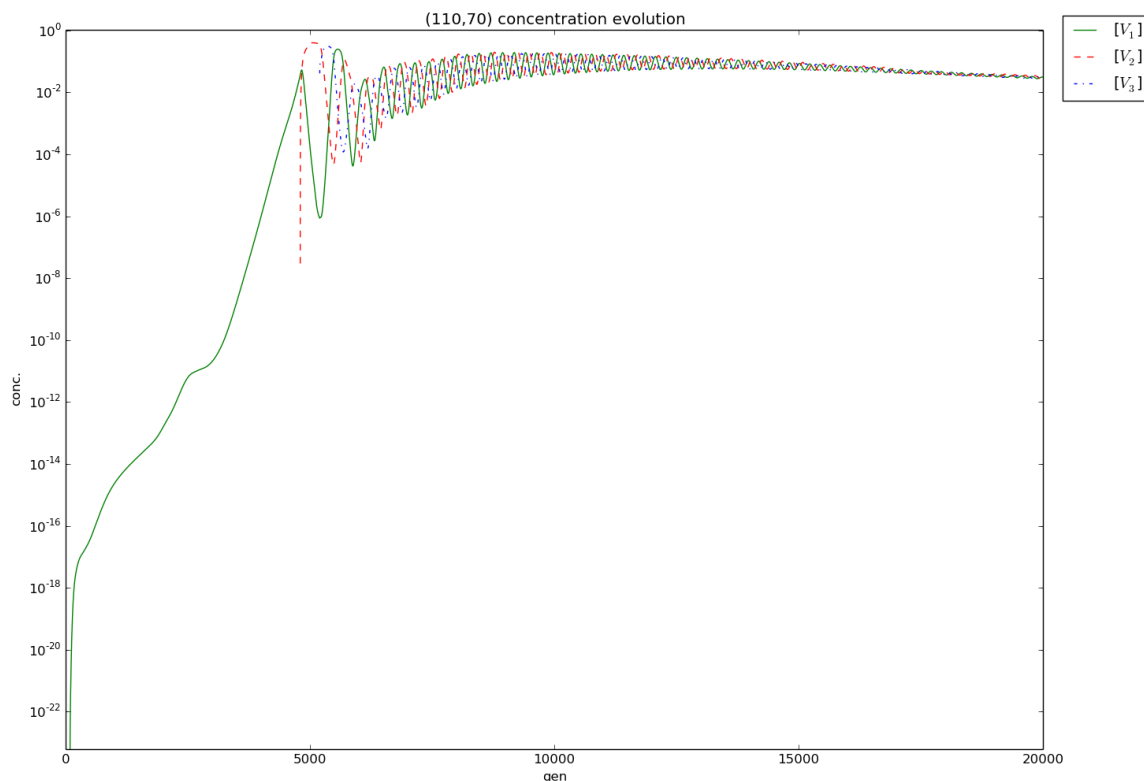


Figure 5.9: Species concentration evolution at grid point (110,70) during the entire duration of simulation 3 (top) and in the interval [4600, 6000]. By the end of the simulation, steady state is nearly reached as can be seen in here by the vanishing oscillations. Mutant V_2 is introduced at gen. 4800 and starts replicating, causing the wild type V_1 levels to start dropping. At gen. 5200 the second mutant is introduced and causes V_2 levels to drop and V_1 to increase. This goes on until about gen. 5500, just before V_1 peaks, with a reversal in V_2 and V_3 evolution. Subsequently, this behaviour repeats yielding out of phase oscillations, with each species holding peak concentration for a short interval.

The cyclic nature of the reaction scheme becomes apparent from the above concentration curves. Since V_3 plays the role of antagonist of V_2 and promoter of V_1 due to the catalytic rates linking them, once it enters the system it aids the replication of V_1 and hinders synthesis of V_2 . However, once V_1 is restored to sufficient levels, since it is the promoter of V_2 it aids in its replication and hinders V_3 , and so on. These oscillations follow the pattern of out of phase increase in species V_i , then V_{i+1} , with decrease in V_{i-1} , where each $i \in \{1, 2, 3\}$ is antagonist of $i - 1$ and promoter of $i + 1$, with $i = 4 \equiv 1$.

To get a clearer picture of how the third species salvages V_1 , stabilizes the system, and why this relation is sufficient to maintain oscillations, leading the system towards steady state or orbit, we plot the concentration space trajectory for the same grid point.

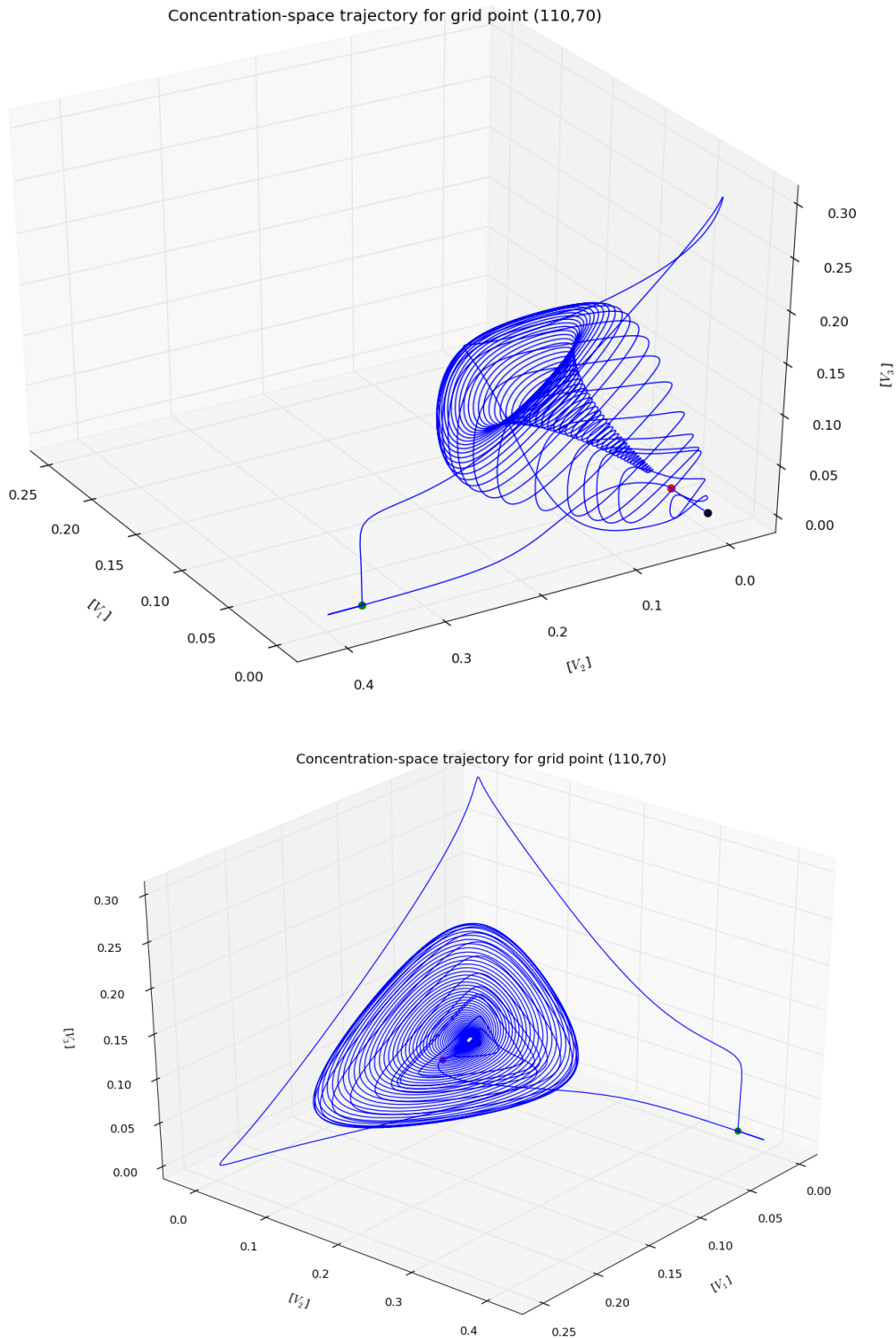


Figure 5.10: (v_1, v_2, v_3) –space trajectory of grid point (110, 70) during simulation 3, from two perspectives. In both, but more apparent on the left hand side view, the start of the trajectory is marked with a black dot, the time of the first mutation event with a red dot, and the second with a green dot. Note that these two mark the times when the mutants were introduced in the system (at different grid points) and are slightly offset here since (110, 70) was chosen manually as close as possible to both mutation points. However, one can distinguish how the trajectory changes direction shortly after each of these moments.

After V_2 is introduced, the 2-species trajectory heads towards the v_1 axis (V_2 starts disappearing) but once the third species appears, this curve becomes embedded in the 3-species space and caught by a global attractor. So as a descriptive explanation of the stable behaviour seen, we could say that since the 3-species hypercycle dynamics feature a global attractor, once V_3 is coupled into the (V_1, V_2) dynamics, the phase space trajectory falls into its basin of attraction.

Simulation 4: failed hypercycle

Here we show a case in which the species forming the hypercycle did not reach stability. The parameters of this system are below. A generation of specific length $\lceil \frac{LN}{\Delta t^2} \rceil = 600$ integration iterations was deemed appropriate for looking at the time evolution.

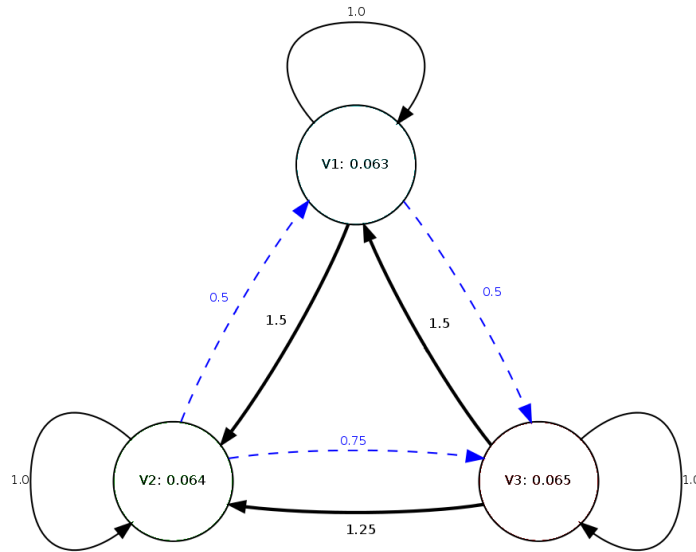


Figure 5.11: Compound hypercycle diagram of simulation 4 parameters. Replication rates r obey Constraint 3. The fuel feed rate is $F = 0.04$.

In this case, the introduced third species has no effect on the concentration levels of the previous two species and simply goes extinct.

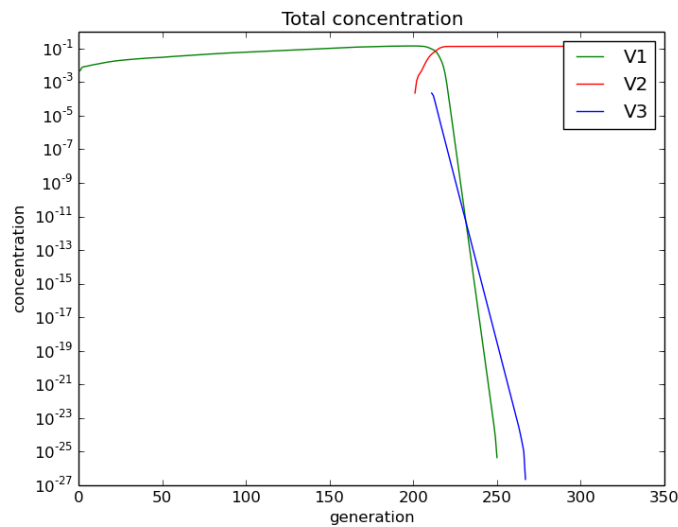


Figure 5.12: Total concentration of the three hypercycle species in simulation 4 (normalised over grid size). Mutants of concentration $\mu = 0.2$ and Moore radius $r_\mu = 2$ were placed at generations 200 and 210. One can see how the introduced V_3 does not manage to spread, nor does it help V_1 return to previous levels, but they both disappear from the system in about 50 generations.

Unlike previous simulations, the system is not brought to a stable orbit or steady state by the extension to three interacting species. As is visible on the cycle diagram above, V_2 is effectively parasitic towards both V_1 and V_3 (although to a lesser degree toward V_3 , as the forward and backward catalytic rates are close). This globally catalytically advantaged relation of V_2 ensures that its growth is unhindered and antagonises the replication of the other two. Notice that the relative degradation rates here play an insignificant role compared to reaction rates.

5.3 Stable hypercycle properties

We now ask what parameters allow for a stable compound hypercycle and if any values allow for different pattern-forming behaviour. As was suggested by the cyclic nature of the catalytic chain, the first simulations tried had forward rates set significantly higher than backward rates, as illustrated by the first three examples in the previous section. During this search, a few properties of these cycles were found.

Directionality

A great many simulations were performed varying \mathbf{r} to identify the class of stable cycles (data not shown here). For simplicity, r_{ii} were kept at 1 since it has been seen that their variation may be equated to varying k_i . It turns out that in order for the hypercycle to be a *permanent* system (all species survive forever, following the definition in [HS87]), it needs to be *directional* with respect to catalytic rates between species, i.e. forward rates must all be greater than backward rates or vice versa. In this respect, the failed cycle example showed previously is no coincidence. This is also the reason for the emphasized depiction of the higher rate in the cycle diagrams. Due to Constraint 3 one could have either of these rates null, in which case the hypercycle becomes of elementary type but still exhibits the same behaviour. The directionality condition holds regardless of degradation rates and implicitly, of formed patterns, which shows some degree of independence of the chemical dynamics from the spatial distribution of molecules and transport processes.

In fact, this difference between r_{ij} and r_{ji} need not be great in order for the cycle to be permanent. However, if the rates are very close, this results in the system reaching a periodic orbit, not a fixed point, as illustrated in the simulation below, featuring a weakly directional cycle.

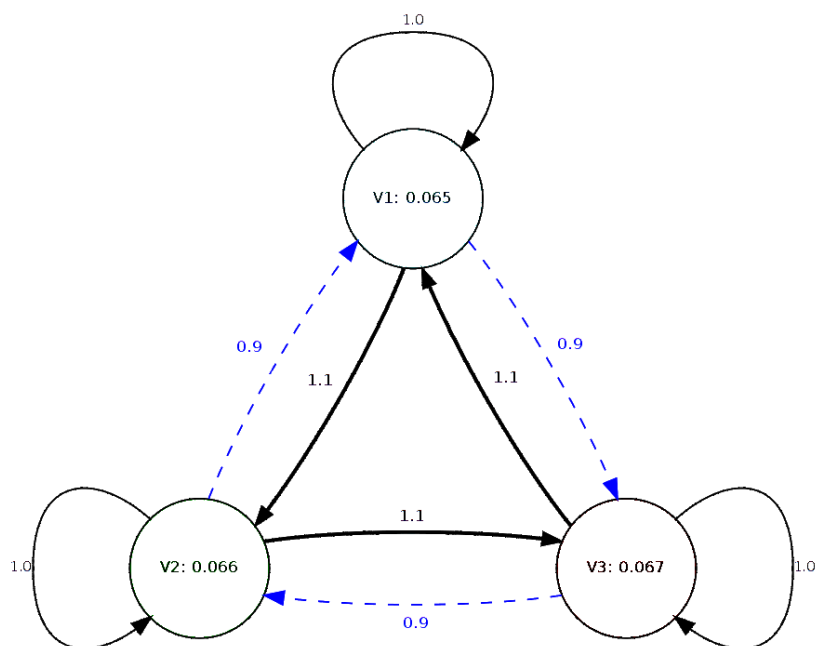


Figure 5.13: Diagram of a compound hypercycle with close forward and backward catalytic links. Replication rates \mathbf{r} obey Constraint 3. The fuel feed rate is $F = 0.04$.

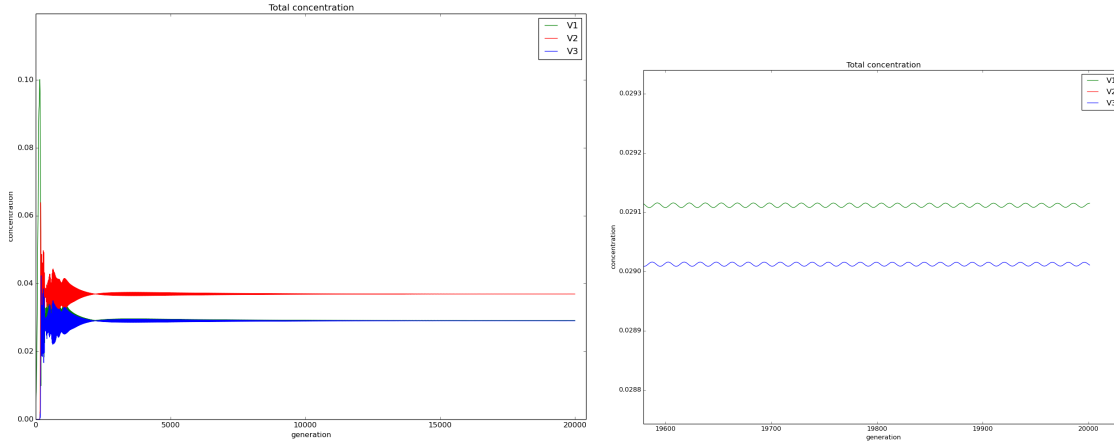


Figure 5.14: Total species concentration (normalised over grid size) of a weakly directional cycle. Generation length was $2 \cdot \lceil \frac{LN}{\Delta t^2} \rceil$. The left hand plot covers the entire simulation while the right hand side provides a zoom at late time. This only features the v_1 and v_2 curves since their oscillations were very small and difficult to see with all three curves fit in, however v_3 follows an identical evolution.

As can be seen from the concentration curves above, the system hits a periodic orbit after 10^4 generations. The patterns at this time are still dividing spots, only the species levels continue to fluctuate. The non-spatial hypercycles composed of up to 4 replicators described in [ES78] were seen to have an asymptotically stable fixed point and as such, this periodic orbit of the spatial model appears as a slight divergence of that result.

Cycles with perfectly equal forward and backward catalytic links were only seen to fail, even when starting from a mix of all three species, leaving only the catalyst with lowest degradation rate. There are exceptions to this in which forward and backward rates are nearly equal. However, these are extremely sensitive to initial conditions, to the point that a different pseudorandom number generator seed (i.e. the randomization of the initial perturbation) leads to its failure. As such, we refer to these as *quasi-stable* hypercycles. A single example was found through the evolutionary simulations to be discussed later. Here, the self-replication rates r_{ii} were also allowed to drift through mutation.

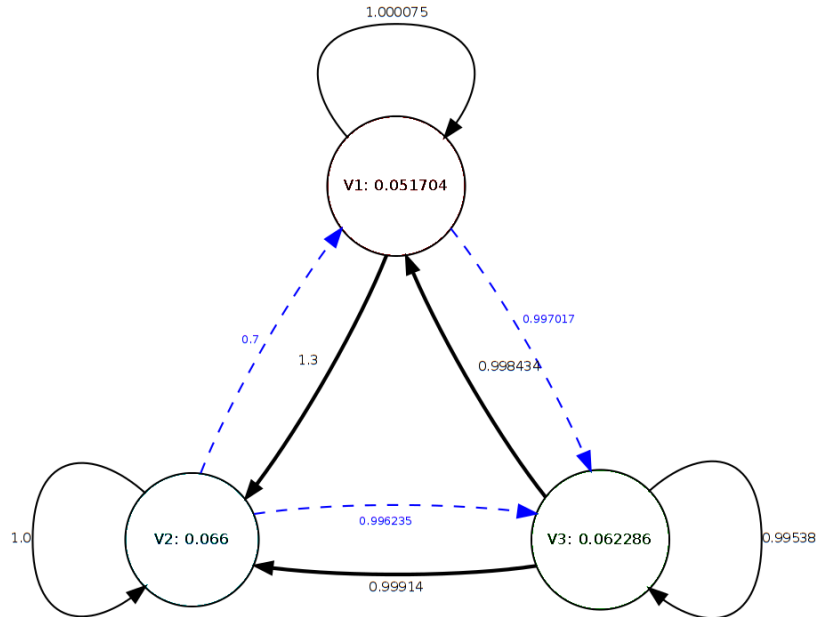


Figure 5.15: Diagram of a quasi-stable compound hypercycle. Replication rates \mathbf{r} obey Constraint 3. The fuel feed rate is $F = 0.04$. V_1 falls outside the pattern-forming domain and corresponds to the homogeneous steady state, while V_2 and V_3 correspond to dividing spots and stripes, respectively.

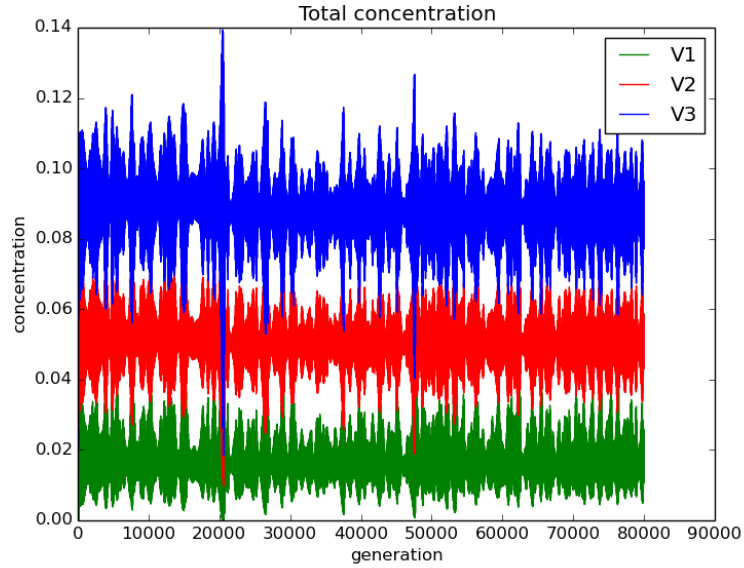


Figure 5.16: Total species concentration (normalised over grid size) of a quasi-stable compound hypercycle. The generation length was $\lceil \frac{LN}{\Delta t^2} \rceil$.

Here, the fluctuations in catalyst levels appear random and do not settle into an orbit, at least not a discernible periodic one. Indeed, at time $t \rightarrow \infty$ it may be that the cycle fails, from whatever initial conditions. We again appeal to the relevance of very long but finite time scales. The pattern at these long times up to $8 \cdot 10^4$ generations is shown below. It consists of a single stripe looping around the system boundaries. Since the species concentrations continue to fluctuate, one can distinguish travelling peaks of each catalyst that also impact the pattern as they traverse the stripe.

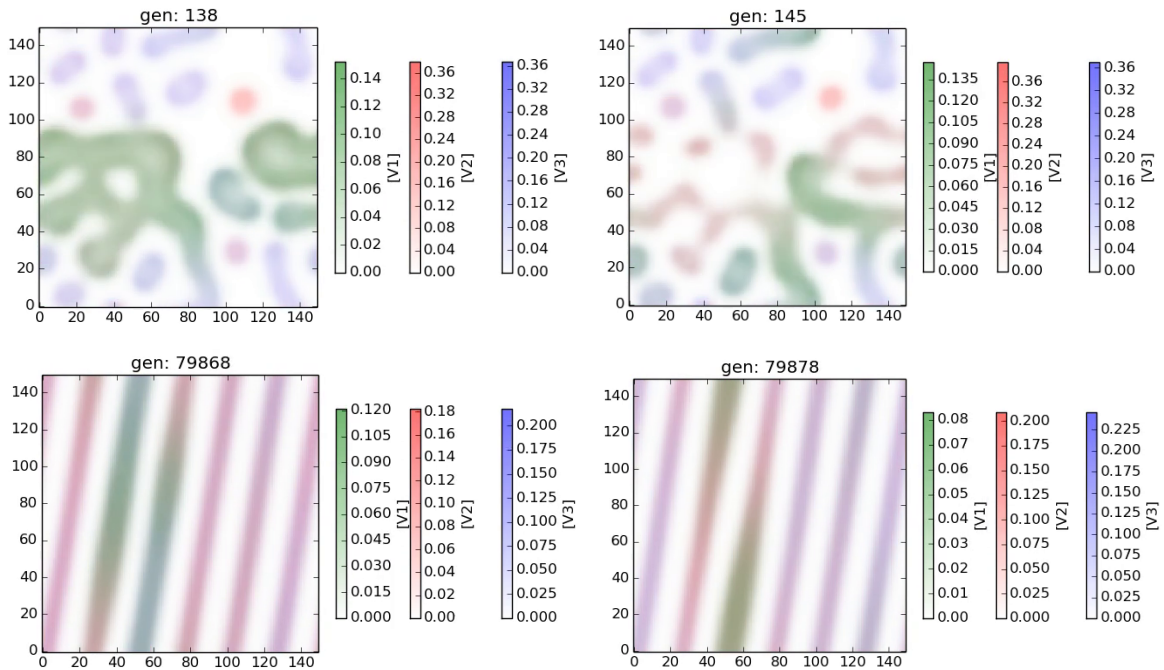


Figure 5.17: Simulation frames of a system featuring a quasi-stable compound hypercycle at early time (top row) and late time (bottom). The three species concentrations are marked with green, red, and blue, respectively. The late time pattern is a stripe that loops across the periodic boundaries and features travelling peaks of each species. In the case of v_1 this also impacts the pattern, as can be seen in the last two frames in the shape of two green-tinted bumps that move towards the upper and lower grid boundaries. These two high v_1 peaks collide and annihilate, leaving a high v_2 section behind.

A discernible feature of this system is that there are large local shifts in pattern type, depending on which species holds local concentration maximum. V_1 corresponds to the homogeneous steady state and whenever it is the dominating catalyst in a certain region the local structural feature expands and then thins as V_1 levels drop. This is distinguishable in the first two simulation frames above as the pattern shifts from spread-out green (high v_1) splotches to thinner spots and stripes.

Cycles that do not fulfil this directionality property and have one component predominantly offering catalytic support to the other two behave similarly to the unstable branched systems described in [ES78], leading to a sole survivor, although those systems do not feature backward catalytic links.

The compound hypercycle has been given less attention in the same paper, due to its improbable role in abiogenesis, though it was characterised to be generally stable (permanent). A later study [SS90] catalogued the phase portraits of concentration simplexes for a non-spatial compound 3-hypercycles. Superimposing results is not trivial and here we have the substrate availability constraint and limited replicator lifespan which might account for this restriction in network topology. There is also the complication that graph representation does not determine system phase portraits uniquely in [SS90]. Further agreement with the results in the previous reference has not been investigated. Safe to say is that strongly directional cycles (with very low back-link rates) behave essentially the same as the elementary cycles, so then the need of directionality (effectively cyclic linkage in this case) is not surprising.

However, if one considers only the reaction network formed with the dominant catalytic links and disregarding self-loops and assuming $r_{ij} \neq r_{ji}, \forall i, j$ or more generally, consider arc weights as the absolute difference of forward and backward rates and oriented in the direction of the larger of the two, this property is consistent with the necessary permanence condition for catalytic networks with $n \leq 5$ species, that they be Hamiltonian (there exists a closed directed path connecting all species exactly once) [HS87]. In particular, there is also consistency with the non-permanence of the 2-species model, i.e. considering only the dominant link (having a purely parasitic species) and assuming all other parameters equal, the network in question no longer has a directed path between all nodes. Furthermore, such a difference network would isolate species nodes for a hypercycle with equal forward and backward rates, corresponding to competing replicators, which here have been seen to lead to a sole survivor, consistent with [ES78]. Note though that the referred results were formulated for (non-spatial) ODEs featuring quadratic autocatalysis.

We also compare the properties obtained here with the analytical results stated in [BPN10] for a spatial extension of the same elementary hypercycle. These are qualitatively very similar, namely that the cycle is permanent but in addition it is shown that steady states of homogeneous concentration distribution are stable to any perturbation for large enough diffusion constants, while heterogeneous steady states have a limited form of stability (not Lyapunov stable). These results are in contrast with the patterns observed here, shown to be stable under strong noise perturbations.

The cited results were derived for networks of interacting catalysts with no fuel consumption (*replicator equations*) under a constant organisation constraint, i.e. conservation of total amount of replicators - essentially equivalent to continuously-stirred tank reactor conditions [HS99]. Here we have cubic autocatalysis with fuel consumption competition in a spatially extended compound hypercycle, which account for the difference in behaviour.

Compound pattern

A structural property of the compound hypercycle explored here is that the pattern formed at steady state is influenced by all three species. Unless they are identical, the compound pattern does not correspond strictly to any one species.

We determined experimentally that this resulting pattern corresponds to a concentration-weighted average of the three degradation rates. To put it slightly more formally, first consider the notion of *structural equivalence* between reaction-diffusion systems. We say that two such systems are structurally equivalent if the patterns they yield at steady state are equivalent. Now let the average degradation rate be given by

$$\bar{k} = \frac{\sum_{i=1}^n (k_i \cdot \int \mathbf{v}_i^* d\mathbf{x})}{\sum_{i=1}^n \int \mathbf{v}_i^* d\mathbf{x}} \quad (5.4)$$

Where n is the number of autocatalyst species with “*” denoting steady state and \mathbf{x} covers the entire system space. That is, \bar{k} is the average k_i weighted by total v_i concentrations. We now state

Hypothesis (Compound pattern rule). *A compound hypercycle with $n = 3$ autocatalysts that reaches a non-trivial steady state is structurally equivalent to a Gray-Scott system with autocatalyst having degradation rate \bar{k} and the same F .*

We use the original Gray-Scott model as reference since, with one exception discussed later, no compound pattern was obtained that could not be also obtained with the single-catalyst model. This is a phenomenological rule that was tested through a large number of simulations by letting the hypercycle systems reach steady state, then running 1-species Gray-Scott simulations with a catalyst having $k = \bar{k}$ until steady state. The patterns always matched.

The above rule can be made less strict if we consider that some permanent cycles reach a periodic orbit in which, although species levels fluctuate, the pattern stays either unchanged or slightly wobbles. In the former case, the rule still holds and in the latter, one could talk about a time average of pattern shape that still obeys the rule.

This rule might also be said to hold as a function of time for small regions containing one structural feature, as was observed for many of the simulations performed. The local ratio of concentrations is reflected in these local patterns. Illustrations are the quasi-stable hypercycle considered previously and systems in the next section. To put it more formally, for such systems there exist non-void subregions Ω of system space and time intervals (t_1, t_2) such that we can define $\bar{k} = \bar{k}(\Omega, t)$ and instead of summing concentrations globally at steady state we do so for these small regions for every time instant in the intervals, i.e. replace integrals above with $\int_{\mathbf{x} \in \Omega} \mathbf{v}_i(t) d\mathbf{x}$ and hold for $t \in (t_1, t_2)$. The relevance of looking at this time dependence is the continuous and sometimes long-lived shifts in patterns that occur before steady states.

Another amendment to the above rule is that it generally holds if species appear sequentially in the system. As we shall see, a novel pattern that does not obey this relation was found for a narrow range of parameters when starting from a mix of all species. We leave the hypothesis statement in a less encumbered form however since the vast majority of systems obey it as such.

5.4 Dynamic patterns

As we have seen in previous sections, the compound hypercycle model exhibits local pattern shifts after the third species is introduced, which go on while diminishing until close to steady state or periodic orbit. This period of pattern change becomes longer as the forward and backward catalytic links get closer in value and may even persist to infinite time for weakly directional cycles.

As such, one could say that these cycles yield *dynamic patterns* composed of structural features that periodically shift between pattern types, as peaks of species concentration travel across the system space (and shift the local \bar{k}). This is different from the original Gray-Scott pattern time evolution, where the behaviour is still exhibited by the same pattern class, whereas here all classes between k_{min} and k_{max} for a fixed F may appear in the system. And since a subset of cycles stays away from steady state for significant periods of time, the pattern alterations become more relevant, as they characterise the overall behaviour of the system.

The quasi-stable hypercycle in the previous section is one example of this behaviour. Even at very long times, periodic local alterations of pattern shape occurred as a function of species levels. Below are a few other examples of such dynamic patterns.

We underline that it is the compound nature of the cycle, featuring close forward and backward catalytic links that allows for this behaviour to emerge. A one-way (elementary [ES78]) hypercycle would very quickly converge to steady state. It was however seen in various simulations that a single weakly directional link was sufficient, acting as a kind of “bottleneck” for the catalytic chain. Also, as may be obvious, the degradation rates of the three species need to be sufficiently far apart for noticeable shifts in pattern type to occur along with concentration fluctuations.

Simulation 1: pulsating spots

Here are cycle parameters that yield pulsating non-dividing spots for very long times, followed by animation frames showing the evolution of the system. The length of a generation was set at the specific length $\lceil \frac{LN}{\Delta t^2} \rceil$.

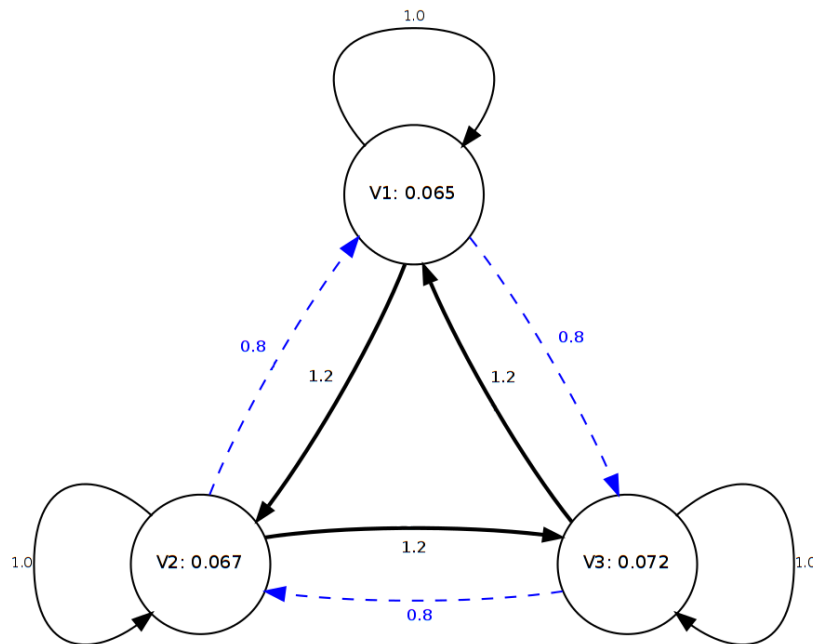


Figure 5.18: Diagram of a weakly directional compound hypercycle that forms a pattern made up of pulsating spots. Replication rates \mathbf{r} obey Constraint 3. The fuel feed rate is $F = 0.04$. Alone, V_1 corresponds to dividing spots, V_2 to non-dividing (stable) spots, and V_3 falls outside the pattern-forming region, in the trivial extinct state.

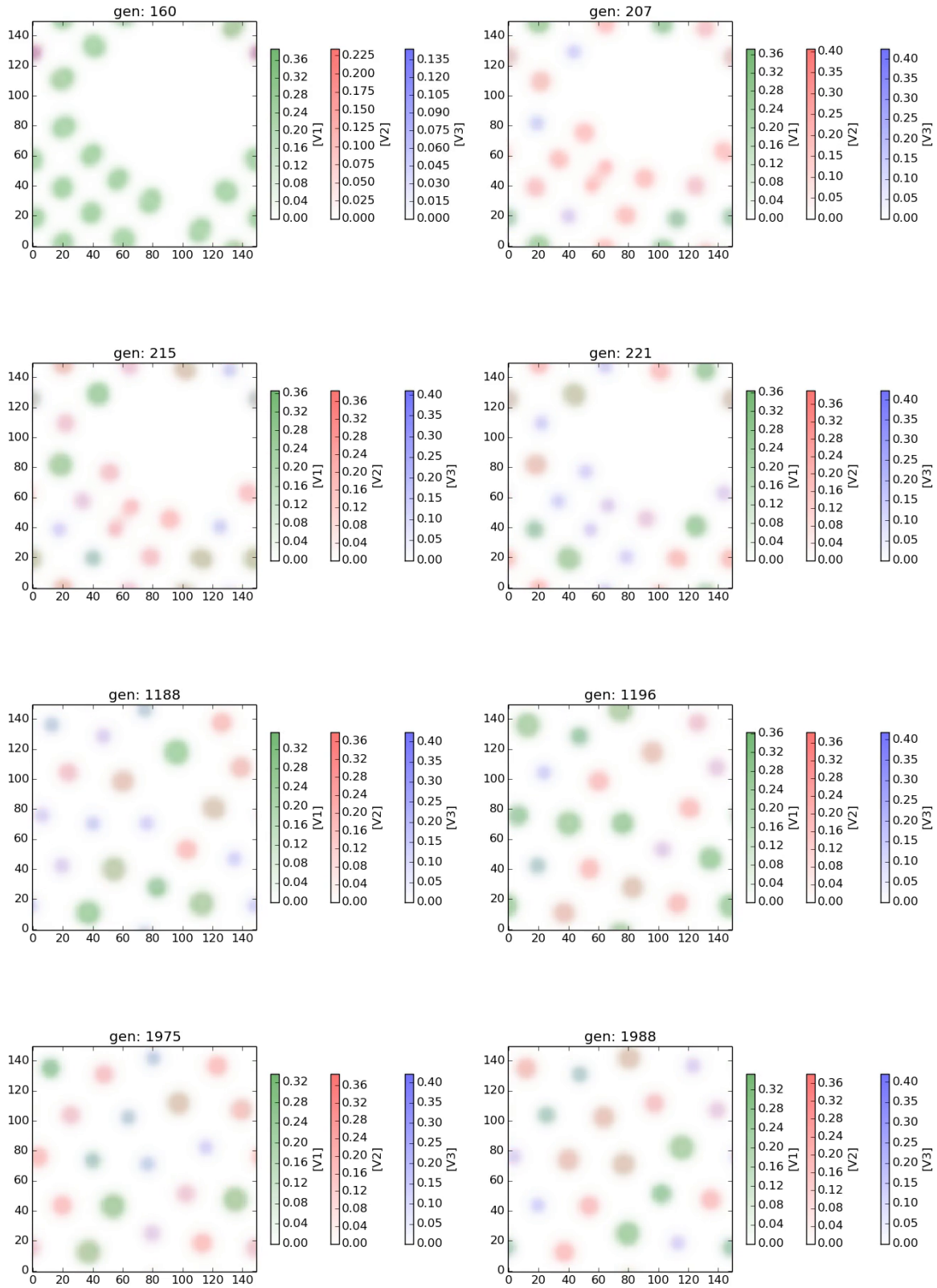


Figure 5.19: Simulation frames showing pulsating spots. At generation 160, all three species are present but not have not yet spread and are confined largely within one spot, situated around coordinates (5, 100). The compound pattern is still dictated by V_1 (dividing spots) but after approximately 40 generations, after more clusters host all species, oscillation in catalyst levels start, leading to change in spot size. High- v_3 spots are of smallest size, the largest are high- v_1 (green) and high- v_2 are of intermediate size. The transition between peak concentrations is reflected by the change in size. Division occurs more rarely and stops quite early, when V_3 levels are low. The last division ends after gen. 215 at coord. (60, 50). The remaining space is filled by translation of the surrounding spots.

As can be seen from the frames above, once all three species are present in the system, a process of concentration and consequently size oscillation begins and continues for a very long time, at largely the same amplitudes. Since V_3 falls inside the “dead” state, whenever it achieves peak concentration inside a spot (while the other two species are at minimum), the spot shrinks as it starts to degrade but is saved by increasing V_1 levels which, due to the dividing nature of its corresponding pattern, increases spot sizes to their largest extent, then followed by V_2 peaking, which reduces radius since they fall within the stable, non-dividing pattern regime. The spots follow the pulsating pattern of green-red-blue, i.e. local $v_1 - v_2 - v_3$ maxima.

Simulation 2: merging and dividing stripes

Here is an example of dynamic pattern featuring stripes that thin out, break apart and subsequently merge back together with a certain regularity. The length of a generation was set at the specific length $\lceil \frac{LN}{\Delta t^2} \rceil$. For this system, the simulation was started from a randomised mix of all species.

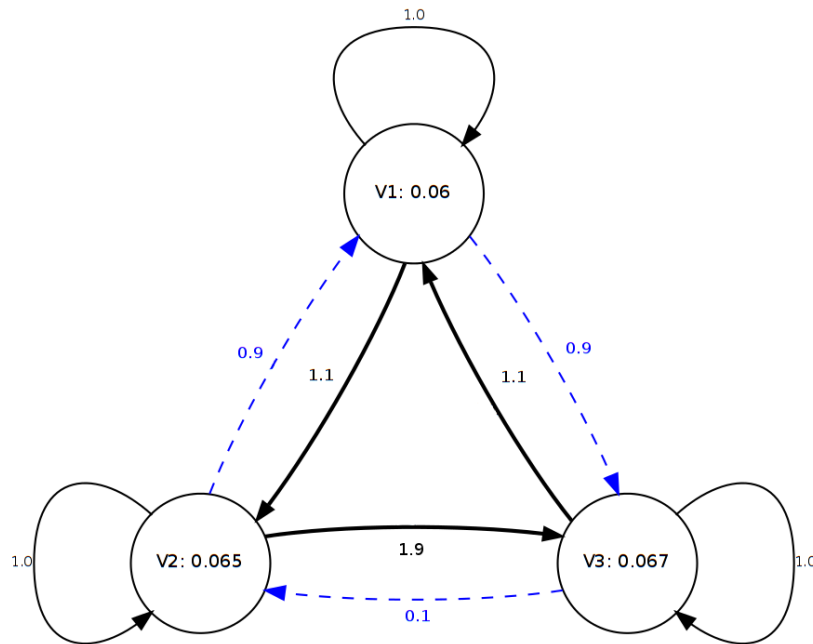


Figure 5.20: Diagram of an overall weakly directional compound hypercycle exhibiting patterns of dividing and merging stripes. Replication rates \mathbf{r} obey Constraint 3. The fuel feed rate is $F = 0.04$. Alone, V_1 corresponds to stripes, V_2 to dividing spots, and V_3 to stable (non-dividing) spots.

Note that the link between V_2 and V_3 is strongly directional $r_{23} \gg r_{32}$. However, this does not change the behaviour and since the initial conditions were a complete mix of catalysts, the system quite quickly reaches a periodic orbit. Below are frames that show the shifting nature of the compound pattern.

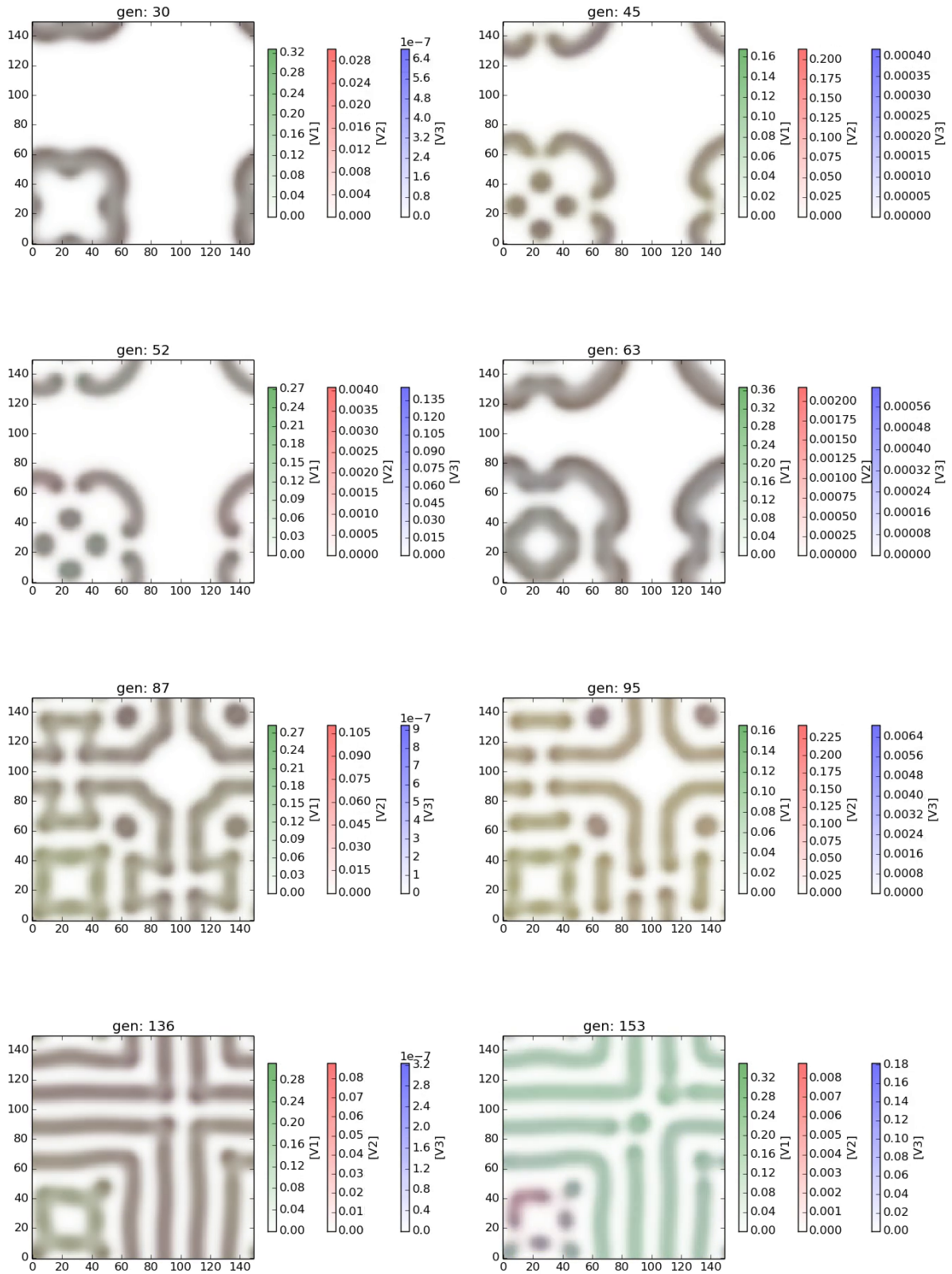


Figure 5.21: Simulation frames showing a dynamic pattern of stripes and spots, starting from a small region containing a mix of all species. The compound pattern first manifests itself as an outward-extending wave, with smaller waves breaking off in its wake and travelling inwards. At about generation 45 the wave stops advancing and the broken off inwards waves shrink to spots. The pattern holds steady in place until about gen. 52, when all its features suddenly start enlarging and merging (gen. 63). Subsequently the wave fronts advance and meet themselves across the periodic boundary, forming a pattern made up mostly of stripes (gen. 87). Due to species fluctuations, this pattern experiences episodes of shrinking and fragmentation followed by engorgement and merging, as seen in the last two time intervals (gen. 87-95, gen. 87-95). The system settles in a stripes-only pattern but still experiences smaller shape transitions up to the end of the simulation, at 1000 gen.

Simulation 3: dynamically dividing spots

The pattern presented here is an interesting counterpart to the dividing spots manifested by the original Gray-Scott model. These compound spots only occasionally divide, when autocatalyst levels reach certain levels. Below are the parameters and animation frames.

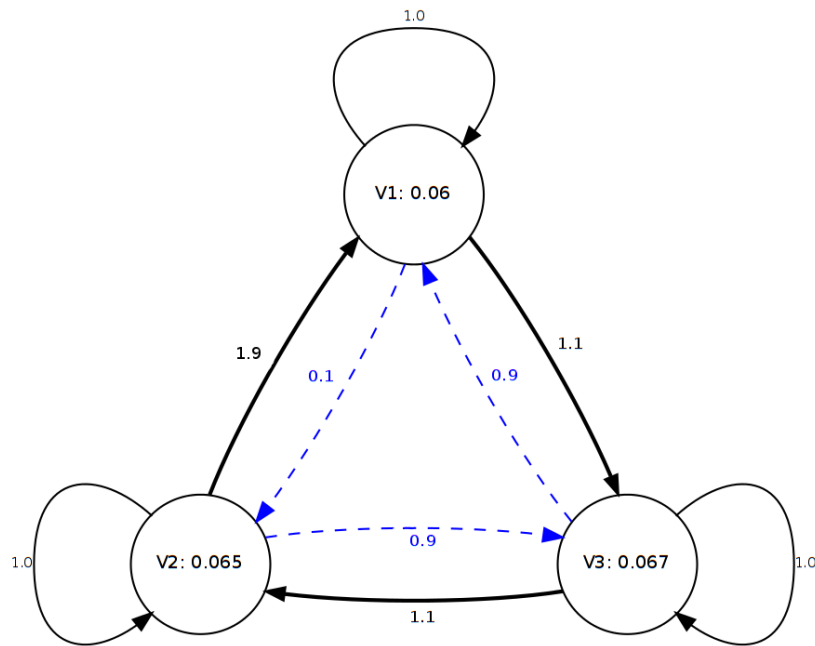


Figure 5.22: Diagram of an overall weakly directional compound hypercycle exhibiting patterns of occasionally dividing spots. Replication rates \mathbf{r} obey Constraint 3. The fuel feed rate is $F = 0.04$. Alone, V_1 corresponds to stripes, V_2 to dividing spots, and V_3 to stable (non-dividing) spots.

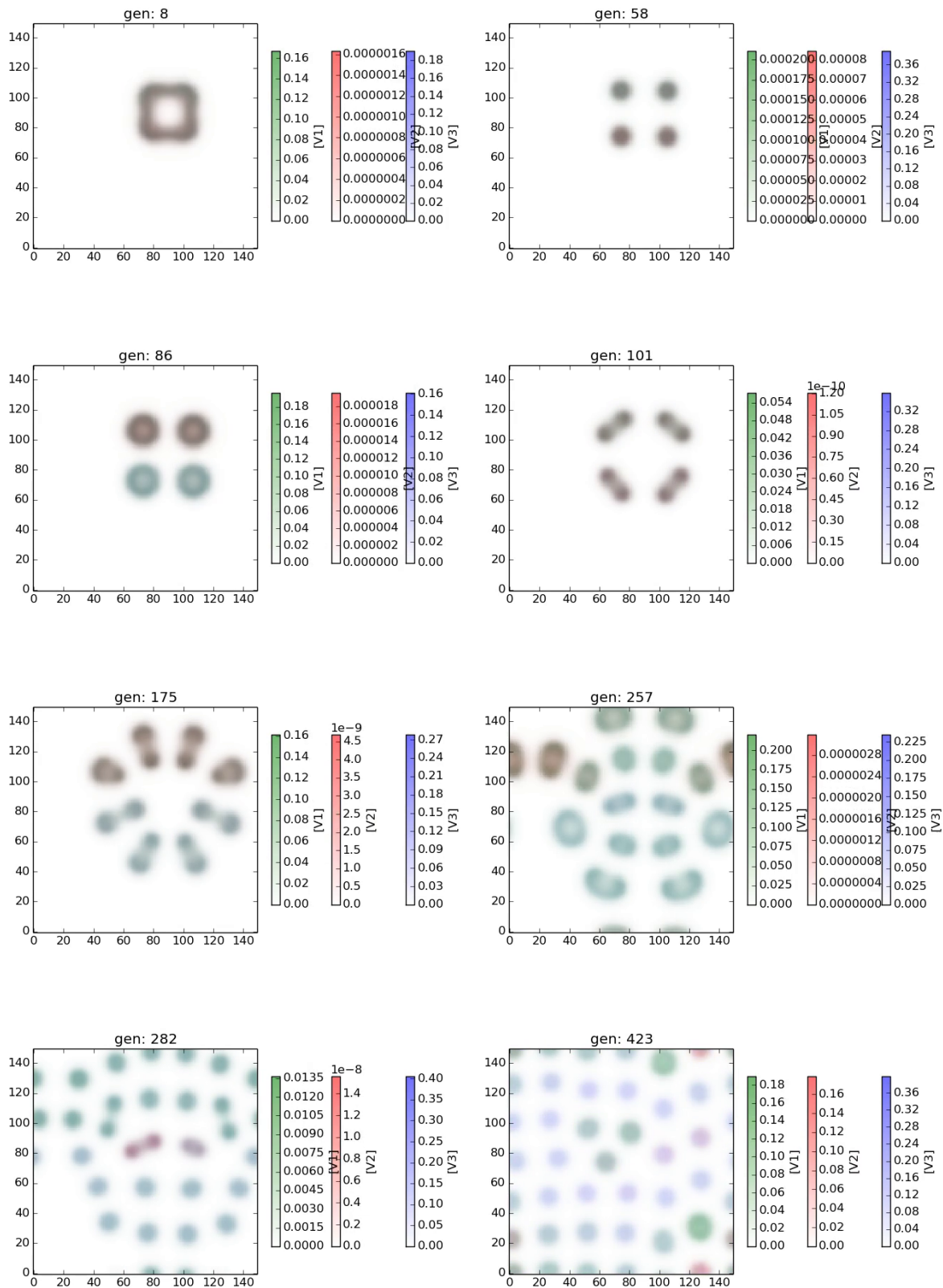


Figure 5.23: Simulation frames showing a dynamic pattern of occasionally dividing spots, starting from a small region containing a mix of all species. The compound pattern first manifests itself as an outward-extending wave that breaks up into 4 spots that remain stationary for about 50 generations, after which, as V_2 levels rise, it undergoes division that completes at about gen. 110. The 8 new spots remain largely stationary and only undergo the same spontaneous division around gen. 170, after which the pattern is once again almost immobile. The next division event occurs at about gen. 250 but it is interesting to note that the spot near coordinates (105, 85) reverts its division and merges back because there isn't enough catalyst-free space around it. After the space has been filled, the spots begin to have faster concentration oscillations, as can be seen from their alternating coloration.

The dividing spots regime of the Gray-Scott model has been likened to cellular division but perhaps this class of hypercycles is closer to the mitosis mechanism in that it features a chemical clock besides the requirement of favourable environment conditions (here, catalyst-free and fuel-rich space around the spots), although mitosis in real cells is irreversible once initiated, in contrast with the behaviour exhibited here. As can be seen from the concentration plots below in conjunction with the animation frames above, division occurs only when the oscillating catalysts reach certain levels. In particular, the spots do not divide most of the time, when v_3 levels are relatively high but do so when there is an increase in v_2 (which by itself corresponds to dividing spots), followed by an increase in v_1 and sharp drop of v_3 .

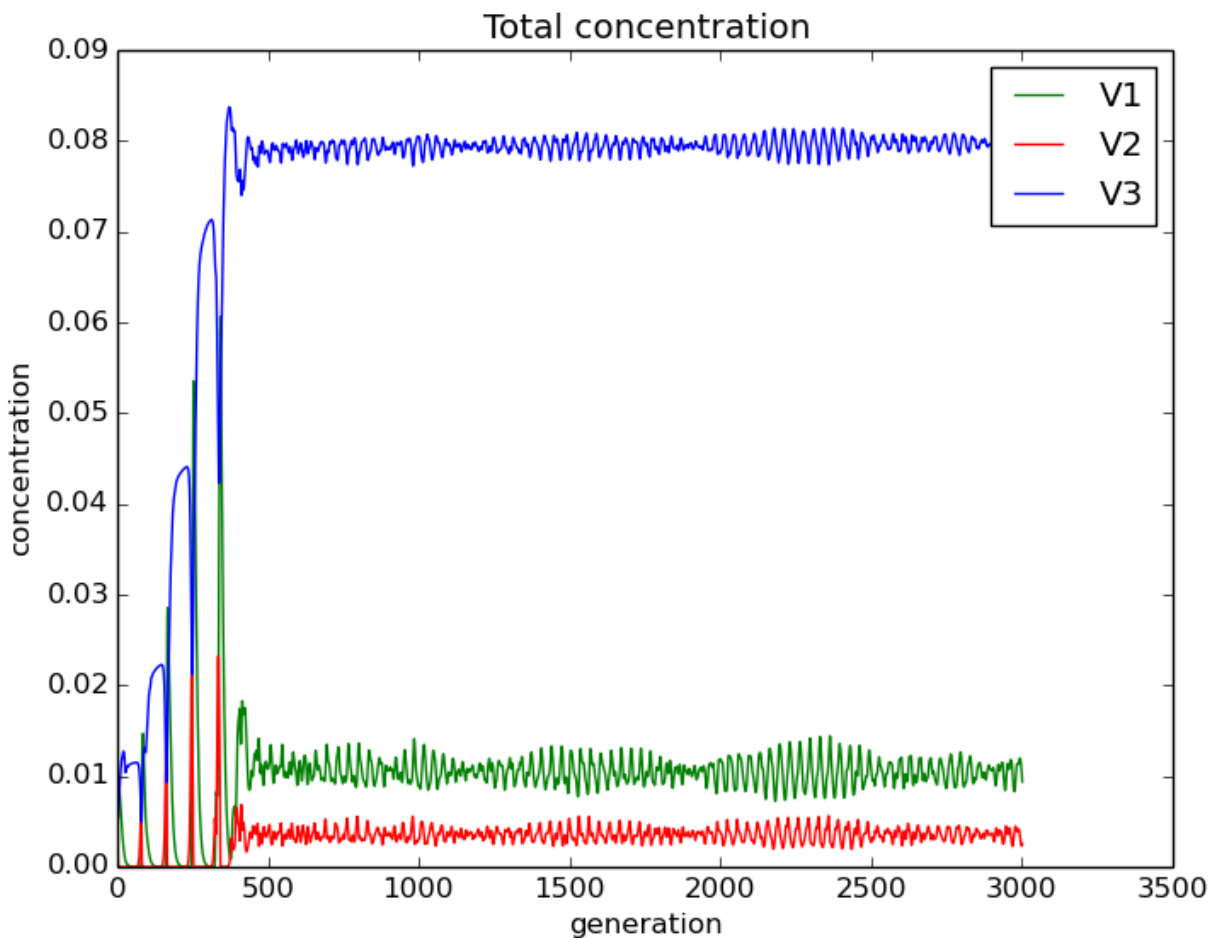


Figure 5.24: Total species concentration (normalised over grid size) of a compound hypercycle manifesting occasionally dividing spots. The generation length was $\lceil \frac{LN}{\Delta t^2} \rceil$ iterations. Up to gen. 400, the spots divide in 4 episodes, corresponding to the sudden deep drops in v_3 (left portion of the plot, close to generations 80, 160, 240). Once they take up the entire system space, the concentration levels quickly settle into an orbit.

5.5 Novel pattern: expanding loop

In this subsection we present an example of compound pattern that could not be equated to any Gray-Scott structure. It is the only novel pattern found in this study and presents some interesting properties.

The structure manifests as a loop that only expands occasionally but which does not break up as in similar Gray-Scott patterns. After it approaches itself over the periodic boundary, a long period of slight adjustments to its shape starts, which bring the pattern to a stable space-filling optimum. Below are the parameters and time evolution of the first case found of this pattern.

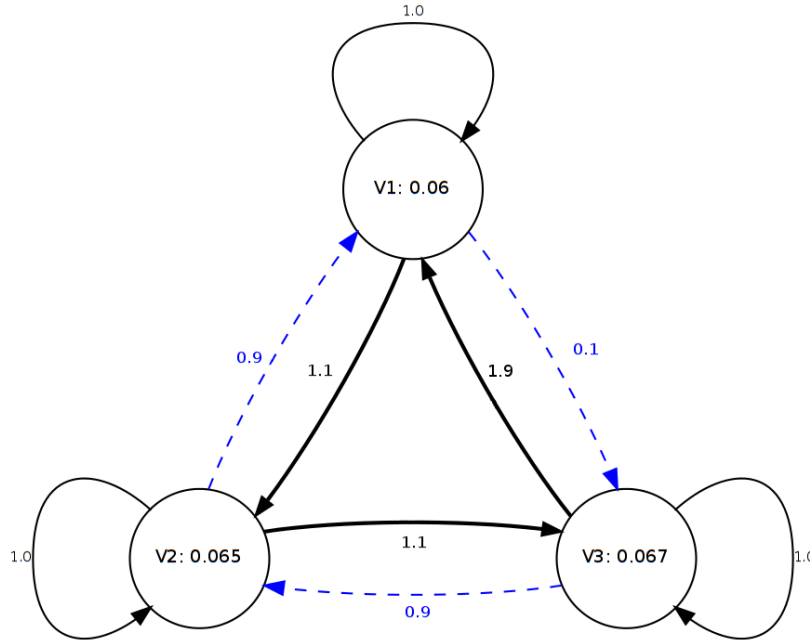


Figure 5.25: Diagram of a novel loop-yielding compound hypercycle. Replication rates \mathbf{r} obey Constraint 3. The fuel feed rate is $F = 0.04$. Alone, V_1 corresponds to stripes that extend and stop at a critical separation when colliding (Pearson θ), V_2 corresponds to dividing spots (Pearson λ), and V_3 to stable (non-dividing) spots (outside Pearson λ , at higher k). As far as directionality goes, the cycle is mostly weakly directional.

The simulation was run to very long times, $5 \cdot 10^4$ generations, with one generation set at $\lceil \frac{LN}{\Delta t^2} \rceil$ iterations. The initial conditions consisted of a perturbation of 20×20 grid cells (1.77% of the grid), containing a mix of all species, with the same concentrations as in all previous simulations before randomisation, i.e. $u = 0.5$, $v_i = 0.25$ in the perturbation and $u = 1$, $v_i = 0$ everywhere else. To better show the behaviour of this pattern we split the frames into the early, expansion period and the later, space-filling period.

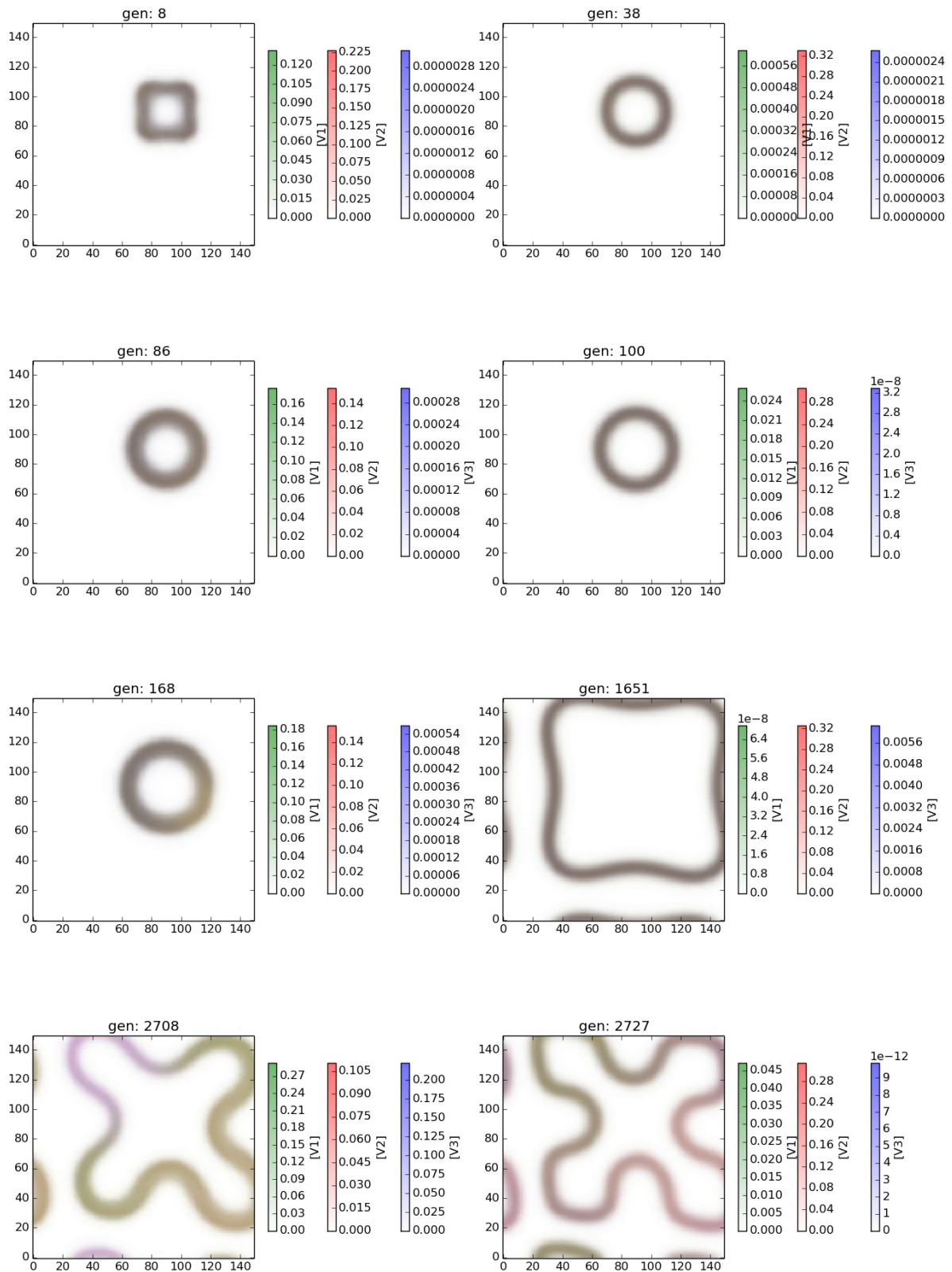


Figure 5.26: Simulation frames showing the loop pattern in its early expanding phase. The pattern first manifests itself as an outward-extending wave but quickly recedes, taking the shape of a symmetrical stationary ring (top row). This shape is retained perfectly for about 50 generations, after which species levels fluctuate and the ring expands in a single growth spurt that lasts about 20 generations, remaining again perfectly stationary afterwards (second row). These expansion events continue but after the ring meets itself the shape changes, with sections expanding inwards, as can be seen in the bottom row that depicts the loop before and after an expansion event.

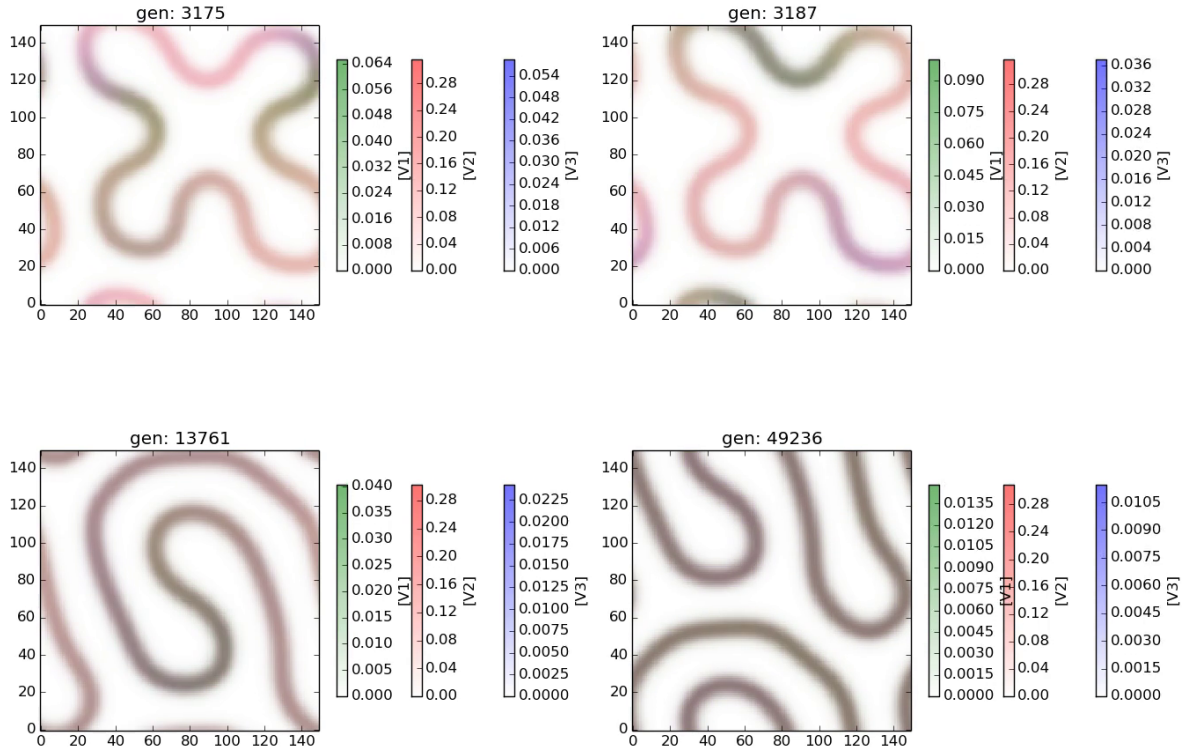


Figure 5.27: Simulation frames showing the loop pattern in its later, shape-adjusting period. After gen. 3000, there are no more spontaneous expansion events but only very slight changes in loop shape. Concentration fluctuations are more frequent and of larger amplitude, and can be seen as travelling peaks along the loop (top row). These slight shape alterations continue until the final pattern is reached some time after gen. $1.3 \cdot 10^4$, after which the loop only translates across the periodic boundary (bottom row).

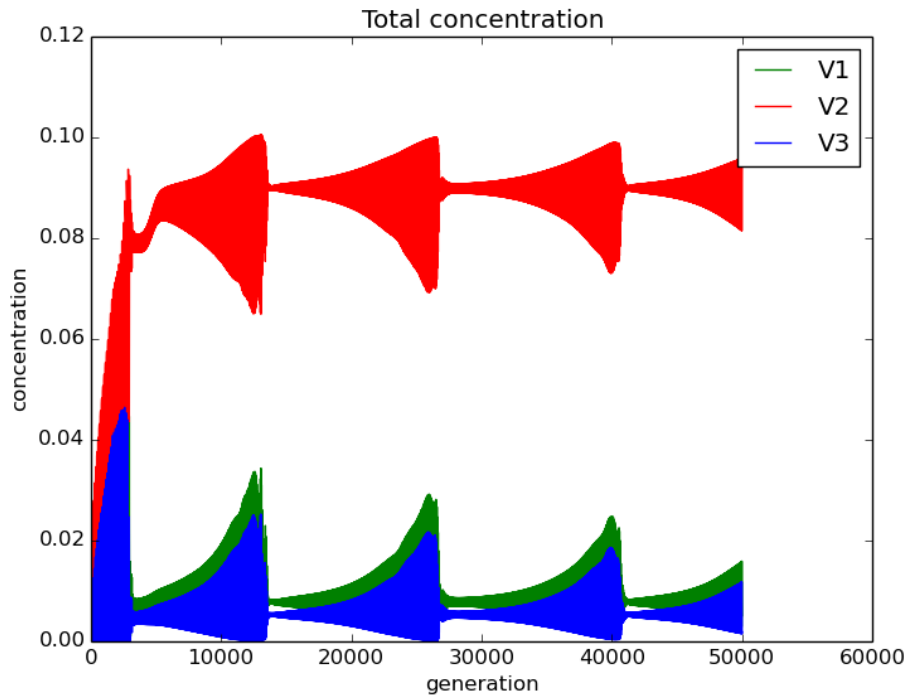


Figure 5.28: Total species concentration (normalised over grid size) of the expanding loop-yielding compound hypercycle. The generation length was $\lceil \frac{LN}{\Delta t^2} \rceil$ iterations. The expansion period featuring episodic growth events lasts until about gen. 4000 and is marked by an increase in pattern coverage but with occasional large changes in species levels. After this interval, the species transition to oscillations around the same mean value. These oscillations have periodic increases in amplitude but the maximum amplitudes reached appear diminishing and the species concentrations are expected to reach a periodic orbit at $t \rightarrow \infty$.

While similar to other patterns made up of loops in the Gray-Scott model (e.g. patterns in $k \in [0.061, 0.063]$ for $F = 4$, see the pattern phase diagram), the essential difference with this structure is that it does not split as it grows and does not break apart or merge sections when meeting itself. Nor does the loop sprout stripes from bends like e.g. the $(k, F) = (0.063, 0.062)$ pattern. An important remark is that this pattern is an exception to the structural equivalence rule stated in the previous section. Towards steady state, the weighted average is $\bar{k} \approx 0.0647$, which corresponds to dividing spots. This was the sole exception to the rule found in this study. This holds even when a few loops are allowed to form, each of these remaining separate while adjusting shape, as shown below. This system has the same parameters as the previous one but with three 20×20 cell initial randomised perturbations.

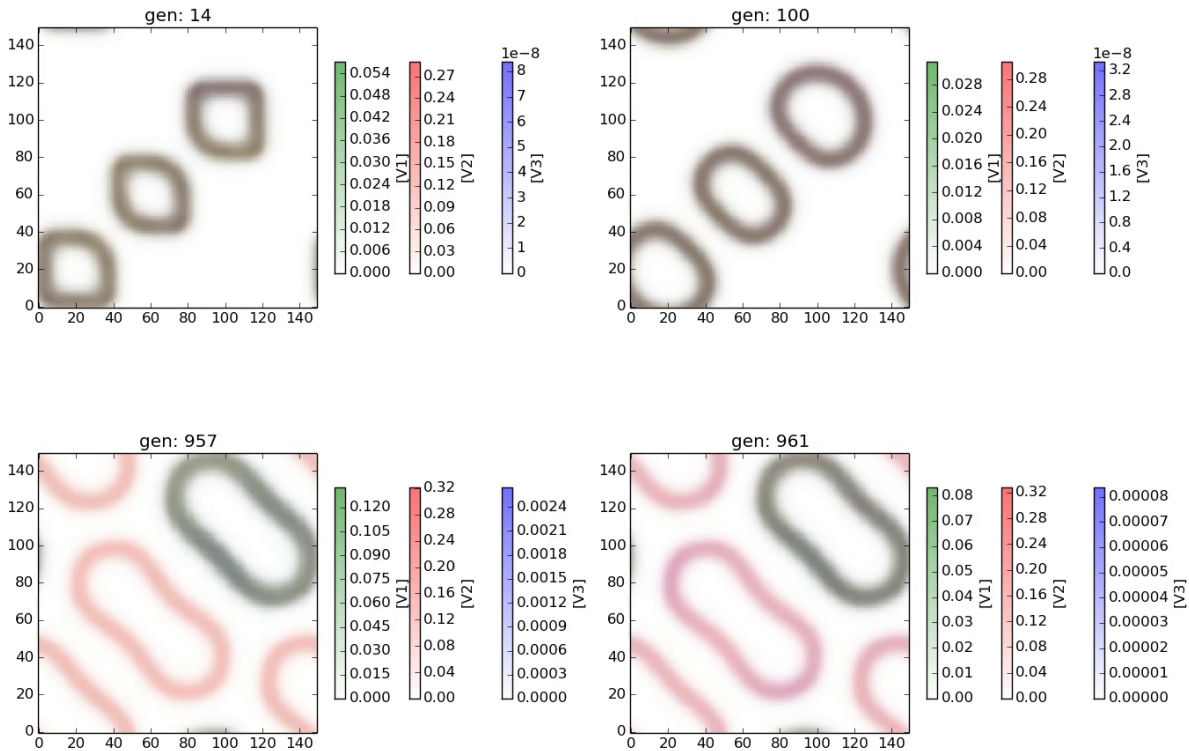


Figure 5.29: Simulation frames showing the expanding loop-yielding system with three loops present, formed from three initial randomised perturbations. Until about gen. 700, the entire pattern is in the expansion phase, featuring occasional growth episodes. Afterwards, while the shapes undergo slight alterations, concentrations start to oscillate with higher frequency around the same mean values, as can be seen by the varying colours of each loop.

The systems featuring multiple loops behave in essentially the same way. The only change is that in the later adjustment period, as the concentrations fluctuate, each loop holds approximately the same species levels and appear as having the same colour. With a single loop, peaks of a single species would visibly travel across its length.

It turns out however that this pattern is quite sensitive to initial conditions: if the initial perturbation holding the mix of species covers a too small or large area, the loop breaks up and the end structure follows the compound pattern rule in the previous section. If the initial mix covers a small area (e.g. 5×5 cells), it forms dividing spots immediately, whereas a mix covering more than 4% of the grid breaks into a shrinking stripe and spots. In both cases, the steady states consists only of spots. Moreover, if too many initial perturbations are placed the forming loops will touch and break apart, resulting in the same end pattern.

Through simulations it was determined that the size of an initial perturbation must lie within $[1, 4]\%$ of the total grid area for it to form a loop. It is also critical that the system start with a mix of all three species; sequential placement through mutation events does not yield stable loops but conforms to the compound pattern rule.

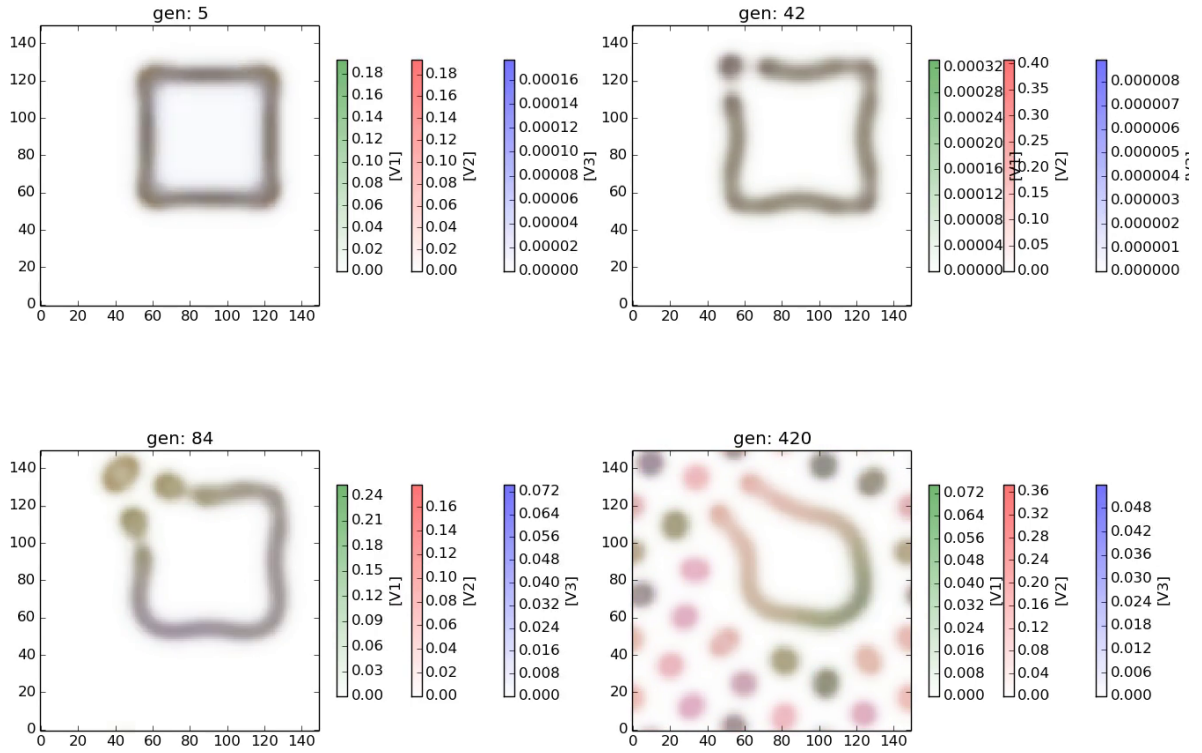


Figure 5.30: Simulation frames showing the expanding loop-yielding system started from a large initial perturbation covering 60×60 grid cells. The wave first formed is not able to retract and form a ring but breaks into a long stripe and a single spot (top row). This spot starts dividing occasionally, when v_2 levels are high (bottom row) while the loop begins slowly shrinking, with spots detaching from its ends either permanently or temporarily (the stripe occasionally swells and reconnects). Ultimately, the pattern will feature only spots.

We have also tried combining starting patterns to see how the stable loop interacts with other structures and found that it becomes destabilised by these and breaks apart. Below are a few frames illustrating this behaviour. Since we could get different starting patterns by setting the initial perturbations sizes, we placed two such mixes initially: once which would yield a loop and a smaller one that would result in dividing spots.

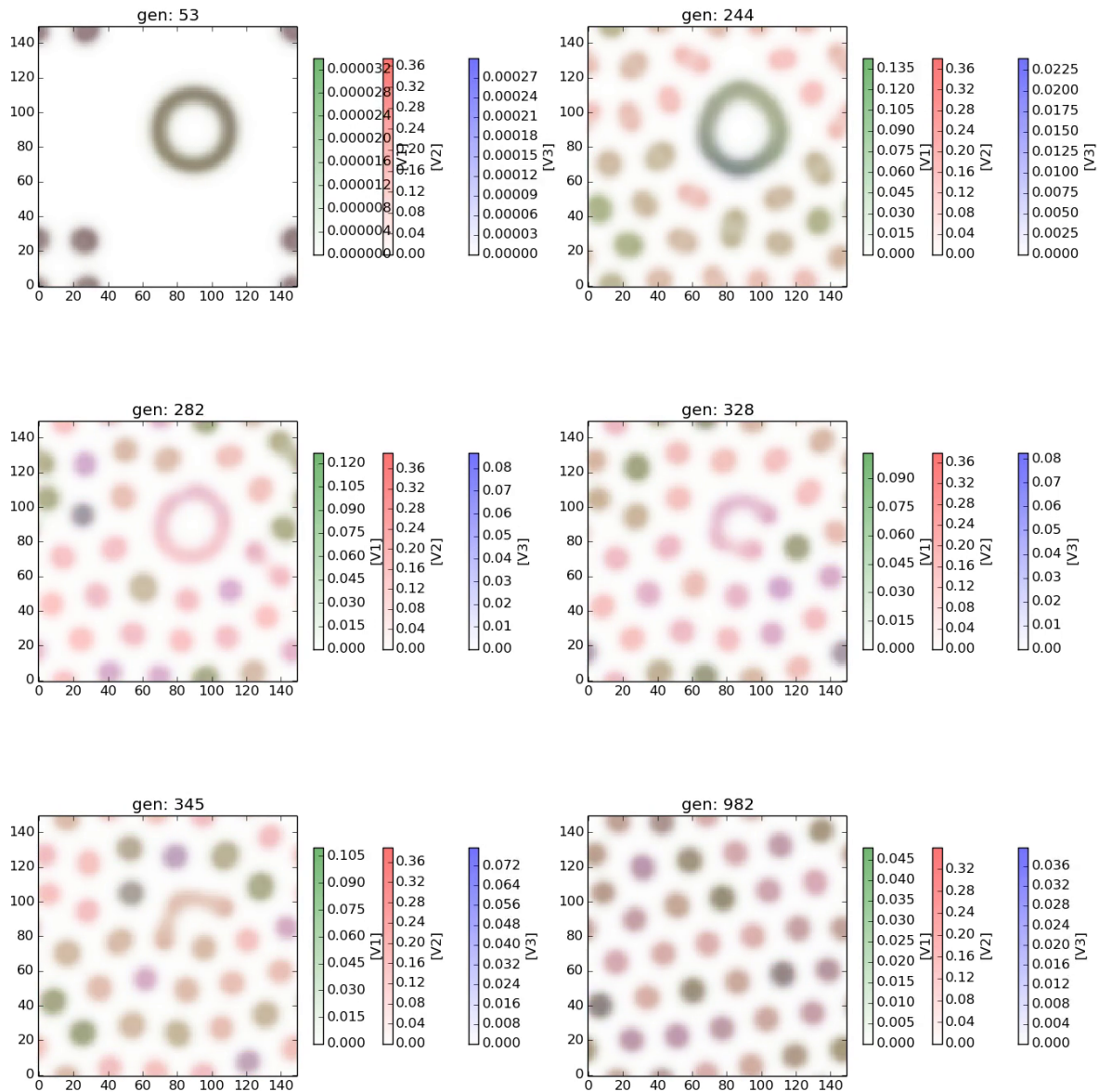


Figure 5.31: Simulation frames showing the interaction of two patterns manifested by the loop-yielding system. The initial conditions consisted of two perturbations of sizes 5×5 and 20×20 containing a mix of all species. The smaller pattern breaks up and forms dividing spots which starts “squeezing” the loop, also causing frequent concentration oscillations within it (which would normally only appear at late times). After 300 generations, the loop breaks up into spots.

We now return to the simple experiment presented at the start of this section to point out another interesting feature of this compound pattern, namely that it exhibits different types of dynamics during its existence. As was pointed out earlier, the pattern’s time evolution is divided in two intervals, called for convenience *expansion* and *space-filling* periods.

We take a closer look at the oscillations during these periods and measure the time between expansion events. Technically, we measure the wavelength (inter-peak distance) of the v_2 curve as a function of time for ease of (visual) inspection. Precisely, these peaks correspond to shortly *before* the events, which start with a sharp drop in V_2 levels and increase of the other two.

Below is the concentration evolution during the expansion period of another run of the simulation first presented in this section. While the exact length of this period varies slightly between simulations due to the initial randomisation, its shape is essentially the same.

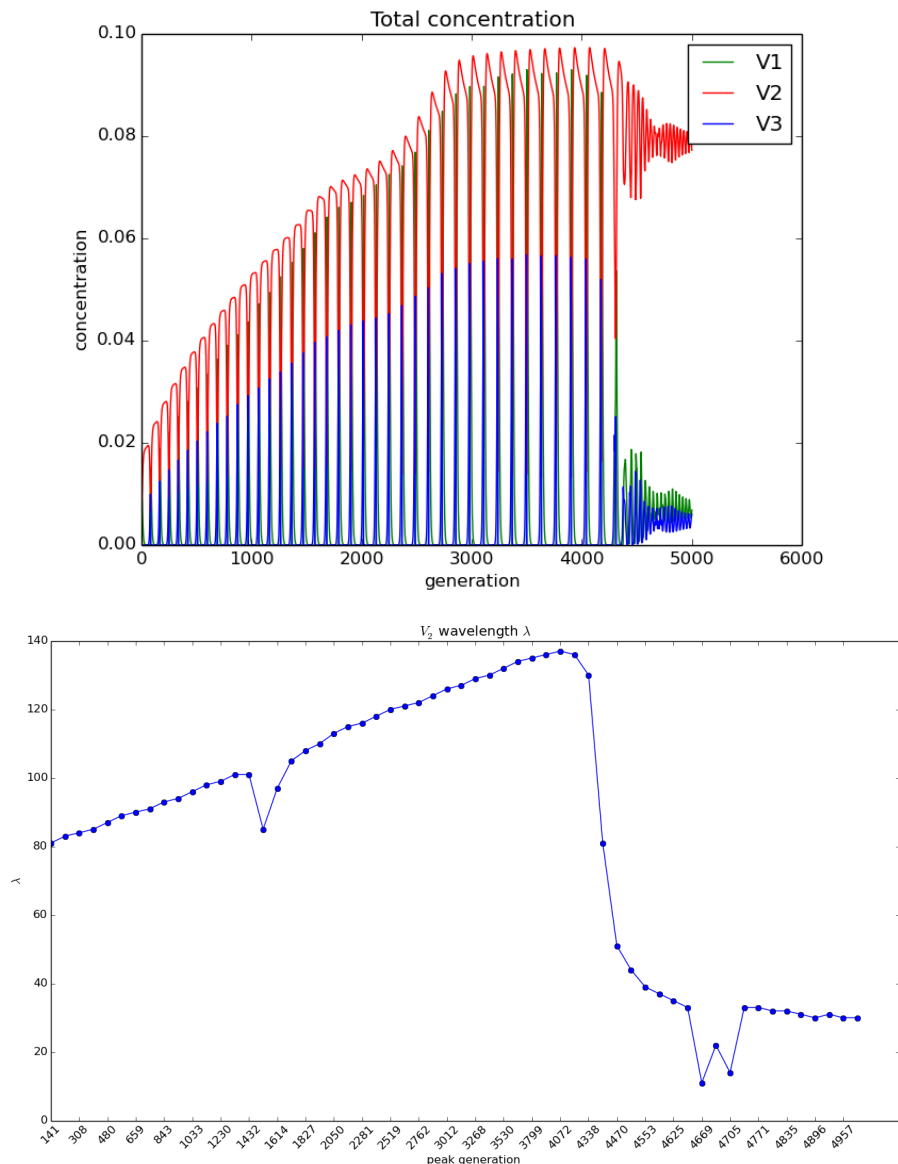


Figure 5.32: Total species concentration (normalised over grid size) of the expanding loop-yielding compound hypercycle (top) and the inter-peak distance (wavelength) of the v_2 curve (bottom), spanning the early expansion period and the start of its space-filling period. The abscissa of the wavelength plot marks the generation of v_2 peak i , starting from $i = 2$, and the ordinate the number of generations from the previous peak $i - 1$. The generation length is $\lceil \frac{LN}{\Delta t^2} \rceil$ iterations.

We see from the above plots that during this early period, the time between expansion events gradually increases. When the loop stops experiencing these spontaneous increases, v_2 's wavelength seems to go towards a constant value. This evolution was seen to be consistent across all simulations run. As perhaps a simple curiosity is that the kink seen in the steadily increasing wavelength slope was found in most of these simulations. It coincides with the moment the loop starts bending inwards after just meeting itself shortly before.

We now look at the long-term oscillatory behaviour of the system for a longer run of the same simulation (but with different random seed). We can see that as $t \rightarrow \infty$, the system finds itself on an orbit. This experiment doubles in that it also confirms the state ultimately reached ($1.5 \cdot 10^5$ generations here).

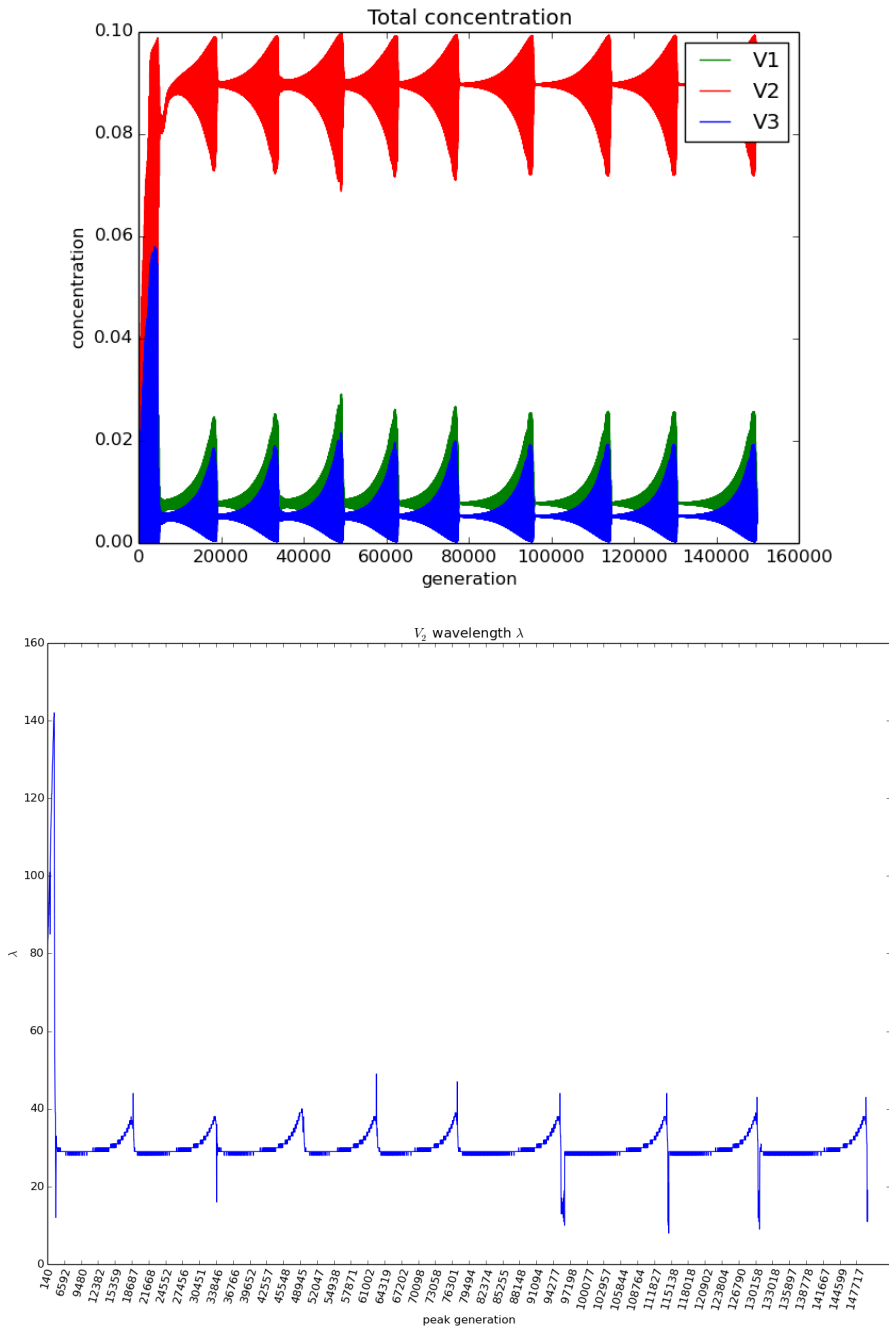


Figure 5.33: Total species concentration (normalised over grid size) of the expanding loop-yielding compound hypercycle (top) and the inter-peak distance (wavelength) of the v_2 curve (bottom), spanning the entire duration of the simulation. The abscissa of the wavelength plot marks the generation of v_2 peak i , starting from $i = 2$, and the ordinate the number of generations from the previous peak $i - 1$. The wavelength spikes in the later oscillatory mode that starts after gen. 5000 coincide with the periodic increases in v_2 amplitude seen in the top concentration plot. The generation length is $\lceil \frac{LN}{\Delta t^2} \rceil$ iterations.

After the expansion period ends, the internal dynamics of the pattern is marked by v_2 oscillations of largely constant wavelength, with periodic spikes of increased inter-peak distance that correspond to the periodic increases in amplitude.

We have also looked at the stability of the loop when subjected to short periods of strong noise. It was observed that the pattern is resistant to these and does not break up, but that a third oscillation mode is induced by the perturbation, characterised by a higher frequency of expansion events.

To illustrate, we ran the same simulation (with a different random seed) for only 5000 generations, covering the expansion period. From generation 1000 to 1020, the system was subjected to strong noise $\bar{\lambda} = 1$. We only show the concentration and wavelength plots, since beside visible speckling during the noise event and slight concentration fluctuations, no essential difference in pattern shape is observed.

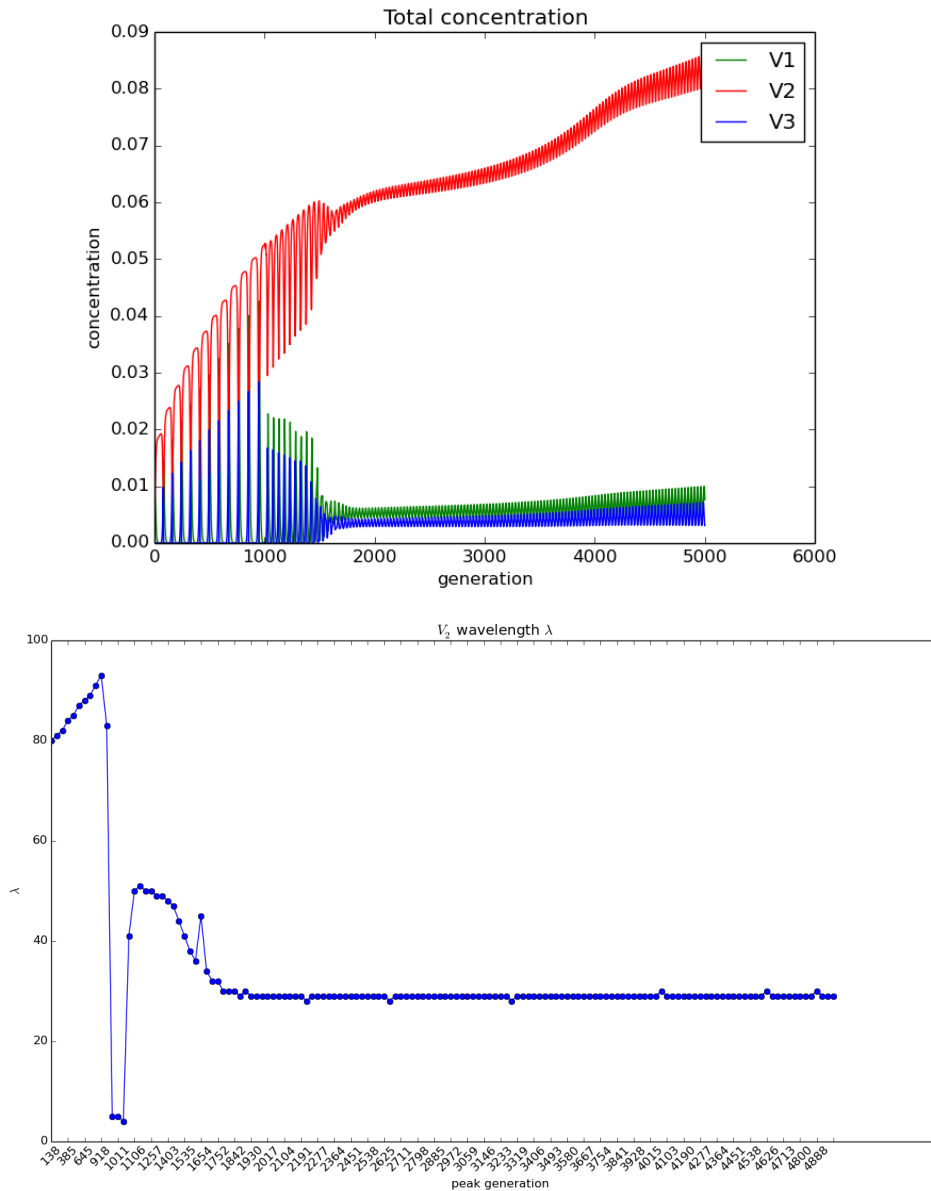


Figure 5.34: Total species concentration (normalised over grid size) of the expanding loop-yielding compound hypercycle (top) and the inter-peak distance (wavelength) of the v_2 curve (bottom), spanning the early expansion period and the start of its space-filling period. The system was under strong noise ($\bar{\lambda} = 1$) for 20 generations starting at gen. 1000, followed by a visible increase in oscillation frequency. The generation length is $\lceil \frac{LN}{\Delta t^2} \rceil$ iterations.

We see that strong noise induces transition from one oscillation mode to another. This happens irrespective of the duration of noise presence. Once the system is thus perturbed, it enters a faster expansion mode with decreasing time intervals between spontaneous loop enlargements. This can be seen in the wavelength plot above, where initially the time between events steadily increases until generation 1000. After the sharp drop in v_2 inter-peak distance caused by the random fluctuations under noise, the time between the expansion events starts to decrease and this period ends quicker, at about 1800 generations.

This fast expansion mode was seen to be stable with respect to subsequent noise events, the overall shape of spontaneous enlargement frequency having the same shape, barring the spikes caused by the noise. The behaviour is shown in the plots below, in a case with two noise events (though the evolution is identical when more occur).

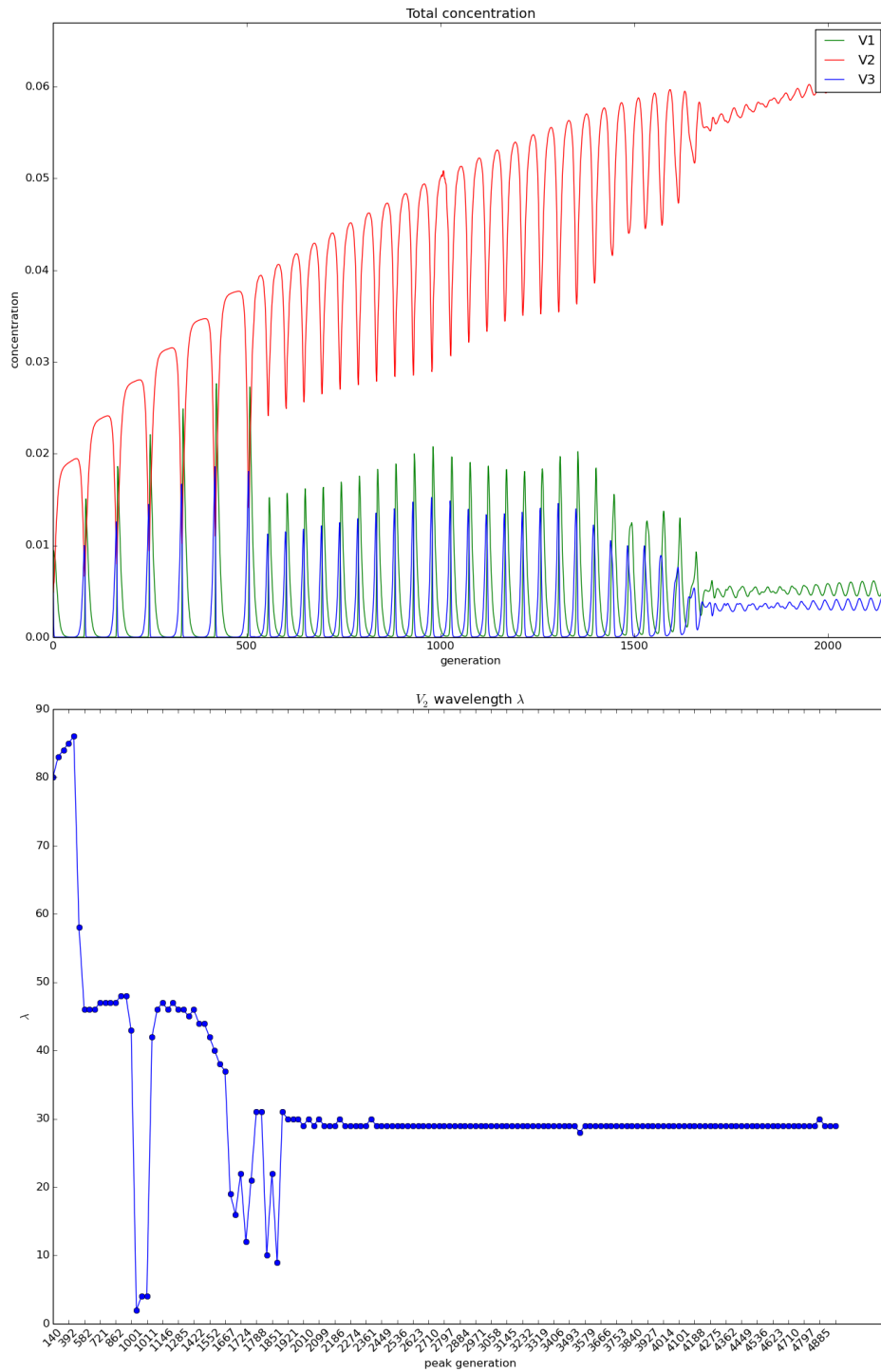


Figure 5.35: Total species concentration (normalised over grid size) of the expanding loop-yielding compound hypercycle (left) and the inter-peak distance (wavelength) of the v_2 curve (right), spanning the early expansion period. The system underwent two strong noise perturbations at gen. 500 and 1000, each lasting 20 generations. The markedly different modes are distinguishable before and after the first noise perturbation in the left plot, with the fast expansion mode unaffected by the second noise event. The generation length is $\lceil \frac{LN}{\Delta t^2} \rceil$ iterations.

We sought to explore the extent of this pattern’s presence in parameter space but as it turns out it may be confined to a very narrow range of values. For the hypercycle presented at the beginning of this section, all non-uniform permutations of weak/strong catalytic links (i.e. values $\in \{1.1, 1.5, 1.9\}$) as well as both cycle directions ($r_{ij} > r_{ji}, \forall i, j$ and vice versa) were tried. The only flexible parameter was the rate $r_{31} \in [1.5, 2]$, with all other deviations being unable to form the pattern. The initial circular wave forms but is unable to hold together as a loop and breaks up, following the compound pattern rule. Similarly, all but minute changes in k_i lead to failure of loop formation. Largely by accident a second set of hypercycle parameters that achieves this behaviour was found, with one k_i in the so-called “u-skate world” region described in [Mun].

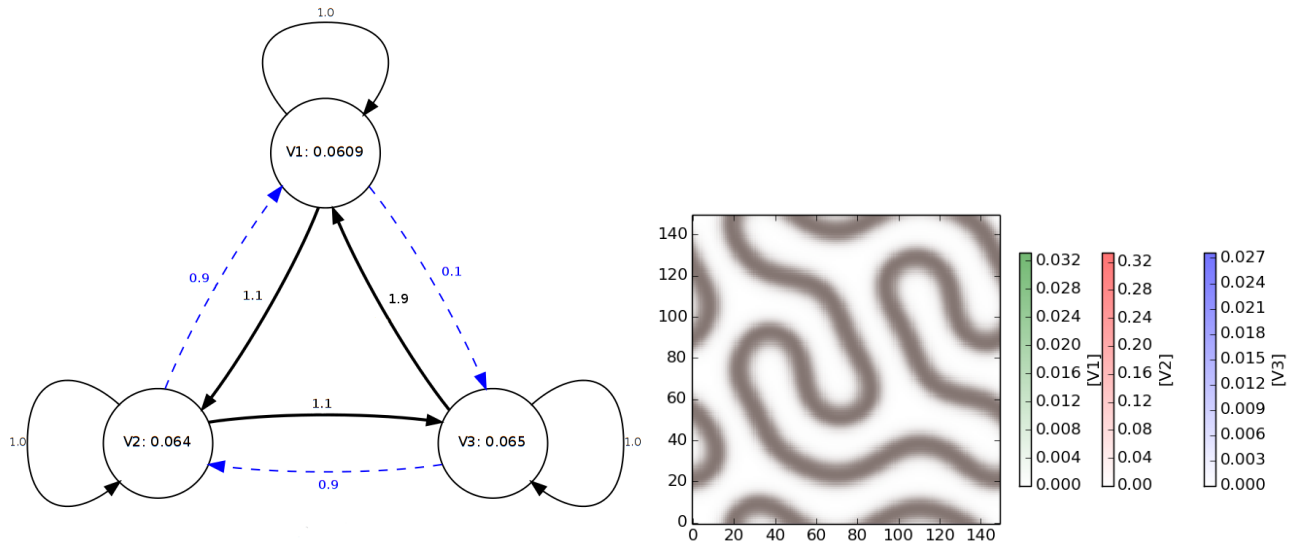


Figure 5.36: Diagram of a loop-yielding compound hypercycle (left) and final pattern shape after 10^5 generations (right). Replication rates \mathbf{r} obey Constraint 3. The fuel feed rate is $F = 0.062$. Alone, V_1 corresponds to a few scattered stripes and non-dividing spots (“u-skate world”, close to Pearson κ), V_2 corresponds to loops and stripes (Pearson κ), and V_3 to stripes and spots (Pearson μ). As far as directionality goes, the cycle is mostly weakly directional.

Interestingly, the final pattern arrived at in all simulations with this cycle look the same regardless of random seed, in the shape reminiscent of a stylised “I” shown above, as is or reflected. Furthermore, this system arrives at a far tighter periodic orbit than the first one, as can be seen in the following plots taken from the same long noiseless simulation that produced the pattern above.

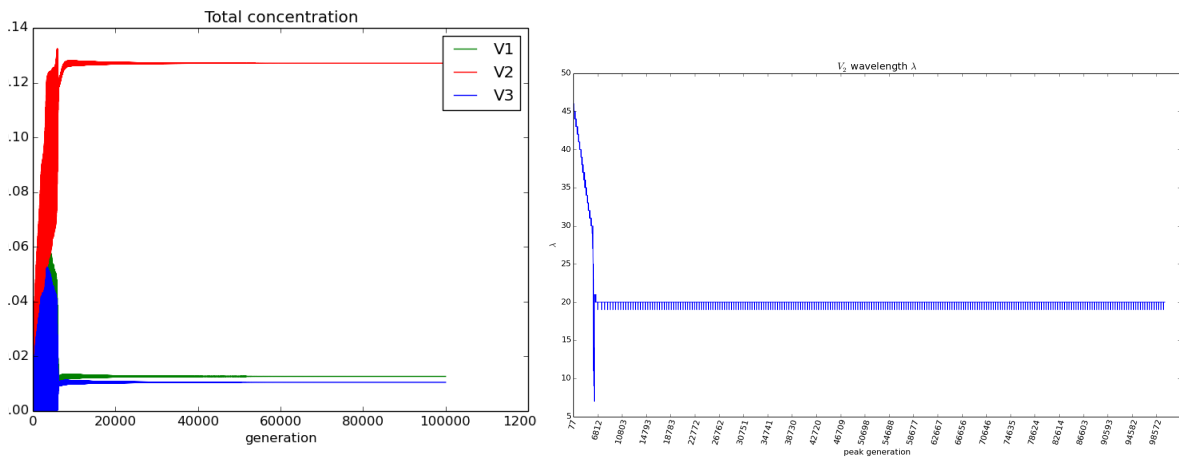


Figure 5.37: Total species concentration (normalised over grid size) of the expanding loop-yielding compound hypercycle (left) and the inter-peak distance (wavelength) of the v_2 curve (right). The expansion mode has decreasing time intervals between spontaneous enlargement events (first portion of the right hand side plot). This period lasts for slightly over 6000 generations, after which the system apparently passes through 3 orbits of increasing duration (clearer for the lower curves in the left hand side plot). The final orbit seems to have been reached some time after gen. $5 \cdot 10^4$. The generation length is $\lceil \frac{LN}{\Delta t^2} \rceil$ iterations.

In contrast with the previous loop-yielding cycle, during the initial expansion period, the time between growth events is decreasing. Noise perturbation causes this decrease to occur more sharply, as can be seen in the following plots from a simulation with strong noise level $\bar{\lambda} = 1$. In this respect, the behaviour is consistent with the previous cycle, in that noise induces an accelerating growth mode.

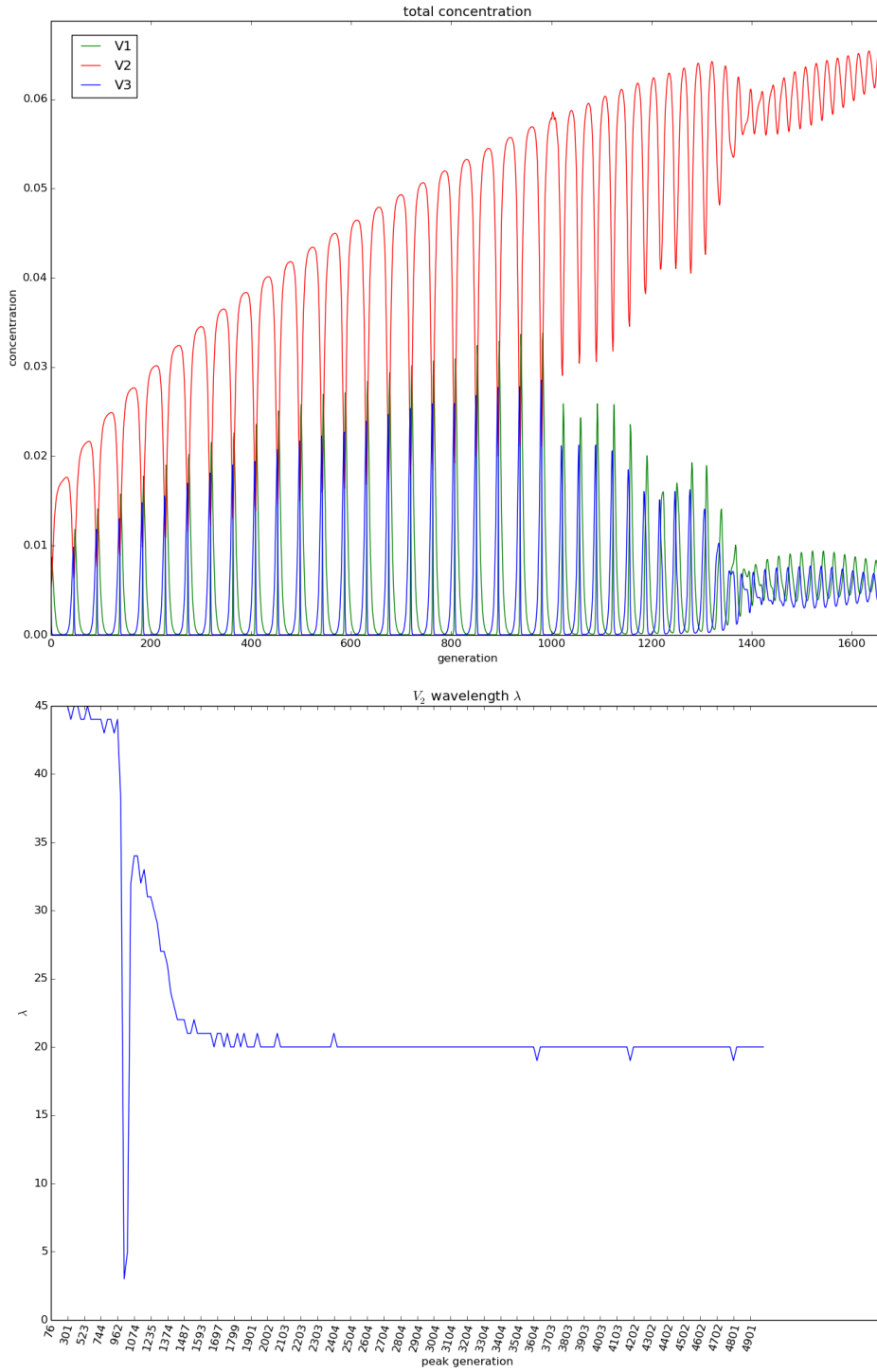


Figure 5.38: Total species concentration (normalised over grid size) of the expanding loop-yielding compound hypercycle (left) and the inter-peak distance (wavelength) of the v_2 curve (right). The system underwent a strong noise $\bar{\lambda} = 1$ perturbation at gen. 1000 lasting 20 generations, after which the decrease in inter-growth intervals becomes sharper (ignoring the downward spike due to noise), until the space-filling period begins, in which the wavelength is overall constant. The generation length is $\lceil \frac{LN}{\Delta t^2} \rceil$ iterations.

It was also discovered that this hypercycle is more flexible to parameter deviations in terms of producing the loop pattern. The size of the initial species mix may be in the range $[1, 75]$ % of the grid area, which is far more permissive. Secondly, rates r_{12} and r_{31} may vary as $r_{12} \in [1.2, 1.5]$ and $r_{31} \in [1.2, 2]$, when changed alone. If r_{12} is increased the spontaneous growth events occur at a much higher frequency (separated by about 5 generations). If r_{31} is set at the lower end of its allowed interval, the system experience more pronounced periodic increases in amplitude during the space-filling period.

These two cycle cases, along with very small deviations in the vicinities of their F and k_i values, were the only instances of this structure formation found. For ease of reference, below is the location in parameter space of the cycles that exhibit this behaviour.

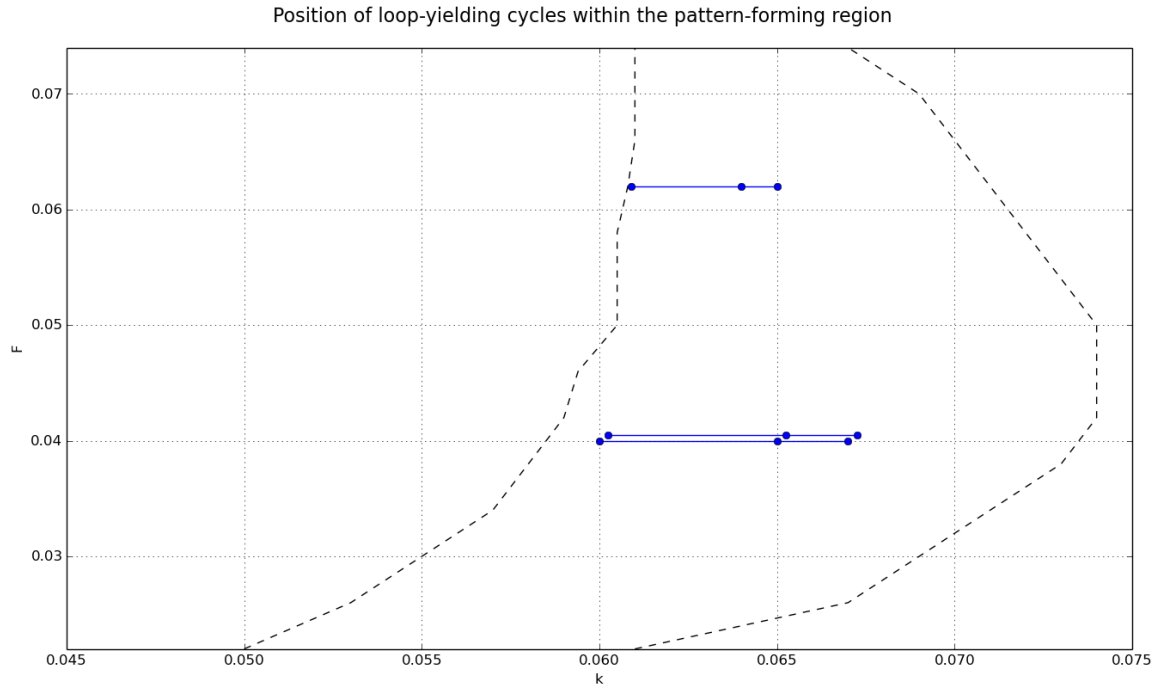


Figure 5.39: Position in (k, F) -parameter space of compound hypercycle parameters that have been confirmed to form the novel loop pattern. Horizontal lines connect the k values of the species in one cycle, with $k_1 < k_2 < k_3$. The dotted boundaries depict the approximate limits of the pattern-forming region and are given for reference (values taken from [Mun]).

At first glance, these positions seem to follow the curvature of the pattern-forming region of the Gray-Scott model. The scarcity of data points is due to the difficulty in locating stable loop patterns. To test their stability, simulations need to be run for very long times and as parameter deviations increased, the loops would ultimately destabilise.

5.6 Evolution simulations

We now move on to an evolutionary scenario for this model in the same vein as the previous ones, to see how its cooperative behaviour influences the parameter direction of the species involved.

Any stable hypercycle reached through these simulations would be the final one, since none of its constituents would become extinct. Therefore the question of these evolutionary simulations becomes: how often does the system encounter stable cycles through random mutation? Or, how common are stable cycles in the evolutionary landscape of the three-species compound hypercycle?

Given the directionality requirement for a stable hypercycle it is perhaps no great surprise that the probability of it arising through unconstrained random mutations is quite small. So these parameter combinations are very sparse points of stability in this landscape. Indeed, in the vast majority of simulations run the systems kept exchanging cycle components as previous ones went extinct, until the time limit would be reached. In fact, these experiments had served to deduce this particular stability condition.

We have used the algorithm described below. The system starts with two species set manually and the first random mutant completes the cycle. Regular checks are performed to see if any species goes extinct and if so, random mutants are introduced to replace them. If all three disappear, the simulation is stopped. This differs from most studies of mutation in hypercycles, e.g. [ES78], [BH91], [CB94], where new species would appear as external components to an internally equilibrated cycle or nearly so. Here these new species are incorporated in the 2-species configuration far from steady state, completing the 3-species hypercycle (they are “internalised”).

Algorithm notes

1. Since the system is only defined with three species, the role of wild type is assigned at each mutation event to one species, upon which the mutant is based. The third species, if present, is assigned the role of some “original” species, otherwise this remains unassigned ($o = 0$). The name means to be purely suggestive, as it is not guaranteed that this species was the wild type 2 mutation events before. The assignment section of the algorithm (lines 21-29) manages these roles in a deterministic manner at every mutation event.
2. The convention used in the evolution scenario is that only received catalytic rates are set through mutation, while the corresponding back-reactions (offered catalytic support) are set by imposing Constraint 2.

Algorithm 5.1 Evolution Simulation 3: Hypercycle evolution

```
1: function MUTATION( $\pi$ )                                ▷ returns mutant parameter as deviation of  $\pi$ 
2:    $\delta_\pi \in \mathcal{N}(0, \sigma_{\Delta\pi}^2)$ 
3:   return  $\pi + \delta_\pi$ 
4: end function

5: function PRESENCE( $v_1, v_2, v_3$ )                      ▷ marks which species present
6:    $x(s) \leftarrow \left( \sum_{i,j} v_s(i,j) > \epsilon \right) \quad \forall s \in \{1, 2, 3\}$            ▷ 1 = True, 0 = False
7:   return  $x$ 
8: end function

9: procedure MAIN

10:  INITIALIZE( $k_1, k_2, r_{11}, r_{22}, r_{12}, r_{21}$ )           ▷ Start with 2 species
11:   $x = (1, 1, 0)$                                            ▷ keeps track of which species present
12:   $o = 1, w = 2, m = 3$                                      ▷ “original”, “w.t.”, “mutant” roles assignment

13:  repeat
14:    SIMULATION STEP( $k_i, r_{ij}$ )

15:    if (another EXTINCT.CHECK generations passed) then
16:       $x \leftarrow$  PRESENCE( $v_1, v_2, v_3$ )
17:      if not ( $x(1)$  and  $x(2)$  and  $x(3)$ ) then                 ▷ at least one extinction

18:        if not ( $x(1)$  or  $x(2)$  or  $x(3)$ ) then                 ▷ full extinction
19:          STOP
20:        end if

21:         $o = w = m = 0$ 
22:        for  $i \leftarrow 1, 3$  do                               ▷ Assign roles to species
23:          if not  $x(i)$  then
24:             $m \leftarrow i$                                      ▷ “mutant” = last not-present index
25:          else
26:             $o \leftarrow w$                                      ▷ “original” = first present species index
27:             $w \leftarrow i$                                      ▷ “w.t.” = last present species index
28:          end if
29:        end for
30:         $k_m \leftarrow$  MUTATION( $k_w$ )
31:         $r_{mm} \leftarrow$  MUTATION( $r_{ww}$ )
32:         $r_{wm} \leftarrow$  MUTATION( $r_{ww}$ )
33:         $r_{mw} \leftarrow 2\sqrt{r_{ww}r_{mm}} - r_{wm}$              ▷ Constraint 2

34:        if  $o \neq 0$  then                                     ▷ The system has a 2nd (“original”) species
35:           $r_{om} \leftarrow$  MUTATION( $r_{ow}$ )
36:           $r_{mo} \leftarrow 2\sqrt{r_{oo}r_{mm}} - r_{om}$            ▷ Constraint 2
37:        end if

38:        INTRODUCE MUTANT( $k_m, r_{mm}, r_{wm}, [r_{om}]$ , at  $\max_{(i,j)}\{v_w\}$ )
39:        RECORD(cycle parameters)
40:      end if                                               ▷ (line 17)
41:    end if                                               ▷ (line 15)
42:
43:  until ENDTIME
44: end procedure
```

Example simulation

We show results from a typical evolutionary simulation, with parameters as follows. The F value was again chosen such that its pattern-forming k interval would be large. The system parameters were the same as the ones used for the hypercycle experiments in the previous section, and the mutant perturbations were of concentration $\mu = 0.2$ and Moore radius $r_\mu = 2$. One generation was set to specific length $\lceil \frac{LN}{\Delta t^2} \rceil$ integration iterations.

F	k_1^0	k_2^0	r_{ij}	$\sigma_{\Delta k}$	$\sigma_{\Delta r}$	$[k_{\min}, k_{\max}]$	$[r_{\min}, r_{\max}]$	ENDTIME
0.04	0.065	0.065	1.0	0.005	0.005	[0.05, 0.07]	[0.0, 2.0]	$2 \cdot 10^5$ gen.

Table 5.3: System parameters for hypercycle evolution simulations. All catalytic rates started with value 1.0 and were made to obey Constraint 3.

During the simulation presented here, 52 hypercycles were present, all of them beginning with the third not forming any patterns since all of its components corresponded to the homogeneous steady state. These transient cycles are long-lived due to the proximity of the constituent species parameters and so a small number take up the entire time of long simulations. However, tendencies in parameter drifts are discernible, as shown in the plots below for the same simulation. Species quickly develop selfish parameter values, as was the case in the previous models. Note that these evolution curves are consistent across all simulations performed.

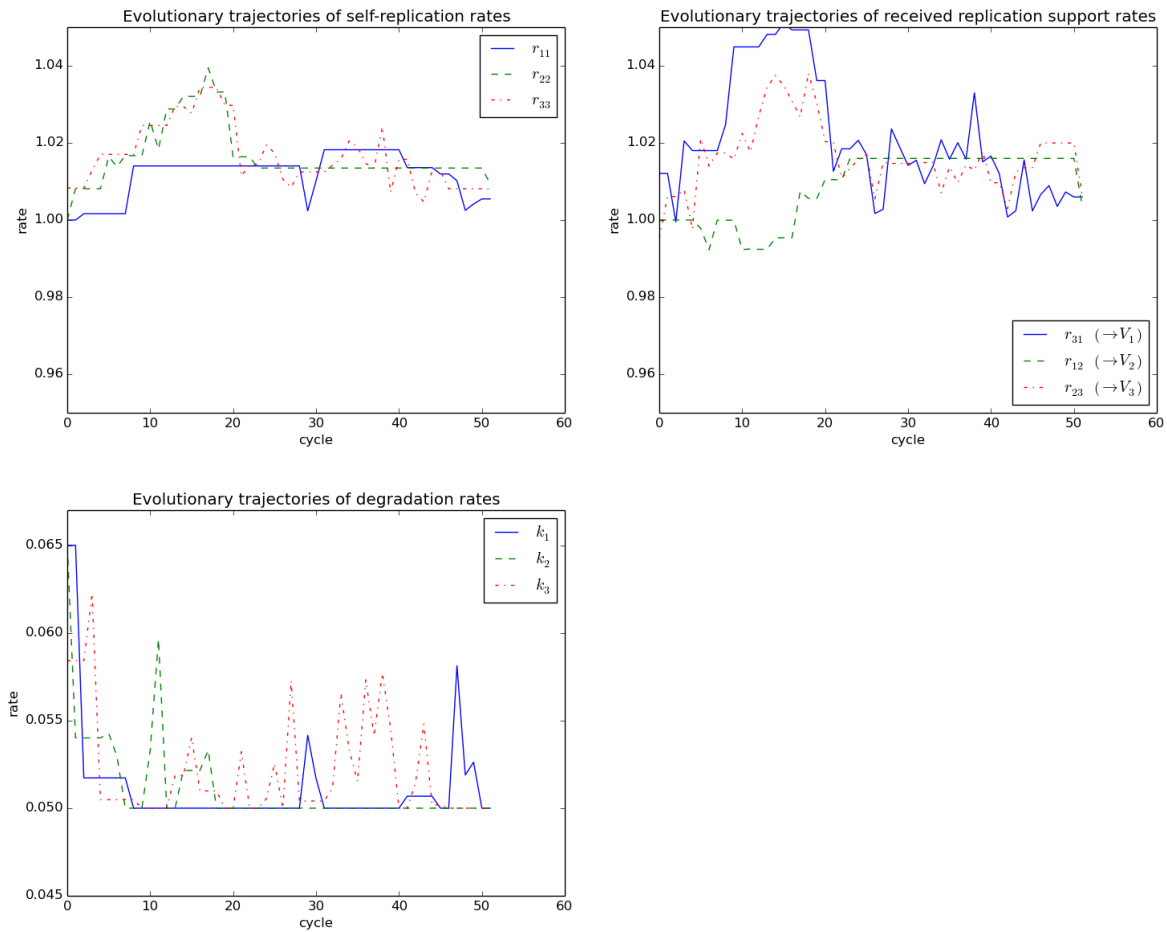


Figure 5.40: Parameter trajectories during a hypercycle evolutionary simulation. Degradation rates k_i quickly drop toward k_{\min} , with occasional increases (bottom row), while self-replication rates r_{ii} (top row, left) as well as received replication support rates $r_{ji}, \forall V_i$ (top row, right) increase and remain above 1.0, leading to species with high self-amplification. One can also observe a slight correlation of these two rate curves.

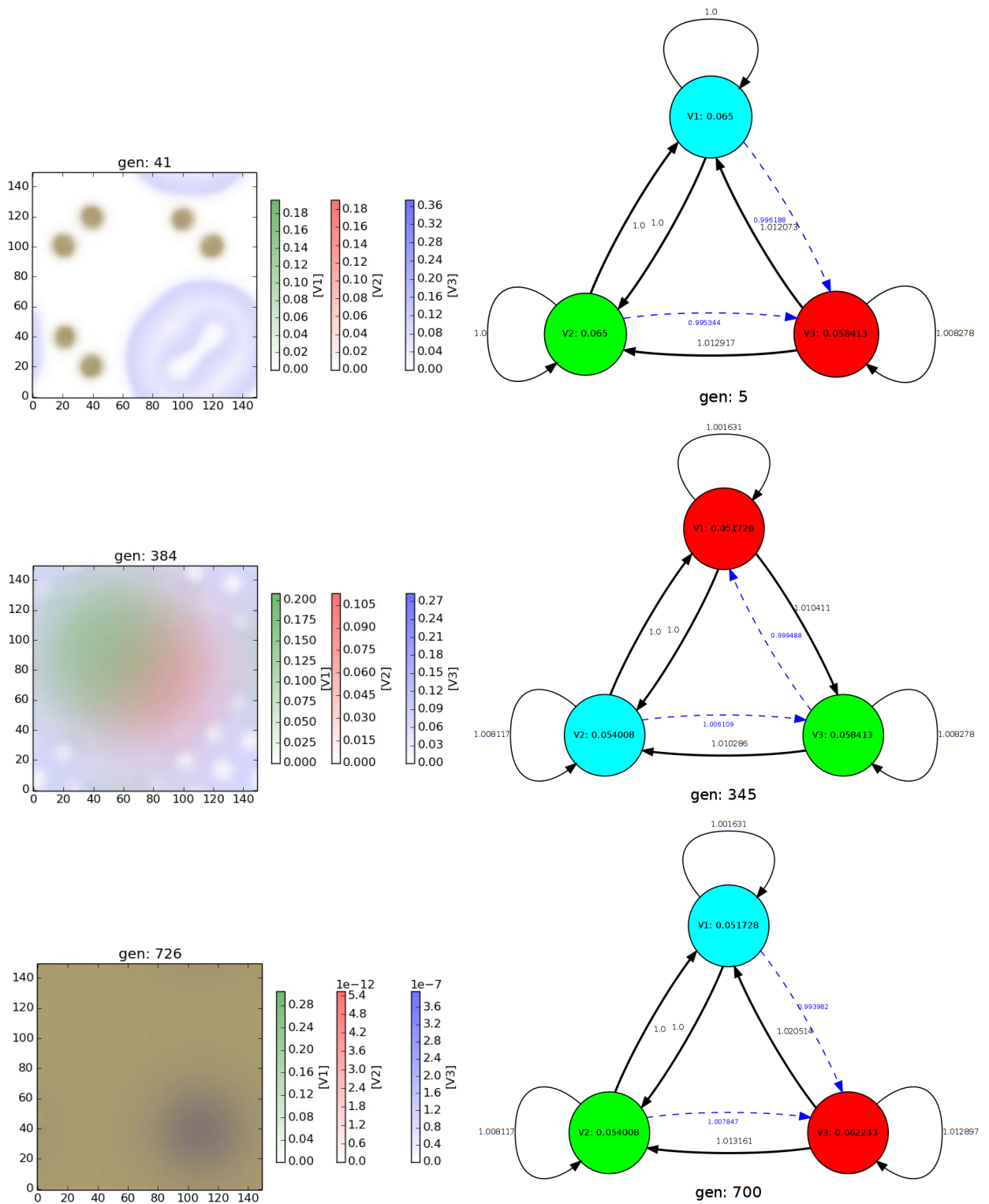


Figure 5.41: Patterns and the hypercycles that produced them from an evolutionary simulation. The right column diagrams are marked with the generation number they first appeared in the system. The colours code for the order of appearance of a species: *cyan* - the “original species”, which was present before the previous mutation event, *green* - “wild type”, and *red* - last mutant introduced as a variation of the wild type. (For clarification of these roles see the algorithm notes.) The animation frames on the left column are taken slightly after their respective cycles were introduced. All cycles starting from the third one produced only homogeneous structures (no patterns).

5.7 Conclusions

We observe that unless set in a cooperative configuration, the three species still evolve toward “selfish” individuals, i.e. high self-replication and received replication support rates, as well as low degradation rates. The correlated increase in rates r_{ii} and r_{ji} , $\forall V_i$ is due to the fact that the latter is set by random mutation as a deviation from the former, but we have mentioned both since their effects are compounded. Given this tendency, when stable cycles are reached, they would have a high likelihood of occurring outside the pattern forming range. This is consistent with the 2-species model, in that evolution drives the system towards loss of structure.

The most important difference from the previous model is that at infinite time these systems will find themselves in a stable cycle configuration, if the algorithm outlined here is to be used, since even if rare, these configuration are cooperative. As such, while only 2 competing species cannot in general coexist, the 3-species compound hypercycle leads to a permanent system through repeated mutation, given ample time.

We have thus seen that the hypercycle allows for cooperative behaviour and the establishment of a permanent system. It also permits a richer array of structure formation in the shape of dynamic patterns, with time-dependant features that emerge out of local species oscillations. While it fits with established criteria of permanence for elementary hypercycles in mixed conditions, the spatial extension of the model along with the added dynamics of the autocatalysts and their competition for a common resource place additional constraints on stable cycle structure. While we cannot argue for the likelihood of evolutionary emergence of such cycles, their behaviour, as well as the abstract nature of this study, warrant their characterisation. In addition, for this model we have discovered a novel pattern, i.e. not reproducible with the simple Gray-Scott dynamics, featuring different types of internal dynamics, albeit a very limited one in terms of parameter-space presence.

Chapter 6

Discussion

6.1 Overview

In this final section we will undertake an overview of the results presented in this thesis and outline the contributions to existing knowledge of similar systems.

Concerning our aim to explore *long-term* evolutionary effects on pattern formation, we conclude that for the systems composed of two and three autocatalysts presented here, the system inexorably heads towards pattern loss and quite quickly so in terms of successive survivors of the replacement process. This is due to the fact that selection favours selfish species which have parameter values outside of pattern-forming range and in the case of the two-catalyst system, it ultimately leads to the appearance of parasites that cause mutual extinction. While there are a few “islands of stability” within the structure-yielding range, as is the case of the stable aggregate patterns in section 4.5 and the stable hypercycle class, the likelihood of reaching them through unconstrained evolution is very small. The fact that patterns themselves are not decisive for evolutionary outcomes but merely reflect (local) populations is most likely due to the PDE nature of the systems since all species may exist in every grid cell. Since the evolutionary direction is dictated by reaction parameters rather than spatial structure, slight transitions in patterns due to noise as in [LHMPM03] would not change this overall direction.

We also sought to understand the effects of spontaneous population variation on patterns. These *short-term* interactions are of dominance by the fitter species, which drive the less fit out from the system and form their own pattern. However, in the 3-hypercycle this replacement is stopped and the interaction is stabilised. Very rich behaviour is obtained in this model, in the form of dynamic patterns that have features which shift their structure in reflection of the local species population ratios. For more catalytically altruistic species this is even more pronounced as long-lived oscillations maintain the continuous changes in pattern features. While each of these features could be obtained with the original single-catalyst Gray-Scott model, to our knowledge the overall result is novel. Moreover, a new kind of pattern was found within this dynamic class in the shape of a stable loop which undergoes episodic growth. This pattern was shown to have varied internal dynamics and to be able to coexist in groups.

We also report that behaviour was essentially identical in environments with varying fuel feed F and/or degradation k_i rates. While the parameter gradients allowed for the forming patterns to vary, as was the case of the phase diagram presented for the Gray-Scott model, the manner in which species interaction occurred was unchanged, the overall pattern behaving as one unit. Hence these results were omitted from this report. This is contrast with the phenomena observed in [BH95b] for a PDE model of an elementary second-order replicator hypercycle with no resource competition but growth limited by a carrying capacity. The study showed that space heterogeneity (degradation rate gradients) confers resistance to strong parasites introduced at steady state. They would be pushed out of the system by spiral fragmentation.

6.2 Parallels with existing models

These results have varying degrees of consistency with existing work, especially in the case of the 3-species compound hypercycle described in this thesis. Due to its improbable role in the early stages of life it has found little attention in such studies. Most models describe elementary hypercycles composed of second-order replicators, which are known to be topologically equivalent to Lotka-Volterra equations [SS03]. In particular they feature quadratic autocatalysis, while here we have a cubic term.

An exception to this prevailing focus is the study of a compound hypercycle in [BH95a], however their cycle features inhibitory back-links. The authors report different behaviour for odd- and even-numbered cycles, though it was stated the negative interactions tended to lead to cycle breakup. They also report non-overlapping population patches that mix and enlarge.

In the non-interacting autocatalysts case first considered in this work, space and the coupled availability of the common resource U complicates competition. Even for fitter mutants, the spread of the initial mutation population constrains its survival. Such non-interacting replicator systems were seen to lead to a sole survivor in the non-spatial setting in [ES78] and in this sense we have consistent results, although selection differs in that the fitness of each species was simply its replication rate and a conservation of the total amount of replicators was in effect.

In contrast with [ES78], resource availability and limited species lifespan induces mutual exclusion in 2-cycles. Furthermore, here we get extinction even for slightly asymmetric interactions, not only for parasitic relationships as in [SS03] for the same non-spatial environment and reaction networks as the previous paper. There is some consistency with [ES78] concerning the 3-cycles, in that they exhibit cooperation and achieve permanence, if only for a subclass thereof. Details about this cycle class have been outlined in the stable cycle properties section of the hypercycle chapter.

As was pointed out in the introduction chapter, cellular automata (CA) models show different behaviour for the same reaction scheme, largely due to their local particle exclusion. Here there is overlap of populations though in wave regimes we do observe population gradient offsets, but there is considerable blending.

A similar approach to ours regarding mutation was taken in [HT03], where a mutant was introduced before population equilibrium. However, they consider only parasitic mutants. The referred work was concerned with a stochastic CA model of an elementary hypercycle with no resource competition. In particular, the authors show that a 2-cycle may coexist indefinitely with a strong parasite and often this invader would be eventually expelled. This configuration would correspond to a broken cycle in this thesis, a case which we did not consider but which we suspect would lead to its failure. In the CA model in [AS06] of an elementary hypercycle composed of second-order replicators featuring faulty synthesis with no resource competition, the populations in the cycle were reported to undergo genetic drift, unlike the species in this work which have a strongly directed evolutionary direction.

Alongside the elementary hypercycle, there has been considerable focus on analysing second-order replicator networks, often under the constraint of constant organisation (total population size fixed by dilution) and assumption of abundant (constant) resources thus with no competition in this respect. While we also assume a constant fuel resupply, it may be locally exhausted by the catalyst populations, especially for the the inflow rates in the pattern-forming region.

Perhaps the closest model and results to our work is to be found in [CB97]. Indeed, the two models are identical for certain parameters if the reaction constraints used here are to be discarded. While our model does not consider varying molecule lengths we do have variation in the self-synthesis rate, which the lengths were inversely proportional to in the respective study. The authors only consider a limited number of network configurations, most notably an elementary hypercycle with no autocatalysis, subjected to an invasion by a parasite also devoid of autocatalysis, which occurs at pattern steady state. The pattern they investigate is described to be the dividing spots classified as λ by Pearson [Pea93]. In an earlier paper with explicitly excluded autocatalysis for the same PDE system [CB94], while not considering a 2-cycle case, the reported behaviour of the (non-invaded) elementary 3-cycle is consistent with the one seen here. Namely the system reaches a time-constant state, though note that for strongly directional (yet still compound) cycles here the system reaches a periodic concentration orbit, even if minute. The invasion of a fitter parasite in their study kills the entire system while less fit ones die out and coexistence is achieved in the limit case of equal fitness, similar to what is observed in this work. To reiterate, the situation in our study differs in that we incorporate the new species into the network as a variation of an existing component. A possible point of contention comes from the authors' hypothesis that any architecture may display clusters. Here however we have seen that non-directional compound hypercycles fail altogether, which contradicts this claim.

Unlike models that assume inherently faulty replication between a fixed number of species, similarly to the rare-event perspective in this thesis, the non-spatial study by [HS98] looks at the effects of introducing a new component. Their model is a non-spatial network that allows bidirectional and negative couplings (inhibitions), with no resource competition. Mutants that were based on a species from the network and inherited only its interactions were seen to be incorporated into the network, as opposed to a randomly coupled new species, that kill the system altogether. This is contrast with our results which feature frequent network failure for mutants closely based on their wild types, unless the necessary coupling are achieved in the 3-cycle. The sharpest difference comes however with their result that all evolved networks through small deviations are permanent, as we have seen

here that minute differences in parameters simply delay extinction in competitive configurations. The important consistency with this study is that the authors also report increase in average fitness in evolved networks, although different parameters are involved, replication rates in [HS98] since species do not degrade but are diluted out (constant organisation conditions), while in our model fitness also comes from degradation rates.

Different forms of mutation produce differing results at least for a non-spatial setting. Such as the continuous (perturbation) treatment in [SS92] of mutation in fixed networks with no resource competition. Mutation in their model tends to drive the system away from extinction of single species and does not cause extinction in stable complete populations. This is in sharp contrast with our results (except for the special stable cycle class) - after a network is formed by the introduction of a mutant, even slightly deviating new species will lead to extinction.

We also make a quick note of another system with behaviour resembling that of our 2-species model, namely the spatial Nicholson-Bailey host-parasitoid model in [BL93], where the host may be viewed as the resource for which parasitoids compete. They also report population overlaps and replacement by a fitter species in spiral patterns.

6.3 On further extensions

A well-known problem of internally equilibrated hypercycles is their vulnerability to external parasitism. In the present model we have seen that the incorporation of a third species with little to high degree of parasitic nature into an existing 2-hypercycle far from steady state may stabilise the system and lead to permanence. If we assume the directionality constraint for a stable cycle fulfilled and think of these as elementary cycles in the direction of the dominating rates (see discussion in the cycle properties section), established properties [ES78] of these networks in the non-spatial case hold. As such, we suspect that longer directional compound cycles would allow permanence and show similar dynamics, reaching a periodic orbit state at infinite time. For this hypothesis we list some results concerning larger systems.

We know that more complex network topologies reduce to hypercycles [ES78]. For uniform coupling terms generally only independent replicators or (elementary) hypercycles remain. We also have from [ES78] that if a cycle has alternative internal paths (short-cuts), only the most efficient path (in terms of catalysis rate) will remain. Since our results show some overlap with the non-spatial elementary hypercycles and the evolutionary behaviour appears decoupled from structure formation to a certain extent, we expect other results regarding arbitrarily complex networks to hold, at least for certain subclasses.

Non-spatial second-order replicator networks under the constant organisation constraint were shown in [HS98] to exhibit a logarithmic increase in the number of constituent species as a function of the number of mutation events. The same result was obtained in [MN94] in a non-spatial replicator metapopulation model of competing parasites. There is a similarity to the model studied here, in that the infecting parasites compete over the common resource of hosts, which are sustained in turn by self-replication. However, it features a strict chain hierarchy of forward replication support and inhibition (negative interaction), and the constant organisation constraint. A consistent result is that for a new species to establish itself, its decay rate (or “virulence”) must lie within a critical range with respect to its wild type.

In the spatially extended multi-substrate and multi-catalyst generalisation of the Gray-Scott model in one dimension [TK01], we have similar behaviour to our results in that spikes of overlapping oscillating populations are formed. This resembles the case of concentration-oscillating spots shown here, although the authors describe rare cases of spikes differing either in peak shape or internal dynamics, with chaotic spikes mixed with fixed point ones.

It was stated in the analytical treatment by [WW14] that for the elementary hypercycle with no autocatalysis, the solution consisting of a single spot pattern is (linearly) stable up to a cycle length of 4 components. Their analysis was of the same model as that in [CB97], where it was shown numerically that these spots were stable for cycles of length 5. Note that this does not entail lack of structure formation but a change in dynamics of larger cycles.

On the other hand, there are also results which stand against the hypothesis stated earlier, such as the numerical survey [SH93] which showed that the probability of achieving permanence in random non-spatial second-order replicator networks of more than 5 components decreases at least exponentially with the number of components.

Appendix A

On numerical issues

As pointed out in a previous paper[CB97], one needs to be careful of stability when performing numerical integration of these dynamics. Most critically here, one needs to avoid the emergence of spurious structural features.

A necessary condition for the stability of (well-posed) initial-value problems solved by finite difference methods is the Courant-Friedrichs-Lewy (CFL) condition, which informally states that the time step length must be smaller than information propagation time on the discrete grid. More formally, “the mathematical domain of dependence must be contained in the numerical domain.” [Tre96] *Domain* denotes all points that may be influenced by a given point x starting from time $t = 0$, whether in the analytical (*mathematical*) system or in the discrete integration space.

For the current system, this condition may be stated as

$$C = \frac{s\Delta t}{\Delta x^2} = \frac{D\Delta t}{\Delta x^2} < C_{\max} \quad (\text{A.1})$$

where s denotes the velocity of information, here taken as the diffusion coefficient since it parametrises the Laplacian spatial operator. C is the so-called “Courant number” and the bounding $C_{\max} = 1/4$. This is to say, the length of the squared space step should be at least 4-fold that of the time step, which is sufficient for the stability of an explicit method used on a parabolic system, as is the case here [Tre96].

In most simulations the ratio has been kept as low as feasible, a typical example being a CFL number for u of $3.15 \cdot 10^{-2}$, with the value for v at half.

As can be seen from the above, the magnitude of the diffusion coefficient is related to the discretisation parameters. Throughout the literature, the value of D is given without explicit reference or functional link to these parameters. Here we have used the following heuristic to set this parameter in our simulations. The idea is to work backwards and assume a given Courant number C_d and derive

$$D = C_d \frac{\Delta x^2}{\Delta t} \quad (\text{A.2})$$

We have found this derivation to work well for $C_d = 10^{-3}$ in the majority of simulations though the essential thing is to have the diffusion coefficient of the same order of magnitude as the right-hand side term above.

The integration method used throughout this work, unless stated otherwise, is the forward Euler method. The midpoint method was also used, but no difference in behaviour could be observed when confining as described above. Therefore, the simple Euler method was deemed satisfactory and chosen for speed. For the same reason, most simulations use a 5-point stencil for the discrete Laplacian operator, especially since its computation was the speed bottleneck of the simulations. As no effective difference was observed in pattern formation following the precision considerations described here, the more accurate 9-point discrete Laplacian was not employed.

Regarding effective null concentration, we have chosen a more realistic value $\epsilon = 10^{-24}$, based on the Avogadro constant (i.e. $\epsilon < 1/6.02214129(27) \cdot 10^{23}$), rather than relying on the implicit machine IEEE 754 specification of lowest non-null representable double precision floating point number, which is 10^{-324} [jee08]. Note though that this value is used for every grid cell, so a mole is a quite high reference value and a ratio over Δx^2 would be perhaps more appropriate, giving a value of e.g. 10^{-14} for most simulations in this report, but for simplicity the aforementioned value was chosen. Visible effects of high cut-offs have been reported to occur for values above 10^{-5} [CB94], many orders of magnitude higher than our value, even with the extra scaling.

Very low values are also worth taking note of, since some patterns were seen to be influenced by them. Specifically, we have found for the fledgling spirals pattern (Pearson α) that as the null cut-off was lowered from 10^{-30} to 10^{-300} , a twofold increase in the number of wave fragments occurred, all other parameters being kept identical. However, concentrations below the ϵ chosen here were deemed unreasonable as the probability of finding any particle in a cell holding these values is effectively zero. So we decided to consider these structural features that appear at machine ϵ as spurious and, besides the numerical experiments performed to decide the above issues of numerical stability, all results presented in this thesis, unless otherwise specified, have employed the 10^{-24} cut-off.

The pseudorandom number generator used was the Tausworthe algorithm (for quality and speed) supplied by the GSL package, with seed given by computer system time. From the same package, the Ziggurat algorithm was used to draw Gaussian random variates.

Appendix B

Simulation movie files

The animations from which frames have been illustrated in this report may be found online at https://github.com/phil-b-mt/sim_animations. Below is a table that indicates the file name of the movie corresponding to each series of frames, as given by figure number. Some simulations described in this report have not had the animations saved, as only a few time intervals were of interest. The movies have been encoded in the H.264/MPEG-4 AVC format and should be viewable with any modern media player (e.g. VLC).

Figure	File name
3.1	simple_sim1.mp4
3.5	simple_sim3.mp4
4.2	ic_sim1.mp4
4.4	ic_sim2.mp4
4.6	ic_evol_ex.mp4
4.7	ic_special1a.mp4
4.8	ic_special1b.mp4
4.9a	ic_special2.mp4
4.9b	ic_special2_cross.mp4
4.14	ic_aggr_noise_perturb.mp4
4.21	fic_evol_ex.mp4
5.2	hcycle_sim1.mp4
5.5	hcycle_sim2.mp4
5.11-5.12	hcycle_sim4.mp4
5.17	hcycle_quasistable_first1000.mp4 hcycle_quasistable_last1000.mp4
5.19	hcycle_dyn1.mp4
5.21	hcycle_dyn2.mp4
5.23	hcycle_dyn3.mp4
5.26-27	hcycle_loop1.mp4
5.29	hcycle_loop2.mp4
5.30	hcycle_loop3.mp4
5.31	hcycle_loop4.mp4
5.41	hcycle_evol_ex.mp4
(*)	unused/hcycle_dyn_ex1.mp4
(*)	unused/hcycle_dyn_ex2.mp4

Table B.1: The last two files marked with (*) have not been described in this thesis but have been provided as they are interesting examples of dynamic patterns.

Appendix C

Software

The software used to perform simulations was developed by the author and is available at <https://github.com/phil-b-mt/egs> under a GPL3 licence. It was written in C++ and uses the OpenMP library for parallelisation and the GNU Scientific Library (GSL) for pseudorandom number generation. GSL routines are guaranteed to be thread-safe by the developers, meaning that no errors are introduced when calculations using them are done in parallel. The simulation program handles the numerical computations only, saving the system evolution for later visualisation and analysis. This was done largely with Python scripts.

Plotting, both of the animations and the various concentration and trajectory plots, has been done with the matplotlib library, versions 1.2.1 to 1.3.1 (the change in versions had no essential effect on the procedures used here).

The correlations in section 4.8 on 2-species evolution were obtained using the functions *scipy.stats.spearmanr()* and *numpy.correlate()* from the Python libraries SciPy (0.9.0) and NumPy (1.6.1), respectively. The Q-Q plots in the same section were done in Mathematica 8.0.4.0.

Bibliography

- [AS06] C. S. Attolini and P. F. Stadler. Evolving towards the hypercycle: A spatial model of molecular evolution. *Physica D: Nonlinear Phenomena*, 217(2):134–141, 2006.
- [BH91] M. C. Boerlijst and P. Hogeweg. Spiral wave structure in pre-biotic evolution: Hypercycles stable against parasites. *Physica D: Nonlinear Phenomena*, 48(1):17–28, 1991.
- [BH95a] M. C. Boerlijst and P. Hogeweg. Attractors and spatial patterns in hypercycles with negative interactions. *Journal of theoretical biology*, 176(2):199–199, 1995.
- [BH95b] M. C. Boerlijst and P. Hogeweg. Spatial gradients enhance persistence of hypercycles. *Physica D: Nonlinear Phenomena*, 88(1):29–39, 1995.
- [BL93] M. C. Boerlijst and M. E. Lamers. Evolutionary Consequences of Spiral Waves in a Host–Parasitoid System. *Proceedings of the Royal Society of London. Series B: Biological Sciences*, 253(1336):15–18, 1993.
- [BPN10] A. S. Bratus, V. P. Posvyanskii, and A. S. Novozhilov. Existence and stability of stationary solutions to spatially extended autocatalytic and hypercyclic systems under global regulation and with nonlinear growth rates. *Nonlinear Analysis: Real World Applications*, 11(3):1897–1917, 2010.
- [CB94] M. B. Cronhjort and C. Blomberg. Hypercycles versus Parasites in a Two Dimensional Partial Differential Equations Model. *Journal of Theoretical Biology*, 169:31–49, 1994.
- [CB97] M. B. Cronhjort and C. Blomberg. Cluster compartmentalization may provide resistance to parasites for catalytic networks. *Physica D: Nonlinear Phenomena*, 101(3):289–298, 1997.
- [ES77] M. Eigen and P. Schuster. The Hypercycle. A principle of natural self-organization. Part A: Emergence of the hypercycle. *Naturwissenschaften*, 64(11):541–65, 1977.
- [ES78] M. Eigen and P. Schuster. The Hypercycle: A principle of natural self-organization. Part B: The abstract hypercycle. *Naturwissenschaften*, 65:7–41, 1978.
- [GM72] A. Gierer and H. Meinhardt. A theory of biological pattern formation. *Kybernetik*, 12:30–39, 1972.
- [GS84] P. Gray and S.K. Scott. Autocatalytic reactions in the isothermal, continuous stirred tank reactor. *Chemical Engineering Science*, 39:1087–1097, 1984.
- [HS87] J. Hofbauer and K. Sigmund. Permanence for replicator equations. *Dynamical systems*, pages 70–91, 1987.
- [HS98] R. Happel and P. F. Stadler. The evolution of diversity in replicator networks. *Journal of theoretical biology*, 195(3):329–338, 1998.
- [HS99] R. Happel and P. F. Stadler. Autocatalytic replication in a CSTR and constant organization. *Journal of Mathematical Biology*, 38(5):422–434, 1999.
- [HT03] P. Hogeweg and N. Takeuchi. Multilevel Selection in Models of Prebiotic Evolution: Compartments and Spatial Self-organization. *Origins of Life and Evolution of the Biosphere*, 33(4):375–403, 2003.
- [iee08] IEEE Standard for Floating-Point Arithmetic. *IEEE Std 754-2008*, 2008.

- [Kam07] N. G. Van Kampen. *Stochastic Processes in Physics and Chemistry*. 3 edition, 2007.
- [LEE04] K. Lindgren, A. Eriksson, and K-E. Eriksson. Flows of information in spatially extended chemical dynamics. *Artificial Life IX: Proceedings of the Ninth International Conference on the Simulation and Synthesis of Artificial Life*, 9, 2004.
- [LHMPM03] F. Lesmes, D. Hochberg, D. Morán, and J. Pérez-Mercader. Noise-Controlled Self-Replicating Patterns. *Phys. Rev. Lett.*, 91(23), 2003.
- [LMOS93] K. J. Lee, W. D. McCormick, Q. Ouyang, and H. L. Swinney. Pattern formation by interacting chemical fronts. *Science*, 261(5118):192–4, 1993.
- [LSYG97] D. H. Lee, K. Severin, Y. Yokobayashi, and M. R. Ghadiri. Emergence of symbiosis in peptide self-replication through a hypercyclic network. *Nature*, 390(6660):591–594, 1997.
- [Mer92] E. Meron. Pattern formation in excitable media. *Physics Reports*, 218(1):1–66, 1992.
- [MN94] R. M. May and M. A. Nowak. Superinfection, metapopulation dynamics, and the evolution of diversity. *Journal of Theoretical Biology*, 170(1):95–114, 1994.
- [MS06] A. Munteanu and R. V. Solé. Pattern formation in noisy self-replicating spots. *International Journal of Bifurcation and Chaos*, 16(12):3679–3685, 2006.
- [Mun] R. Munafò. *Reaction-Diffusion by the Gray-Scott Model: Pearson's Parameterization*. unpublished material, available at <http://mrob.com/pub/comp/xmorphia/index.html>, under Creative Commons Attribution-NonCommercial 2.5 License.
- [Mur03] J. D. Murray. *Mathematical Biology*, volume I, II. Springer New York, 3rd edition, 2003.
- [Pea93] J. E. Pearson. Complex patterns in a simple system. *Science*, 261:189–192, 1993.
- [SCS+03] I. Scheuring, T. Czárán, P. Szabó, G. Károly, and Z. Toroczkai. Spatial models of prebiotic evolution: soup before pizza? *Origins of life and evolution of the biosphere : the journal of the International Society for the Study of the Origin of Life*, 33(4-5):319–355, 2003.
- [SH93] P. F. Stadler and R. Happel. The probability of permanence. *Mathematical biosciences*, 113(1):25–50, 1993.
- [SS90] P. F. Stadler and P. Schuster. Dynamics of small autocatalytic reaction networks—I. Bifurcations, permanence and exclusion. *Bulletin of mathematical biology*, 52(4):485–508, 1990.
- [SS92] P. F. Stadler and P. Schuster. Mutation in autocatalytic reaction networks - an analysis based on perturbation theory. *Journal of mathematical biology*, 30(6):597–631, 1992.
- [SS97] E. Szathmáry and J. Maynard Smith. From Replicators to Reproducers: the First Major Transitions Leading to Life. *Journal of theoretical biology*, 187(4):555–571, 1997.
- [SS03] B. Stadler and P. F. Stadler. Molecular Replicator Dynamics. *Advances in Complex Systems*, 6(1):47–77, 2003.
- [SS06] J. Sardanyés and R. V. Solé. Bifurcations and phase transitions in spatially extended two-member hypercycles. *Journal of Theoretical Biology*, 243(4):468–482, 2006.
- [TK01] H. Takagi and K. Kaneko. Differentiation and replication of spots in a reaction-diffusion system with many chemicals. *EPL (Europhysics Letters)*, 56(1):145–151, 2001.
- [Tre96] L. N. Trefethen. *Finite Difference and Spectral Methods for Ordinary and Partial Differential Equations*. unpublished text, available at <http://people.maths.ox.ac.uk/trefethen/pdetext.html>, 1996.
- [Tur52] A. Turing. The Chemical Basis of Morphogenesis. *Philosophical Transactions of the Royal Society of London. Series B, Biological Sciences*, 237(641):37–72, 1952.
- [WW14] J. Wei and M. Winter. *Mathematical aspects of pattern formation in biological systems*. Springer, 2014.